DEPOSITIONAL AND DIAGENETIC CONTROLS ON POROSITY EVOLUTION OF THE MIOCENE DAM FORMATION CARBONATES; AL-LIDAM AREA, EASTERN SAUDI ARABIA

BY

MOAZ ABD ALTAWAB MOHAMMED ALI SALIH

A Thesis Presented to the

DEANSHIP OF GRADUATE STUDIES

KING FAHD UNIVERSITY OF PETROLEUM & MINERALS

DHAHRAN, SAUDI ARABIA

In Partial Fulfillment of the

Requirements for the Degree of

MASTER OF SCIENCE

In

GEOLOGY

NOVEMBER 2015

KING FAHD UNIVERSITY OF PETROLEUM & MINERALS

DHAHRAN- 31261, SAUDI ARABIA

DEANSHIP OF GRADUATE STUDIES

This thesis, written by **Moaz Abd Altawab Mohammed Ali Salih** under the direction his thesis advisor and approved by his thesis committee, has been presented and accepted by the Dean of Graduate Studies, in partial fulfillment of the requirements for the degree of **MASTER OF SCIENCE IN GEOLOGY.**

Dr. Osman M. Abdullatif
(Advisor)

Dr. Abdulaziz Al-Shaibani
Department Chairman

Dr. Khalid Al-Ramadan
(Member)

Dr. Salam A. Zummo
Dean of Graduate Studies

Dr. Dave Cantrell
(Member)

3/5/16
Date

Dedication

Every challenging work needs self efforts as well as guidance of elders especially those who were very close to our hearts.

My humble efforts I dedicate to my sweet and loving

Mother (Mameeto) & Father

Whose affection, love, encouragement and prays of day and night make me able to get such success and honor.

This work is also dedicated to soul of my Grandma (Habba), my brother (Hamada Batta), my sister (Mayyar), my uncle (Osman Gailab) and his family who have provided moral strength and encouraged me to complete this study.

ACKNOWLEDGMENTS

I would to thank the Geosciences Department and King Fahd University of Petroleum & Minerals for offering me this opportunity to complete my graduate studies. I also would like to thank the Center for Petroleum & Minerals/Research Institute at King Fahd University of Petroleum & Minerals, as well as Saudi Aramco for supporting this work.

My immense thankfulness to my supervisor, Dr. Osman Abdullatif for his support, and invaluable guidance throughout my journey at King Fahd University of Petroleum & Minerals. Special thanks also go out to my committee members, Dr. Khalid Al-Ramadan and Dr. Dave Cantrell, for their insights and constructive comments and their huge efforts during field. Also I want to express my gratitude to Dr. Hassan Eltom for being a great guider through all the stages of my research. My thanks go also to Dr. Lamidi Babalola for his efforts and support during this research.

TABLE OF CONTENTS

LIST OF TABLES

LIST OF FIGURES

LIST OF ABBREVIATIONS

LST	:	Lowstand System Tract
TST	:	Transgressive System Tract
HST	:	Highstand System Tract
MFS	:	Maximum Flooding Surface
TS	:	Transgressive Surface
SB	:	Sequence Boundary

ABSTRACT

Full Name : Moaz Abd Altawab Mohammed Ali Salih

Thesis Title : Depositional and Diagenetic Controls on Porosity Evolution of the Miocene Dam Formation Carbonates - An Outcrop Approach. Al-Lidam Escarpment – Eastern Saudi Arabia

Major Field : Geology

Date of Degree : November, 2015

The Miocene Dam Formation in the Al-Lidam area of eastern Saudi Arabia consists of a succession of mixed siliciclastic-carbonate sequences that were deposited during Miocene (Burdigalian) times. Stratigraphic equivalents of the Miocene Dam Formation occur as hydrocarbon reservoir intervals in the Arabian Plate in Iraq and Iran.

Previous studies have demonstrated that reservoir quality in carbonate rocks is mainly controlled by depositional setting and post-depositional diagenesis. Carbonate minerals are more susceptible to diagenesis than are their siliciclastic counterparts. This diagenetic susceptibility is mainly due to the high chemical reactivity of carbonate minerals. Diagenetic processes can be either porosity enhancing and/or porosity destructive.

In this study, based on description of the lithology, sedimentary structures, texture, fossil content, and diagenetic features, fifteen lithofacies were identified within the Miocene Dam Formation in the study area. These lithofacies were deposited on, a low angle dipping, carbonate ramp under supratidal, beach, intertidal and shallow subtidal conditions. Carbonate diagenesis has been examined using different analysis tools, including: thin-section petrography, SEM, XRD, XRF and cathodoluminescence. These analyses tools have shown that the studied succession, especially the intertidal grainstones

and packstones, are influenced by extensive meteoric diagenesis that led to formation of moldic and vuggy porosity. In addition to these dissolution related porosities, meteoric diagenesis is also observed in the form of meniscus, microstalictitic and equant calcite cement. Marine diagenesis was also observed, but it was restricted to the beach grainstone and subtidal quartz wacke-packstone lithofacies, in the form of aragonite and high magnesium calcite cement on the grain margins. Shallow burial conditions were inferred by grain contacts represented by point, suture and concavo-convex contacts. In some intervals, such as in the mud-dominated wackestones, hairline-thick fractures were observed. Mimetic dolomitization for the whole succession was also observed. The association of dolomite with evaporites minerals led to the interpretation that dolomitizationas sabkha-evaporative dolomitization model.

Sequence stratigraphic approach was used in order to link the diagenetic processes to depositional setting and relative sea level fluctuations. Three fourth-order, shallowing-upward sequences were identified in the study area, and they are separated by two sequence boundaries. A clear relation between sequence surfaces and diagenetic processes was observed; the meteoric related diagenetic processes and dolomitization increase upwards (towards the sequence boundary) in each sequence. Porosity and permeability measurements have shown that the highest values are associated with the high stand systems tract (HST) of each sequence, followed by the transgressive systems tract (TST) and the low stand systems tract (LST). This was attributed to the fact that the (HST) is dominated by more grainy sediments in association with dissolution related porosities, while the (TST) and (LST) are dominated by muddier sediments with less influence of meteoric dissolution. The results of this study might help in understanding of diagenetic

processes, and consequently the porosity and permeability distribution within hydrocarbon reservoirs.

ملخص الرسالة

الاسم الكامل: معاذ عبد التواب محمد علي صالح

عنوان الرسالة:

التخصص: الجيولوجيا

تاريخ الدرجة العلمية: نوفمبر 2015

متكون الدام في منطقة اللدام في شرق المملكة العربية السعودية يتكون من تتابعات صخرية مختلطة من الرواسب الفتاتية و رواسب الكاربونات والتي ترسبت خلال العصر الميوسيني. الرسوبيات المكافئة لتكوين الدام في الصفيحة العربية تمثل خزانات للنفط في كل من العراق وايران.

أثبتت الدراسات السابقة أن نوعية الخزان في الصخور الكربونية يتم التحكم فيها بشكل رئيسي من قبل النظام الترسيبي بالاضافة الى عمليات النشأة المتاخرة التي تؤثر على جودة الخزان. معادن الكربونات أكثر عرضة لعمليات النشأة المتأخرة أكثر من نظرائها في معادن الرواسب الفتاتية .ويعزى هذاالى الأصل الاحيائي لمعظم المعادن كربونات مقارنة مع الرواسب الفتاتية. ويمكن لعمليات النشأة المتأخرة إما أن تعزز و/أو تقلل مسامية الصخور.

في هذه الدراسة، استنادا إلى وصف الخصائص الصخرية، وهياكل الرسوبية، والملمس، والمحتوى الأحفوري، وملامح النشأة المتأخرة، تم تحديد خمسة عشر سحنة صخرية ضمن تشكيل الدام الميوسيني في منطقة الدراسة. وقد ترسبت هذه السحنات على منحدر ترسيبي ذوو زاوية منخفضة تحت ظروف ترسيب فوق مدية، بين مدية، شاطئية وتحت مدية ضحلة.

تم تحليل عمليات النشأة المتأخرة المتعلقة بصخور الكربونات باستخدام أدوات التحليل المختلفة، بما في ذلك: رقيقة المقطع الصخري، المجهر الماسح الألكتروني، تشتت الحيود السيني، وميض الحيود السيني والإستضاءة بالأشعة الكاثودية. هذه التحاليل أظهرت ان التتابعات المدروسة، وتحديدا الطبقات الحبيبية البين مدية، قد تأثرت بعمليات النشأة المتأخرة الناتجة عن المياه العذبة والتي أدت الى تكوين مساميات مختلفة تتضمن: المسامية القالبية، الفجوية والداخل حبيبية. وبالإضافة إلى هذه المساميات ذات الصلة الذوبانية، لوحظت عمليات النشأة المتأخرة أيضا في شكل انواع من السمنتة تتضمن: الغضروف المفصلي، السمنت المتدلي وايكوانت الكالسيت. ولوحظ أيضا عمليات النشأة

المتأخرة البحرية، ولكن اقتصر ذلك على الطبقات الحبيبية الشاطئة وطبقات الواكي-باكستون التحت المدية الغنية بالكوارتز ، في شكل اسمنت الأراغونيت و الكالسيت العالي المغنيسيوم على هامش الحبوب. تم الاستدلال الظروف الدفن الضحلة بنقاط الاتصال بين الحبوب والممثلة في نقاط اتصال نقطية، خياطية والمحدب-المقعر. في بعض الطبقات، كما هو الحال في طبقات الواكيستون التي يهيمن عليها الطين، لوحظت كسور رفيعة جدا. وقد لوحظ أيضا الدولومايت التقليدي والذي أثر على كل الطبقات. تجمع الدولوميت مع معادن المتبخرات ادى إلى تفسير الدلمتة بأنه تكون تحت ظروف السبخة والتبخر.

تم استخدام تسلسل النهج الطبقي من أجل ربط عمليات النشأة المتأخرة مع الترسيب والتقلبات النسبية لمستوى سطح البحر. وقد تم تحديد ثلاثة متواليات رابعة التكوين والتي تتضاحل الى اعلى في منطقة الدراسة، ويفصل بينهما حدود تسلسل اثنين. ولوحظ وجود علاقة واضحة بين أسطح التسلسل وعمليات النشأة المتأخرة. عمليات النشأة المتأخرة ذات الصلة الزوبانية، والدولومايت يزيدان صعودا (نحو حدود التسلسل) في كل تسلسل. وقد أظهرت قياسات المسامية والنفاذية بأن القيم العليا ترتبط مع أنظمة الترسيب العالية من كل تسلسل، تليها أنظمة الترسيب المتقدمة ومن ثم أنظمة الترسيب المنخفضة .ويعزى ذلك إلى أن أنظمة الترسيب العالية يهيمن عليها المزيد من الرواسب الحبيبية بالإضافة لوجود المساميات التي لها علاقة بالزوبان، فيما ان انظمة الترسيب المتقدمة والمنخفضة يغلب عليها الرواسب الطينية مع وجود أقل للمساميات الزوبانية.

يمكن الإستفادة من نتائج هذه الدراسة لفهم توزيع عمليات النشأة المتاخرة في خزانات النفط التحت الارضية وبالتالي يمكن بواسطتها معرفة توزيع المساميات المختلفة في انطمة الترسيب المختلفة.

CHAPTER 1

INTRODUCTION

1.1 Introduction

The susceptibility of carbonate rocks and sediments to post-depositional cementation and leaching, that affect the primary porosity and permeability values is higher than that of siliciclastics (Table 1.1) (Longman 1980; Moore 1997; Morad et al. 2012; Moore and Wade 2013) . Non-structural hydrocarbon exploration in carbonate rocks is different from that of sandstones where the major pore system occurs as inter-granular pores between sand grains. Thus, the highest porosities in siliciclastic successions can be predicted as a function of depositional facies alone, and so exploration tends to focus on identification and delineation of sand bodies with only secondary emphasis placed on cementation, leaching and other diagenetic processes. In contrast, carbonate rocks, display a wide variety of pore types as described by Choquette and Pray (1970), that can form independently of depositional facies (Longman, 1980; Makhloufi et al., 2013; Morad, Ketzer, & De Ros, 2013; Tucker, 1993). Thus, for hydrocarbon exploration in carbonate rocks, equal emphasis should be given to the interpretation of depositional and diagenetic controls on porosity. Outcrop studies are one of the effective tools that have been used in hydrocarbon exploration (Thurmond et al., 2005).

Table 1.1: Comparison of diagenesis influence on porosity in both sandstones and carbonates (adapted from Choquette & Pray, 1970)

Aspect	Sandstones	Carbonates
Amount of primary porosity	Commonly 25% to 40%	Commonly 40% to 70%
Amount of ultimate, postdiagenetic porosity	Commonly half or more of initial porosity: typically 15% to 30%	Commonly none or only a small fraction of initial porosity: 5% to 15%
Types of primary porosity	Almost exclusively interparticle	Interparticle commonly predominates; intraparticle and other types important
Pore diameter and throat size	Closely related to particle size and sorting	Commonly bear little relation to particle size or sorting
Uniformity of pore size, shape and distribution	Fairly uniform	Variable, ranging from fairly uniform to extremely heterogeneous, even within a single rock type
Influence of diagenesis	May be minor: reduction of primary porosity by compaction, cementation and clay precipitation	Major: can create, obliterate or completely modify porosity; cementation and solution important
Influence of fracturing	Generally not of major importance	Of major importance, when present
Permeability-porosity interrelations	Relatively consistent: commonly dependent on particle size and sorting	Greatly varied: commonly independent of particle size and sorting

They overcome many of the limitations associated with subsurface well data (high vertical resolution but lack of information from inter-well spacing) and seismic data (low vertical resolution). Understanding and interpreting the depositional and post-depositional processes that initiated and influenced porosity in the reservoir-equivalent strata that are presently exposed at the surface will help in filling the gap between large-scale but low resolution seismic data and small-scale well data (Thurmond et al.2006).

Well-exposed Miocene-age rocks in the Al-Lidam escarpment of eastern Saudi Arabia (Figure 1.1) provide an excellent area for outcrop studies, where more than 40 outcrops of Miocene Dam Formation are well exposed. There, the Dam Formation occurs as a mixed clastic-carbonate succession that was deposited during the Miocene (Burdigalian) time in a closed embayment (Alkhaldi, 2009), with a tidal setting that ranged from supra-tidal to inter-tidal and shallow sub-tidal (Irtem, 1986).

Stratigraphic equivalents of the Miocene Dam Formation are hydrocarbon producing intervals in Iraq and Iran, and in some fields they act as seal rocks for underlying reservoirs (Al-juboury & Mccann, 2008).

The carbonate sequences of the Miocene Dam Formation have been affected by the diagenetic processes in term of the dissolution of skeletal grains, cementation and other diagenetic processes (Alkhaldi, 2009; Irtem, 1986).

Diagenetic processes that have an influence on the petrophysical properties of carbonate reservoirs occur in different diagenetic environments (Tucker, 1993; Flügel, 2010) (Figure 1.2A). These diagenetic environments are: marine diagenetic environment, meteoric diagenetic environment, and burial diagenetic environment, with each environment having its own diagenetic processes and products (Figure 1.2B).

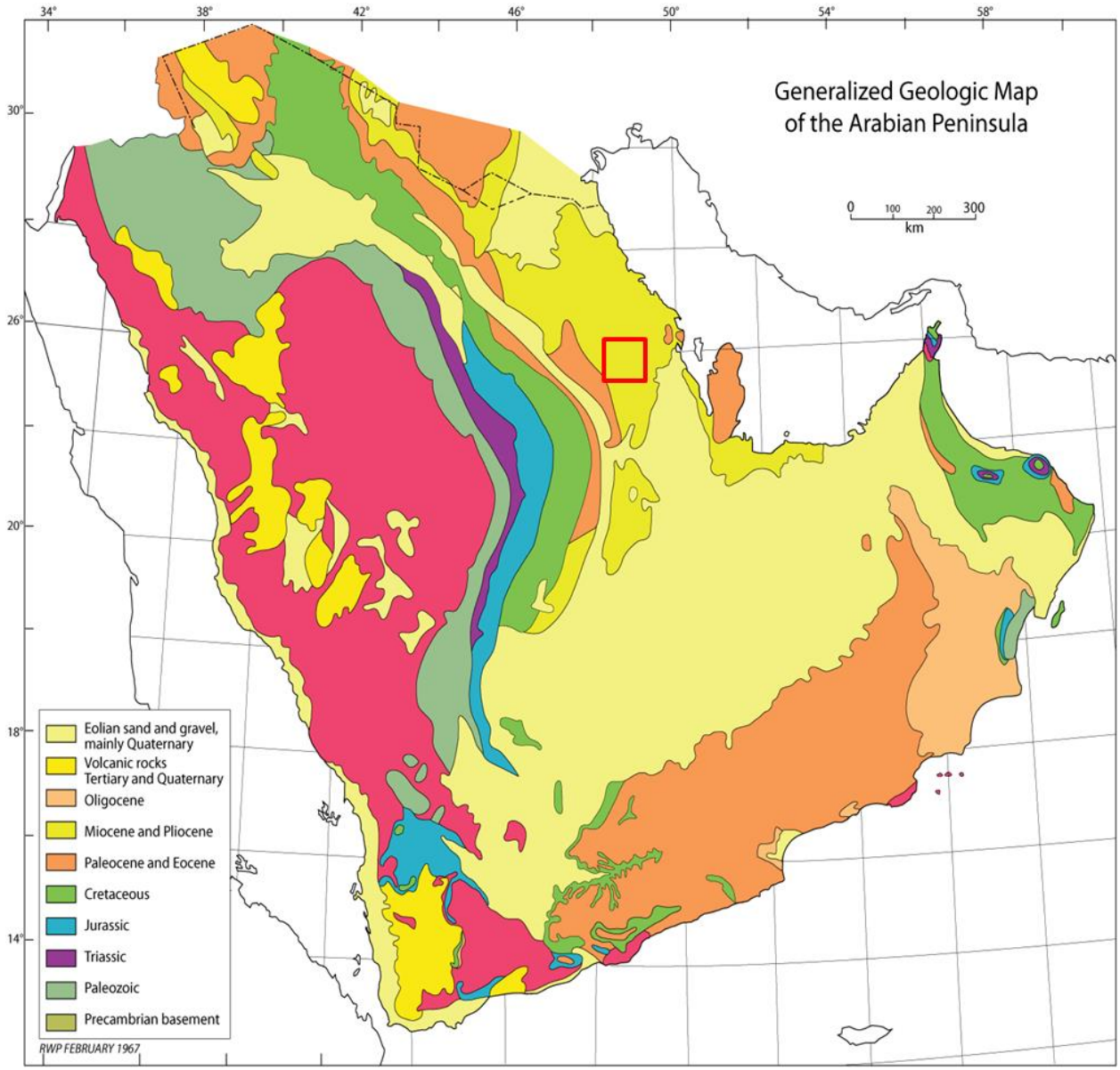

Figure 1.1: Generalized geologic map of the Arabian Peninsula, with the Miocene and Pliocene strata marked by dark yellow at the east with the red rectangle showing the location of the study area (after Powers, 1963).

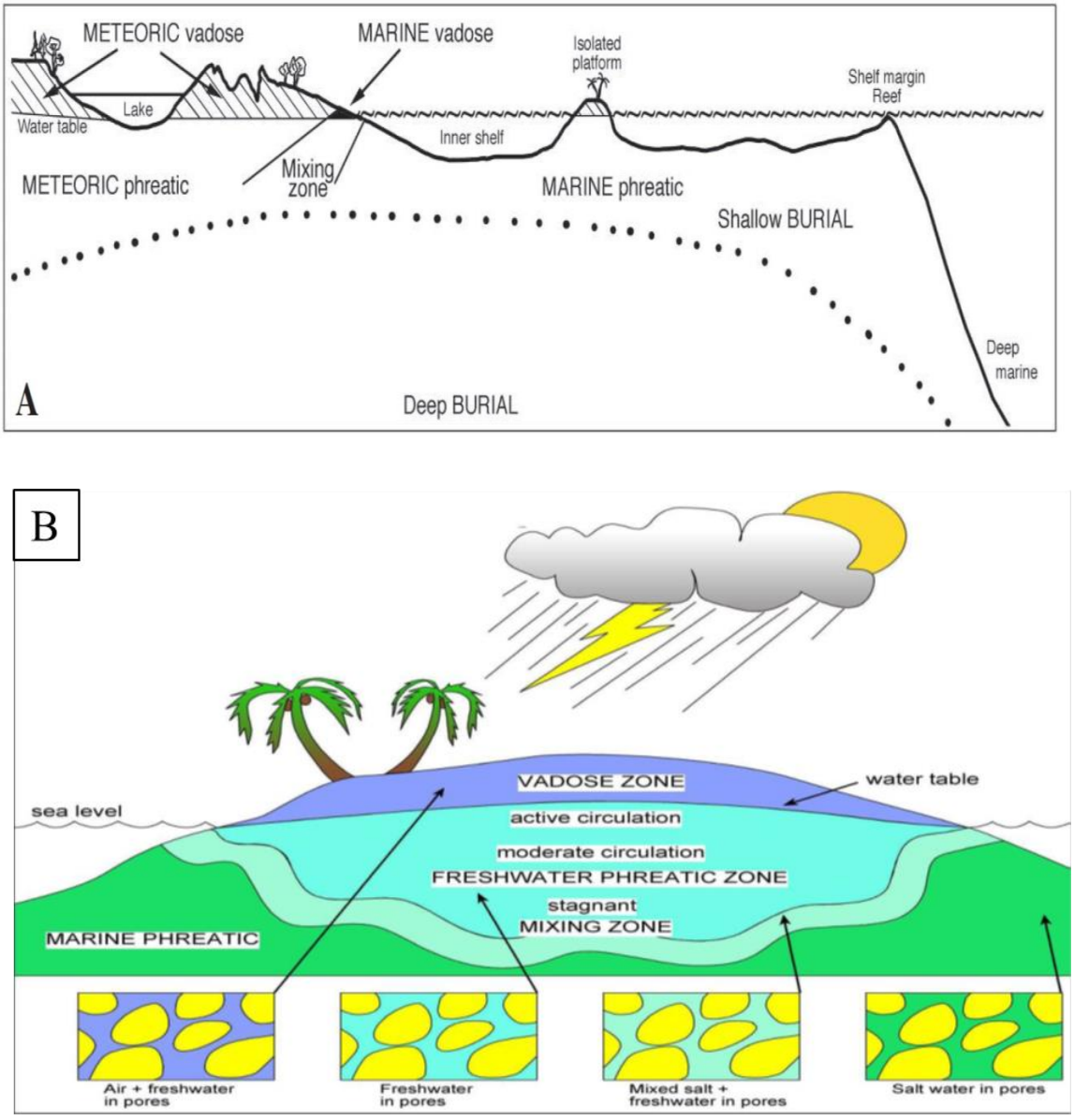

Figure 1.2: (A) Sketch diagram shows the different diagenetic environments (Flügel, 2010). (B) Diagenetic environments and the type of pore water within different diagenetic environments (Cui, 2012).

1.2 Objectives

Changes in relative sea level drive changes in pore fluid chemical composition that in turn control the early mineralogical stabilization and porosity evolution (Tucker, 1993; Morad et al. 2012). Therefore, putting carbonate diagenesis into a sequence stratigraphic framework facilitates a better understanding of the distribution of diagenetic patterns in a carbonate succession and permits a degree of predictability.

This study aims to investigate porosity and permeability evolution as a response to diagenetic processes and alterations of the Miocene Dam Formation carbonates that are cropping out in Al-Lidam area, Eastern Saudi Arabia, and as part of collaborative program between Geosciences Department (KFUPM), Center for Petroleum and Minerals (Research Institute/KFUPM), and Saudi Aramco. The study also tries to link the diagenetic processes to the sequence stratigraphic framework, which is established by another contemporaneous study (Bashri, 2015).

1.3 Study Area

The study area is located in the Eastern Province of Saudi Arabia, about 70 km to the west of Dammam city, north of Dammam-Ar Riyadh highway. It is located between 49° 28′ 30″ & 49° 31′ 30″ East and 26° 15′ 45″ & 26° 14′ 15″ North (Figure 1.3). Outcrops of the Miocene Dam Formation are exposed in the study area and have a general strike NNW-SSE (Figure 1.4). In association with Miocene outcrops, there are several sand dunes in the study area, which may reach up to 13 m height and 200 m width.

Figure 1.3: Satellite image showing the location of the Study Area.

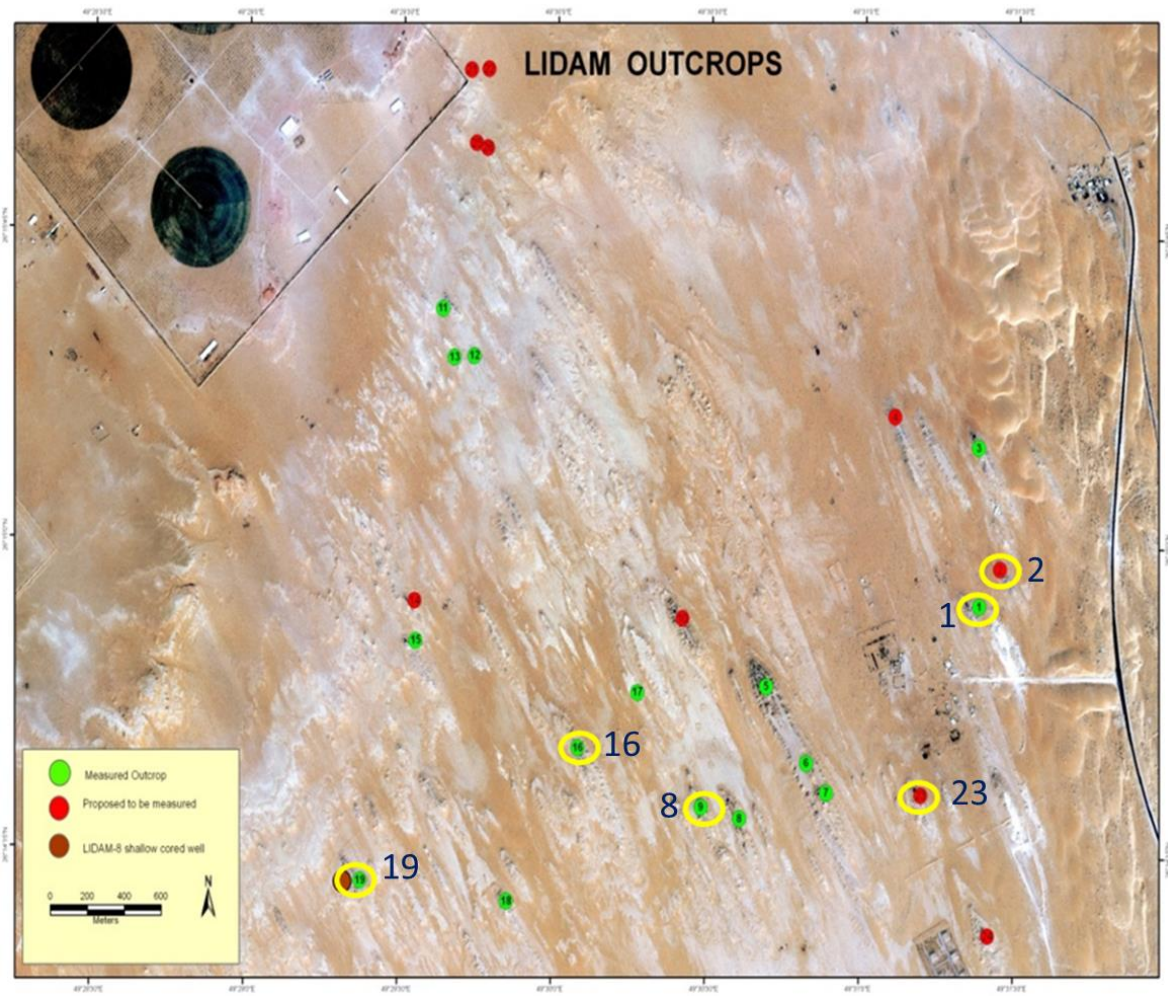

Figure 1.4: Satellite image showing the measured outcrops in the study area. The studied outcrops are shown by yellow circles.

1.4 Tectonic Regime Related to the Study Area

The present day Arabian Plate comprises all types of tectonic boundaries; extension and sea floor spreading along the Gulf of Aden and the Red Sea, collision along Bitlis Suture and Zagros, and transform movement along the Dead Sea. The Precambrian Arabian Shield bounds the asymmetric Arabian Plate basin to the west. The basin deepens gently eastward with the maximum depth reached at the front of the Zagros fore-deep zone (Konert et al., 2001).

The Precambrian Arabian Shield is formed by accretion of micro-continental terranes and island-arcs (Stoeser & Camp, 1985) overlain by post cratonic volcanics and sediments. The final Precambrian event was the Amar collision (640–620 Ma) that terminated the Arabian Plate fusion along the north- trending Amar suture (Al-husseini, 2000).

Stampfli and Borel, 2002 developed a plate tectonic model for the entire planet to describe the tectonic setting of the Paleozoic and Mesozoic , using the plates' buoyancy, plate boundaries locations, and the distribution & geochemistry of magmatic bodies and mid oceanic ridges (MOR) spreading rates. The proposed time of Neo Tethys rifting initiation, according to their results, is in the Late Carboniferous to Late Early Permian and is concurrent with separation of the Cimmerian plate from Pangea and the closure of the Paleo Tethys (Figure 1.5).

Muttoni et al., 2009 used paleo-magnetism and stratigraphy of Permian lateritic soil profiles in Iran and Pakistan to study the opening of the Neo Tethys; their results were similar to the Stampfli and Borel model. After the opening of the Neo Tethys, highly variable (spatially and temporally) paleo facies were deposited in the Arabian Plate basins.

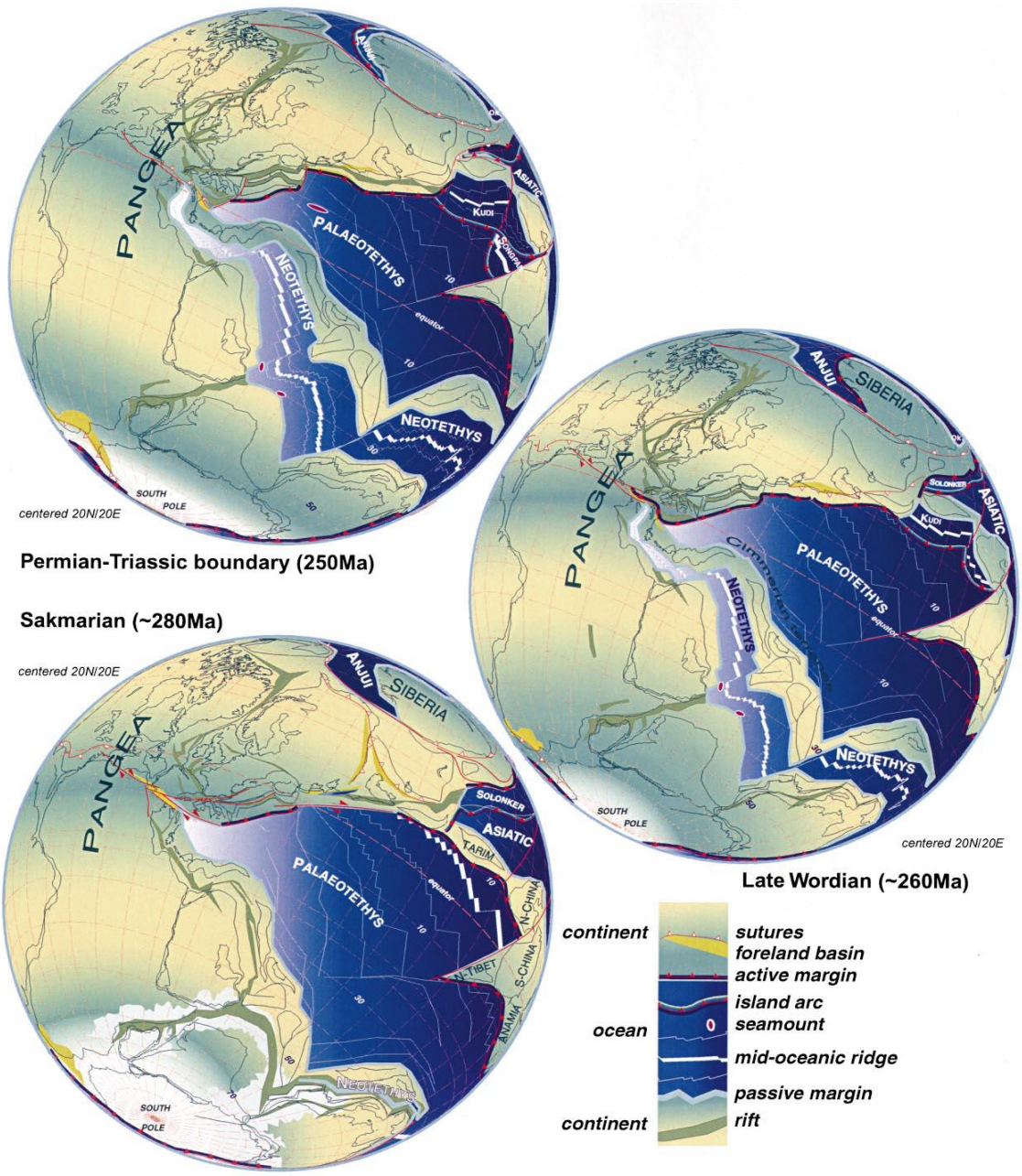

Figure 1.5: Orthographic projection explains the chronological stages of Neo Tethys creation and its relation to the Arabian Plate location (Stampfli and Borel, 2002).

During the Late Permian to Middle Triassic, a new passive margin developed with Neo-Tethys. Shallow-marine and arid evaporitic environments developed and a regional carbonate regime spread over the eastern Arabian Platform. This deposited the Late Permian Khuff Formation and its regional equivalents. During the Late Triassic to Early Jurassic, the southern part of the Plate and the southeastern edge of the Arabian Shield were uplifted and contributed massive floods of terrigenous clastics toward the northeast (Minjur and equivalent formations). In the late Middle Jurassic, a carbonate regime was dominant throughout the region, and even the western shelf of the Arabian Basin hosted reefal limestones and buildups (upper Dhruma Formation and the Tuwaiq Mountain limestone). During the Late Jurassic, in central Arabia, slow but progressive infill of the intrashelf basins took place through repetitive shoaling-upward carbonate cycles of Hanifa and Jubaila Formations. At the beginning of the Cretaceous, the Arabian Basin was rapidly infilled, first by carbonates and later by terrigenous clastics (Buwaib and Biyadh formations). Neo-Tethys became compressive and began to close during the Late Cretaceous, and shallow marine carbonates were deposited southward across Sinai into the depression that marked the proto-Red Sea rift (Ziegler, 2001).

During Miocene time, there was repeated interchange between the dominance of shallow marine carbonates & evaporites and siliciclastics in the foreland areas of the Arabian Plate, with dominance of the deep marine facies in the northern & eastern fore-deep parts of the Neo Tethys margin (Ziegler, 2001).

During the Miocene (Burdigalian) times, the Red Sea rifting took place and Arabia started to separate from Africa, and the Gulf of Aden also opened (Ziegler, 2001).

Through collision of Arabia with Eurasia, inversion in the Palmyrides and the Sinjar uplift occurred during Miocene times as well as minor transpression in the Euphrates Graben (Sawaf

et al., 1993). Collision with Asia occurred at the eastern flank of the Arabian Plate which was indicated by the thrusting of the Sanandaj-Sirjan zone onto the Plate. As a result, a huge amount of continental to deltaic clastic deposits and shallow-marine shales were deposited in the Zagros fore-deep areas. Post-Asmari Miocene to Recent sediments reached a thickness of over 5,000 m in the Dezful Embayment of the Zagros Basin (Koop et al., 1982).

Volcanic activity was widespread and prolonged in western Arabia beginning at about 12 Ma (Camp & Roobol, 1991) and represents a second phase of volcanic activity associated with the opening of the Red Sea. Historical eruptions (e.g. at Al Madinah in AD1256) show that volcanism is still in progress. Basaltic lava fields (harrats) extend intermittently from Yemen through western Saudi Arabia and Jordan, and as far north as southern Turkey. They have a total surface area of about 180,000 sq km and constitute one of the world's largest basalt provinces (Ziegler, 2001).

The north-trending Hercynian lineaments of the Central Arabian Arch extend far north into the Zagros foredeep. They separate on the western (Iraqi) side the massive wedge of the Lower Fars clastics and evaporites from the eastern Gachsaran salt marshes of the Khuzestan Province, (Agha Jari and Dam formations) and shallow-marine carbonates (Guri Formation) in the Fars Province. The hypersaline deposits relate to a relative fall in sea level at the end of the Oligocene (Ziegler, 2001). The marine connection, or 'Tethyan Seaway' of Goff et al. (1995), became obstructed along the narrow foreland basin so that basinal evaporites began to precipitate in the former foredeep. Around the Arabian Arch, a halo of mainly continental (Hadrukh Formation) to transitional-marine sediments (Dam Formation) were deposited (Figure 1.6). In the interior of the Arabian Plate, age-equivalent lacustrine sediments belong to the Hofuf Formation (Ziegler, 2001).

Due to uplift of the western part of the Arabian Shield, rapid erosion and denudation of the interior occurred and vast amounts of gravel become incorporated into the Hofuf Formation. The clastic components are primarily quartz and igneous and metamorphic rock fragments, but sedimentary rock fragments (particularly from the Jabal Tuwayq escarpment) also occur.

The Arabian Platform has three main structural elements. These are; (a) north-trending highs such as Qatar Arch and Ghawar Anticline; (b) northeast-trending structures such as Khleissia trend and (c) northwest-trending structures such as Ma'rib and Azraq grabens (Konert et al., 2001). The three main structural elements are shown in (Figure 1.7). The study area (al Lidam), which is the type locality of the Dam Formation, lies in the Arabian Basin which contains faults that follow the N-S trend. This basin contains the famous Ghawar Field which is the biggest oil field worldwide.

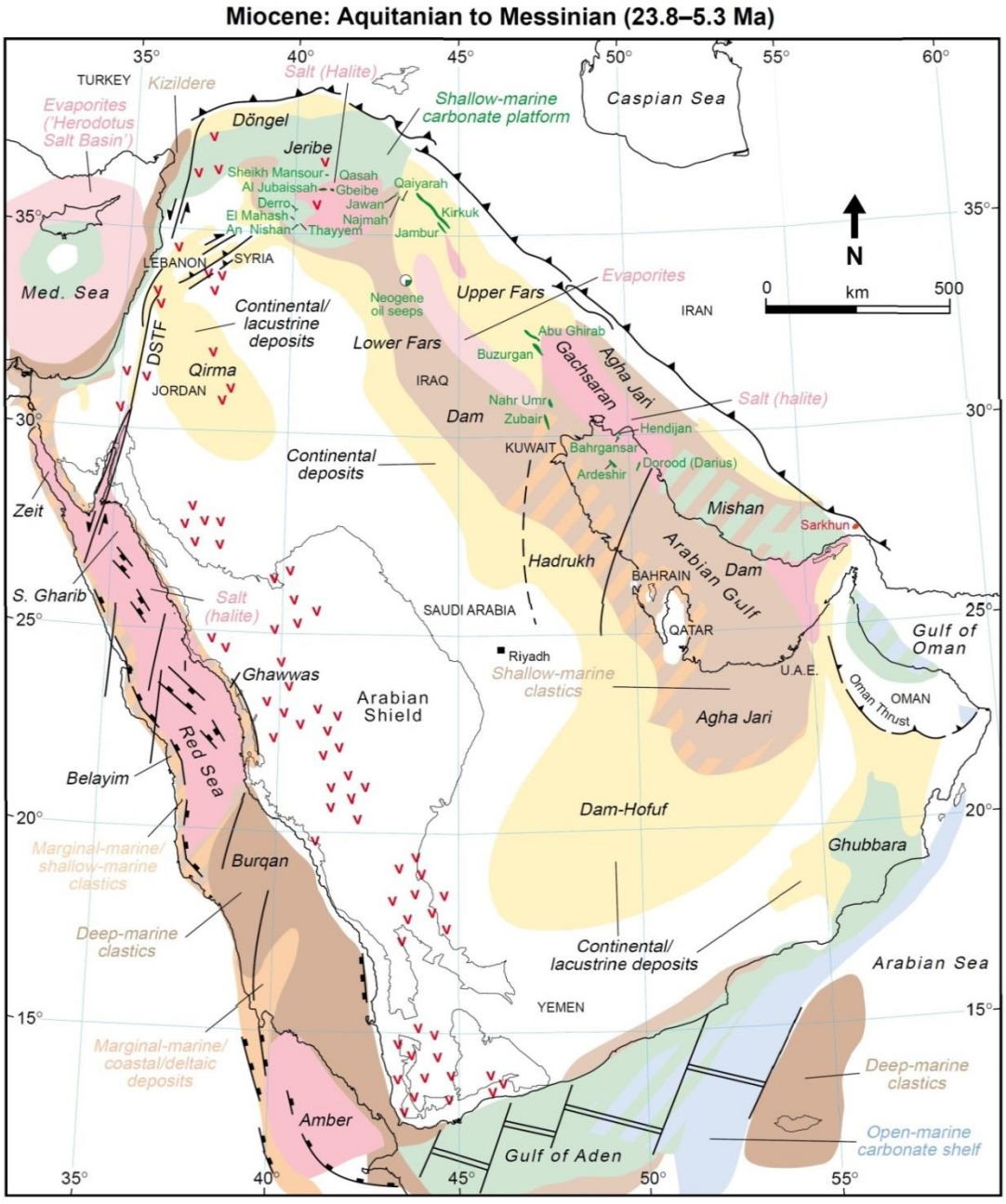

Figure 1.6: Paleofacies map of the Arabian Plate during the Miocene (Ziegler, 2001).

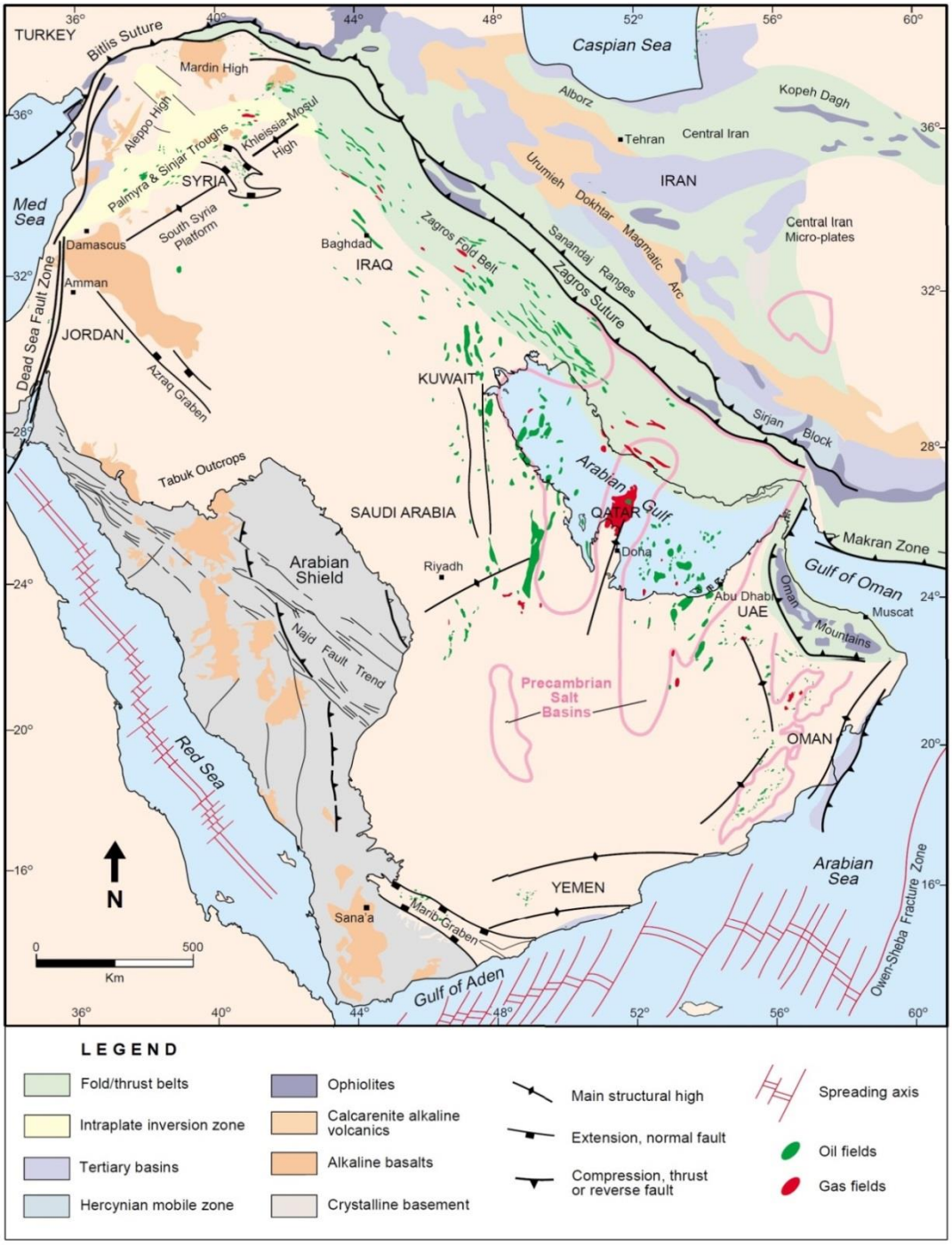

Figure 1.7: Location and major tectonic elements of the Arabian Plate (Konert et al., 2001).

CHAPTER 2

LITERATURE REVIEW

2.1 Previous studies Related to the Dam Formation

The name of the Dam Formation was first used by Max Steineke and T.W. Koch for a coastal Miocene succession (Powers et al, 1966). The name first appeared, in formal sense, in a paper by Thralls & Hasson, (1956).

The Miocene Dam Formation has been examined by several studies since the 1930's, especially in Qatar. Several of these studies are briefly described as follow;

Steineke et al. (1958**)** described the details of the Dam Formation at its type section in Jabal Al-Lidam (Lat 26° 21′ 42″ N. Long 49° 27′ 42″ E.) where the lower part of the formation crops out. They stated that the Dam Formation at its type locality is composed of about 90m of pink, white and gray marl and red, green and olive clay with minor sandstone interbedding (Figure 2.1). They described various marine fossils but the most important fossils, which were considered as marker fossils, are echinoids and specifically *Echinocyamus sp*. and *Archaias sp*. near the base of the formation.

Powers et al. (1966) described the Dam Formation at its type locality, and stated that the Dam Formation is underlain by sandstones of the Hadrukh Formation, and overlain by clay, sandstone and gravel of the Hofuf Formation.

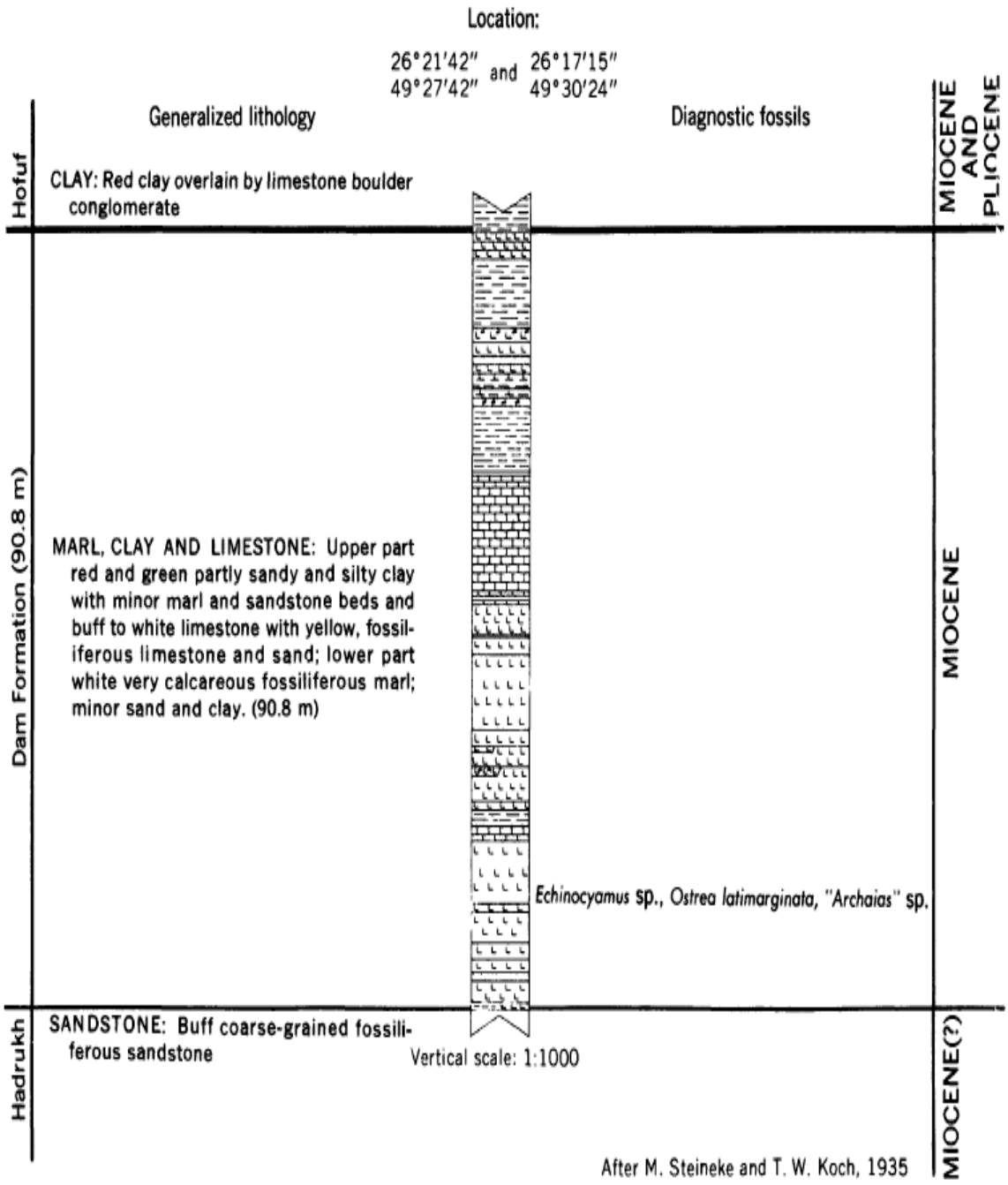

Figure 2.1: Dam Formation type section. (After M. Steineke and T. W. Koch, 1935).

Irtem (1986) studied the lower part of the Dam Formation in the Al-Lidam area. He could identify three upward deepening cycles. Theses cycles start by supra-tidal gypsiferous claystone, grading upward into inter-tidal sandstone and shallow sub-tidal thinly bedded oolitic grainstone at the top. He found closely spaced columnar stromatolites (2 to 5 cm in cross section and 3 to 20 cm in height) in association with the oolitic grainstone bed of the third cycle. Thus, he interpreted the stromatolites as being deposited in the same environment as the oolitic grainstone bed.

Weijermars (1999) studied the surface geology, lithostratigraphy and the rate of growth of Dammam Dome. He described the Miocene Dam Formation at three locations (Table 2.1): Jebel Um Ar Rus (where the Dam Formation unconformably overlies the Rus Formation), Jebel Midra Al Janubi (where Dam Formation unconformably overlies the Midra Member of Dammam Formation) and Jebel Midra Ash Shamali. At both Jebel Midra Ash Shamali and Jebel Midra Al Janubi, he described the Dam Formation as a series of a mixed clastic – carbonate sequences at the base that are overlain by stromatolitic beds. He reported the presence of various fossils including vertebrate bones and ungular teeth of *Perissodactyl* or *Artiodactyl*. At Jebel Umm Ar Rus, *Peneroplis farensis* has also been reported from the Dam Formation (Henson, 1950), and is used as an index fossil for basal Fars rocks of the Miocene in Iraq.

Al-saad and Ibrahim (2002) studied aspects of stratigraphy, micropaleontology and paleo-ecology of the Dam and found that its microfossils are predominantly benthic foraminifera and are represented by 38 species of which most are milioline and one is a larger form.

Table 2.1: Tertiary tectonostratigraphic time-table for the Dammam region (Weijermars, 1999).

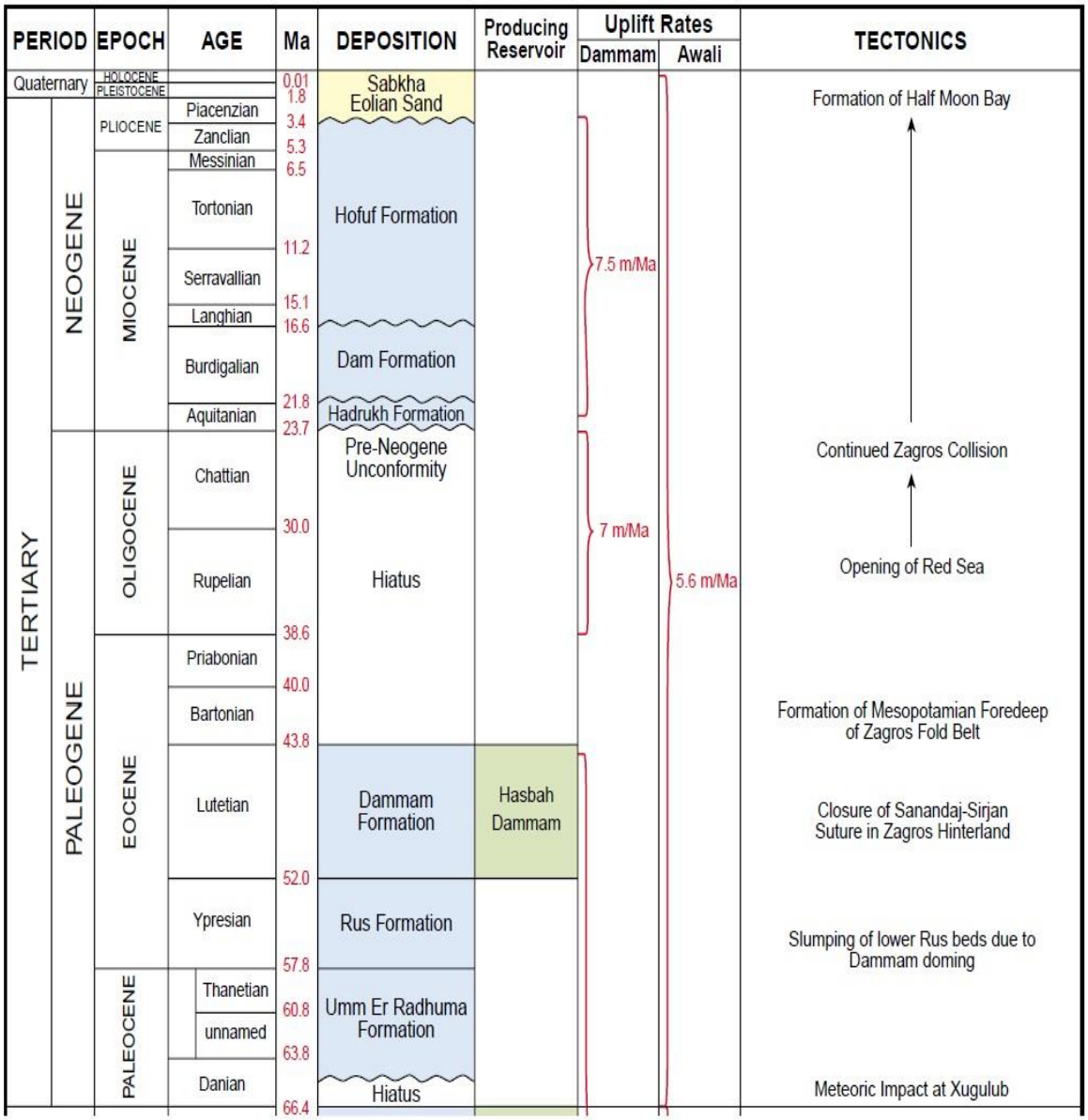

They also stratigraphically subdivided the Dam Formation in Qatar into two new formal members. The basal Al-Kharrara Member [or Salwa member as defined by Dill et al., 2005] is made up of limestone, marl, and claystone, while the overlying Al-Nakhash Member is a cyclic assemblage of carbonate, evaporite, and algal stromatolite facies. This study grouped the lithofacies into four major types of which limestone, subdivided into six sub-facies, is dominant. They concluded that Al-Kharrara member was deposited in warm (25°-30°C), clear, shallow waters of the inner neritic zone (0-35 m) that had an elevated salinity (35%-50%) and a vegetated substrate. They also concluded that the Al-Nakhash member was probably formed in an oscillating, very shallow-marine environment (0-10 meters deep, including tidal flats), under warm climatic conditions that eventually led to the accumulation of evaporites and algal stromatolites.

Dill et al. (2005) studied the Dam Formation at the Southern Dukhan Anticline, SW Qatar and they subdivided the Formation into seven members. Those are from bottom to top; Lower Salwa, Middle Salwa, Upper Salwa, Lower Al Nakahsh, Middle Al Nakhsh, Upper Al Naksh, and Abu Samrah Members. They noticed 54 different types of fossils within the seven members of Dam Formation, but they were dominated by bivalves, gastropods and foraminifera. Based on mineralogy, paleontology, chemical and isotope analysis, they interpreted the depositional environments of the Dam Formation. The Salwa members are composed of interbedded siliciclastics and calcareous sediments, which were interpreted as being deposited in meso- to micro-tidal environments. These environments grade up into macro-tidal conditions which resulted in the deposition of the Al Nakhsh members, and then to wave-dominated micro-tidal conditions which resulted in the deposition of Abu Samrah

Member. They mentioned that the stromatolites were found only in Al Nakhsh Members, and the maximum growth of the stromatolites was found in the Middle Al Nakhsh Member.

Al-Enizi (2006) compared the Dam Formation foraminifera from Jebel Midra Al-Janubi with present day foaminifera from the Arabian Gulf. He identified 51 species from the Dam Formation (including *Borelis melo melo,* confirming a Middle Miocene age), and 47 species from the Gulf samples. He found that the foraminiferal diversity tended to increase with water depth and decrease with salinity. His study indicated that the Dam Formation foraminifera commenced deposition under adverse, hypersaline conditions during a slight marine transgression in the Middle Miocene. Succeeding normal salinity and small-scale marine transgressions led to an increase in foraminiferal diversity, with subsequent formation of foraminiferal grainstones, packstone and wackestones.

Alkhaldi (2009) developed a high resolution sequence stratigraphic framework for the Dam Formation in the Al-Lidam Area. He described it as a mixed carbonate–siliciclastic succession that was deposited during Middle Miocene within a closed embayment. He divided the Dam Formation in the studied outcrop into three composite sequences; he subdivided composite sequence 1 and 2 into high frequency sequences. He interpreted the lower part of each composite sequence to be comprised of TST, followed by a HST comprised of bio-clastic grainstone dominated channels. On the other hand, he interpreted the upper part of the two composite sequences as composed of TST, followed by a HST comprised of prograding banks and bio-clastic channels.

2.2 Literature Review Related to Carbonate Diagenesis

Carbonate diagenesis has been a major topic of research for several decades, starting with the fundamental observations made by Sorby in the mid-19th century. In the next pages, some studies about carbonate diagenesis are briefly shown.

Longmann (1980) studied carbonate diagenesis textures from near surface environments. He has shown that most of the cementation and secondary porosity development in carbonate rocks occurs at relatively shallow depths in one of four major diagenetic environments; the vadose zone, meteoric phreatic zone, mixing zone, and marine phreatic zone. He also mentioned that the climate, changes in relative sea level, rate of subsidence and deposition and mineralogical composition of the sediments, are the major controls on porosity modification in carbonate rocks and sediments.

Tucker (1993) has shown that the carbonate diagenesis can be integrated with the relative sea – level and climate, leading to linking between carbonate diagenesis and the sequence stratigraphy. Depending on the climate and pore filling fluids, he suggested that each system tract will be subjected to specific diagenetic processes. He also mentioned that the different dolomitization models can be tied in a sequence stratigraphic framework.

Morad et al. (2012) linked the diagenesis and sequence stratigraphy of both siliciclastic and carbonate reservoirs. They used this integration as a powerful predictive tool in reservoir quality models. Their study proved that many diagenetic processes such as cementation, dissolution, clay minerals precipitation, intergranular porosity evolution, and even the mechanical diagenetic

processes are highly controlled and related to the sequence stratigraphic surfaces. They also stated that the climatic conditions dominating during subaerial exposure have a great influence on the type and extent of the diagenetic processs.

CHAPTER 3

METHODOLOGY

3.1 Introduction

The methods used in this study consist of extensive field work and measurement and description of six sections, measurements of both porosity and permeability from core plugs, thin section preparation and description, X- Ray Diffraction (XRD) analysis of representative samples to identify the mineralogical components of the rock samples, X-Ray Fluorescence (XRF) analysis to recognize the elemental components and percentage in each sample. Scanning Electron Microscopy (SEM) imaging was also carried out on representative samples to clarify small scale diagenetic features and micro-porosity which can't be seen under polarizing microscopy. Cathodoluminescence microscopy was also used to understand the fundamental diagenetic relationships between grains, matrix, cements, porosity evolution, and common replacement reactions that occur in the examined samples.

3.2 Field Work

The field investigation targeting the Burdigalian Dam Formation was carried out in the Al-Lidam area, Eastern Saudi Arabia. Detailed description of six outcrop sections was conducted, and one hundred eight samples were collected during the field investigations. The field descriptions identified and described the sedimentary facies and structures and their lateral and vertical continuity. Diagenetic features that appear at outcrop scale were also described.

Outcrop high resolution photos were taken for documentation of lithofacies and sedimentary structures. A photomosaic was constructed so as to provide an overview of the study area and was integrated with high resolution proximal photos to show details of the lithofacies, sedimentary structures and diagenetic features. The interpreted stratigraphic and depositional sections of each outcrop based on measured sections and high resolution proximal photos were integrated with the distal outcrop photo using CS6 Software.

Samples were collected from each outcrop on a bed by bed basis, to make a correlation between sedimentary units at different studied outcrops and to recognize the lateral change of lithofacies as well as diagenetic features across the studied traverse.

3.3 Laboratory Work

3.3.1 Porosity and Permeability Measurements

Collected samples were examined slabbed, and photographed to show the texture and structures of the different facies at various scales. Core plugs were drilled and prepared from each sample for porosity and permeability measurements.

Plugs taken were 1 inch (2.5 cm) in diameter and approximately 0.25 - 3 inch (0.0635 - 7.62 cm) in length. Porosity measurements were made for each core plug using Core Test TPI – 219 Helium Porosimeter, while permeability measurements were made using Hassler Core holder assembly permeameter.

3.3.2 Thin-Section Petrography

Thin sections were prepared from all samples using the standard thin section preparation technique. Samples are initially vacuum-impregnated with blue-dyed epoxy resin to assist in

the identification of porosity. Alizarin Red S stain was applied so as to differentiate calcite from dolomite. Detailed thin section petrography was carried out to identify the texture, mineralogy, grain types, bioclasts content, cement types, granulometry, and pore-type distribution and all diagenetic features that can be observed under optical microscopy.

3.3.3 Scanning Electron Microscope (SEM)

Eighteen samples were selected for scanning electron microscopy (SEM) to identify micro-porosity, grain shape, cement, and matrix. SEM was performed in the fresh broken surface of selected samples. Samples were gold coated so as to avoid sample charging (Goldstein and Yakowitz, 1975). SEM is an essential aspect in this study to address the micro-scale heterogeneity within the lithofacies and to identify the small scale digenetic features that cannot be observed under optical microscopy.

3.3.4 Powder X-ray Diffraction (XRD)

Powder X-ray diffraction was performed on twenty five samples to identify the mineral composition for each lithofacies and the percentage of each mineral. Selected samples were crushed and powdered. Each of the powdered samples was placed in a sample holder with a 20 μm square capacity. The scan range was fixed from 10 to 90 degrees to identify a wide range of minerals. The Standard Measurement software (Rigaku package) is synchronized with the personal computer (PC). The data were processed using PDXL2 integrated X-ray powder diffraction software to match the peaks with the minerals in the database of the ICDD PDF software.

3.3.5 Powder X-ray Fluorescence (XRF)

Seventy eight samples were ground and prepared for XRF analysis. Five to eight grams were taken to measure the chemical composition and to identify the major elements ratios in each sample. JEOL JSX-1000S ElementEye™ X-ray spectrometer with a 4 kW generator was utilized for this analysis.

3.3.6 Cathodoluminescence

Eight samples were examined under cathodoluminescence microscopy at Saudi Aramco, to distinguish different mineral species and to estimate their abundance; to interpret different mineral paragenetic sequences and different mineral generations (characterized by different crystallization conditions so by different trace elements resulting in different luminescence); ·to detect zoning in minerals because CL contrasts may be generated in some favorable cases by chemical contrasts of only a few ppm in activator elements such as Mn^{2+}, REE, Fe^{3+}, Ti^{4+}, etc.

The CL microscopy used for this study is CITL Cold Cathodoluminescence 8200 mk3 unit operated at (10 to 14 kv and 180 to 240 μa beam current) attached to Nikon microscope with Leica camera.

3.4 Office Work

Software packages were used in this study including Easy Core for drawing the stratigraphic sections, Adobe Photoshop CS6 for constructing the photomosaic and Adobe Illustrator for drawing the depositional model.

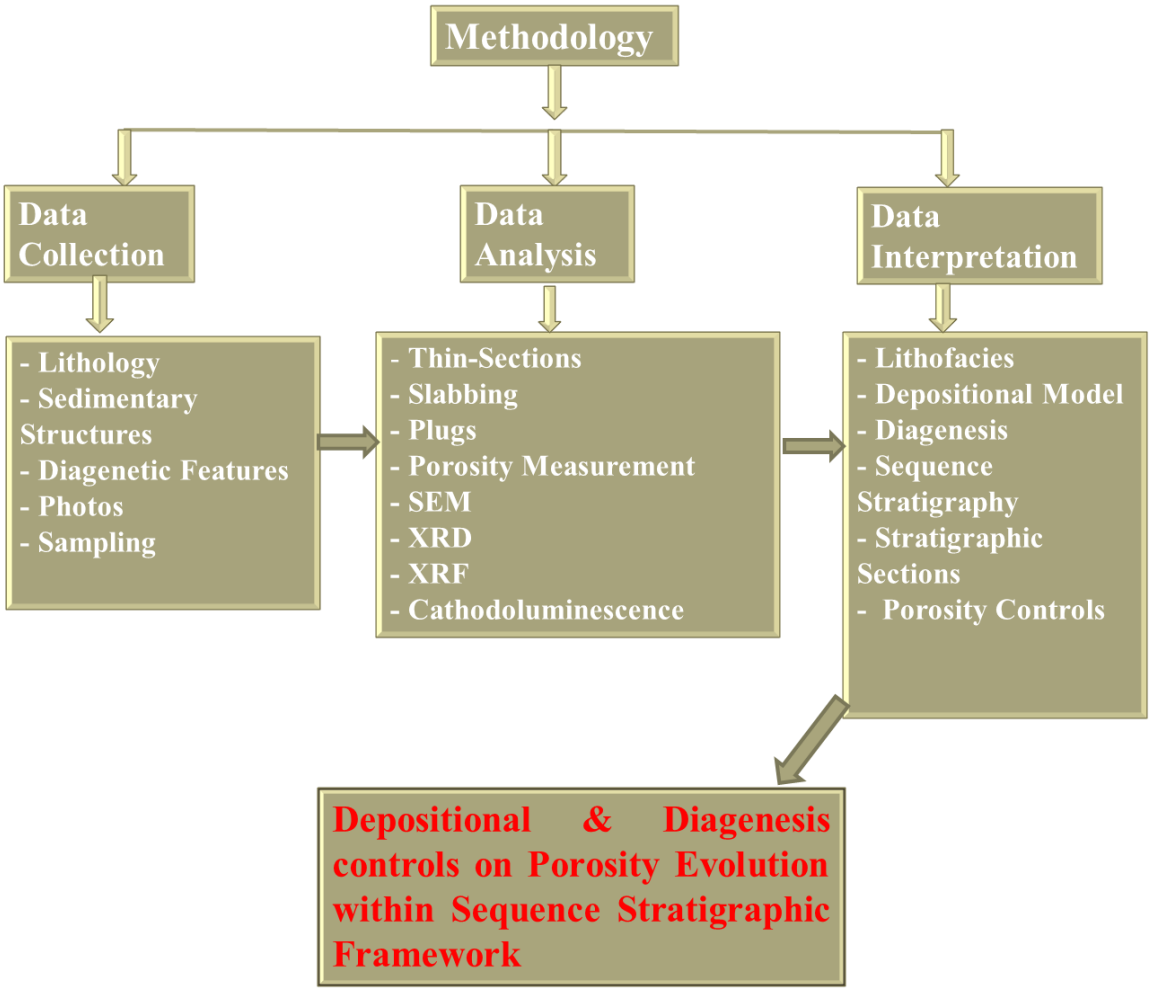

Figure 3.1: Methodology chart of this study

CHAPTER 4

SEDIMENTOLOGY AND LITHOFACIES

4.1 Dunham Classification

The Dunham classification system for carbonate sediments and rocks was devised by Robert J. Dunham in 1962, and refined by Embry and Klovan in 1971 (Figure 4.1) to include sediments that were organically bound during deposition. Dunham's scheme focuses on the depositional fabric of carbonate rocks, and divides them into four main groups based on relative proportions of mud-supported vs. grain- supported particles. His efforts deal with the question of whether or not the grains were originally in mutual contact; and therefore self-supporting, or whether the rock is characterized by the presence of frame builders and organic binders.

4.2 Depositional Lithofacies

Using Dunham's classification, the Dam Formation in the study area was described in term of texture, color, bioturbation, lithology, sedimentary structures, and bio-component. The described lithofacies are as follow:

4.2.1 Channelized Medium Sandstone Facies (f 1):

Description: greenish grey, medium grained, medium to well sorted, extensively bioturbated sandstone with a sharp base that cuts through the underlying lithofacies (f 4). The channel ranges in thickness from 0.3 – 2.0 meters, with a 9.0 meter width.

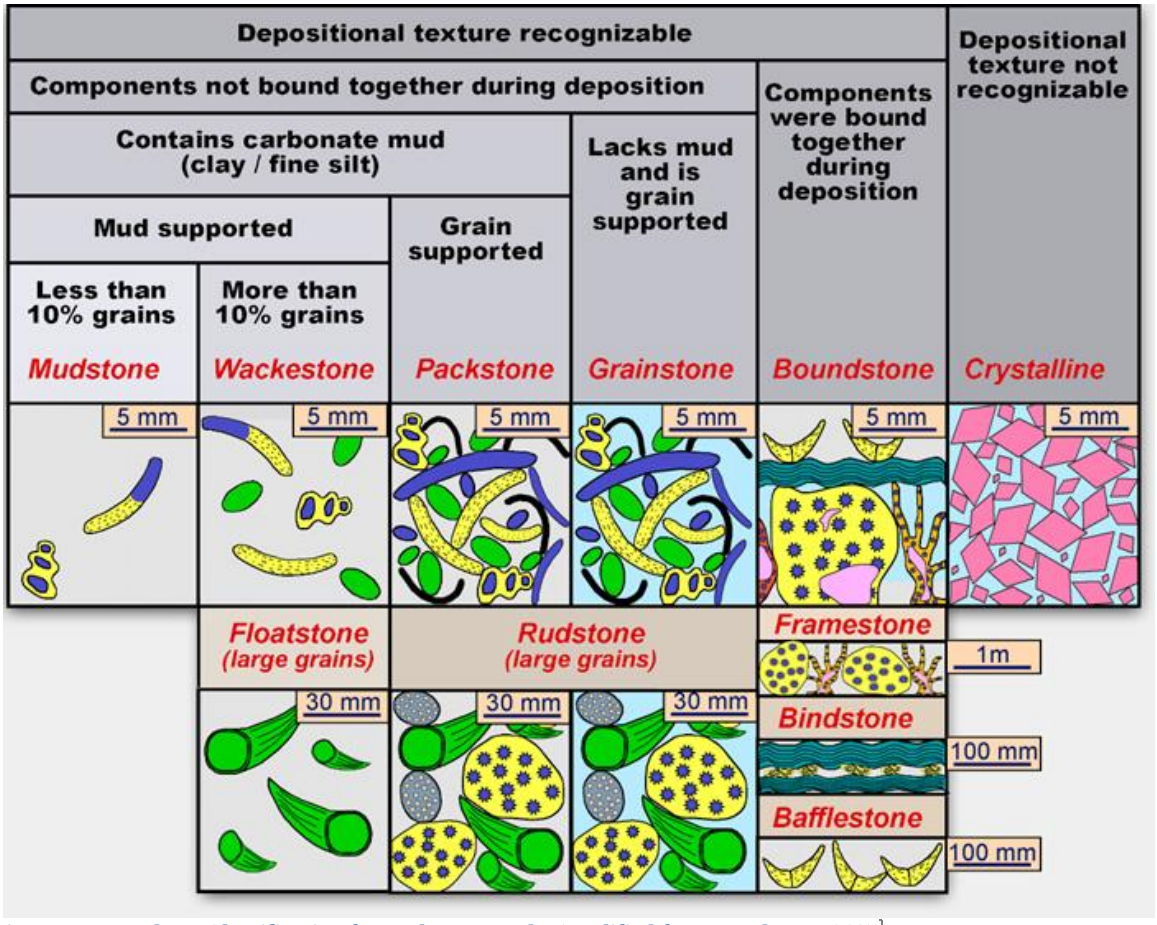

Figure 4.1: Dunham Classification for carbonate rocks (modified from Dunham, 1962).

Bioturbation has partially obscured the sedimentary structures such as bidirectional cross-bedding. This lithofacies appears only in outcrop No 23 (Figure 4.2A & 4.2B) (see the map in Figure 1.4).

Interpretation: the sharp boundary at the base of this lithofacies with the channel shape shows that it was deposited under subaqueous flow condition with high energy that led to cut through the underlying facies. The bidirectional current indicates tidal influence during deposition of this lithofacies. Thus, this lithofacies is interpreted as estuarine fill deposits (Lasemi et al., 2012)**.**

4.2.2 Interbedded Mudstone and Evaporites Facies (f 2):

Description: Reddish to greenish mudstone interbedded with beige to white color evaporite beds (Figure 4.3A). It was found in outcrop 2, 23, and 8 (see the map in Figure 1.4) with a thickness ranging from 0.5 m to 1.2 m. The mud shows some mud cracks while the evaporite beds are partially dissolved, which has led to deformation of the overlying beds and formation of nodules of chicken wire anhydrite (Figure 4.3B). Stratigraphically, in the western part of the study area (outcrop 23 and 8, see the map in Figure 1.4) this facies overlies the cross bedded grainstones (f 11 & f 15) that are pervasively dolomitized as shown by XRD analysis (Figure 4.3C) and underlies sandstone-mudstone facies (f 4) while in the eastern part (outcrop 2 and 1, see the map in Figure 1.4) the overlying siliciclastic facies are absent.

Figure 4.2: (A) outcrop photograph of estuarine fill facies (f 1) cut through underlying facies (f 4). (B) Intense bioturbation within estuarine fill facies.

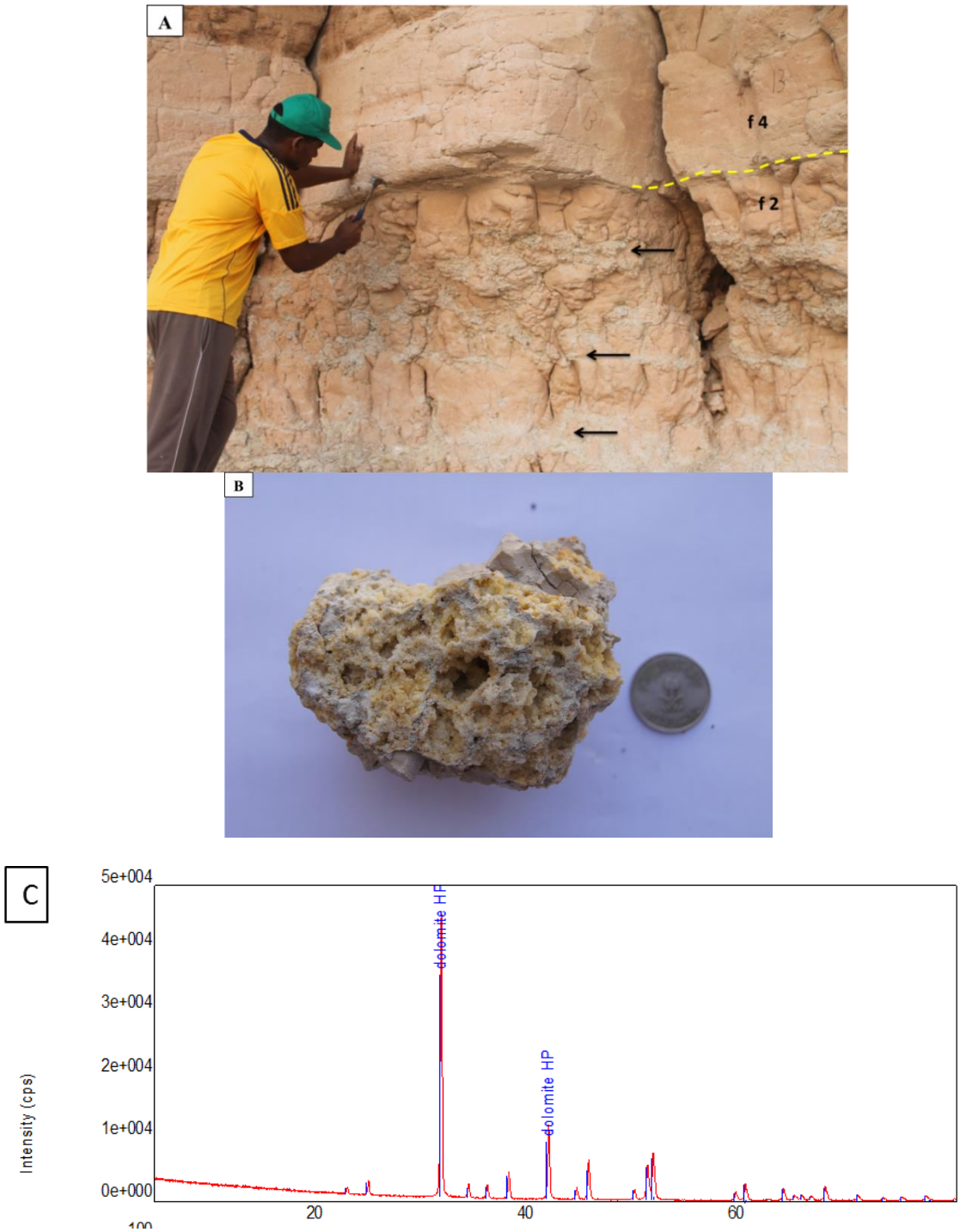

Figure 4.3: (A) outcrop photograph of Interbedded mudstone and evaporite facies (f 2). (B) Hand specimen showing the dissolution of anhydrite and formation of chicken wire anhydrite. (C) XRD diffractogram shows pervasively dolomitized grainstone facies (f 11) that underlies (f 2).

Interpretation: the fine grain size of the mudstone indicates deposition in a low energy environment. The mud cracks and the red color indicate influence of oxidizing subaerial exposure. The association with evaporites indicates deposition from hypersaline water under arid climate condition. The deposition of evaporites from sea water led to the incorporation of calcium ions into the evaporite minerals, and consequently an increase in the Mg: Ca ratio of the interstitial fluids (Tucker and Wright, 1990). Those Mg – rich fluids served to dolomitize the underlying beds. From previously mentioned features, this facies was interpreted as sabkha deposits.

4.2.3 Stromatolites (f 3):

Description: Stromatolites are layered bio-chemical accretionary structures formed in shallow water by the trapping, binding and cementation of sedimentary grains by microbial mats of micro-organisms, especially cyanobacteria (Riding, 1999). This facies is abundant in all outcrops, and it was found at different stratigraphic levels with a thickness ranging from 5 cm up to 50 cm.

Several morphologies of stromatolites were found in the study area including; columnar, conical, branching, stratiform, and domal, stromatolites (Figure 4.4A, 4.4B). Tepee structures and mud cracks were found in association with some stromatolite morphologies, especially the conical stromatolites.

Interpretation: The presence of stratiform laminites indicates deposition under low energy environments while the domal stromatolites indicate a relatively higher energy (Boggs, 2006).

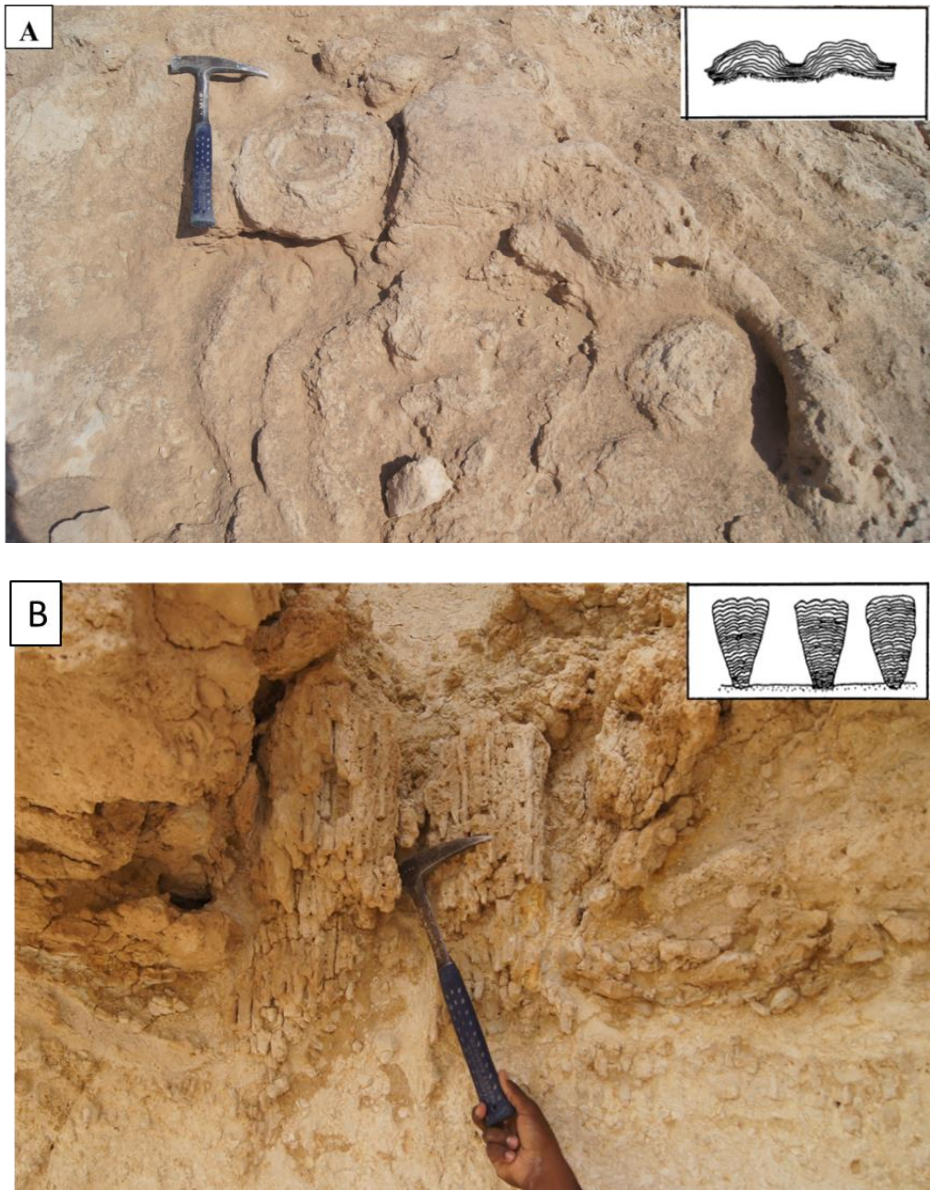

Figure 4.4: (A) Outcrop photograph of domal stromatolites at outcrop 1. (B) Columnar stromatolite at outcrop 16.

The presence of conical and domal stromatolite indicates a deposition in relatively deeper water with greater accommodation space than did the stratiform types (Swart et al., 2009). The association of stromatolites with mud cracks and tepee structures indicate subaerial exposure. This facies were interpreted as it was deposited in the shallow intertidal to supratidal environments.

4.2.4 Interbedded Cross-bedded Sandstone and Mudstone Facies (f 4):

Description: reddish to greyish, slightly cracked mudstone beds interbedded with light grey to yellowish, fine grained, bioturbated, wavy bedded calcareous sandstone beds (Figure 4.5A and 4.5B). This facies has a highly variable thickness, ranging from less than 1 m to about 3.4 m. This facies was found in the western part of the study area (outcrops 23, 8 and 16), but was not seen in the eastern part (outcrops 1 and 2) (see the map in Figure 1.4). It has been cut by estuarine fill sandstone (f 1) in outcrop 23 and it overlies the mudstone-evaporite facies (f 2) in outcrop 23 and 8. It is capped by stromatolite facies (f 3) in outcrops 8 and 16.

Interpretation: the alternation between mud and sand indicates that there were fluctuations in energy during deposition, with mud being deposited during periods of low energy conditions as inferred by fine grain size, and sand being deposited during periods of relatively higher energy processes as inferred by wavy bedding and coarser grain size. The desiccation cracks within mud indicate subaerial exposure, while the wavy bedding in the sandstones indicates shallow water conditions. According to these evidences, this facies was interpreted as it was deposited in shallow intertidal environment (Lasemi et al., 2012).

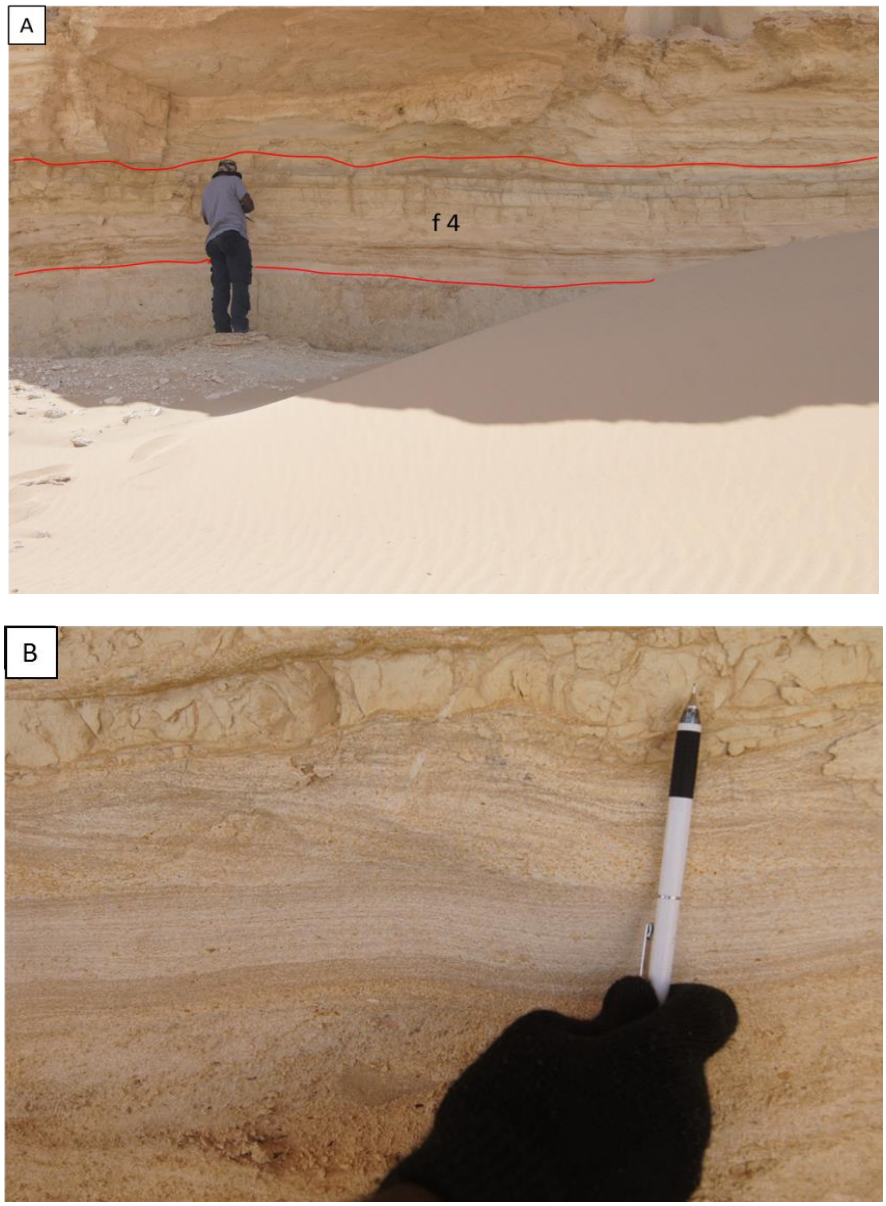

Figure 4.5: (A) Outcrop photograph of interbedding between mudstone and sandstone (f 4) at outcrop 8. (B) Desiccation cracks of mudstone and wavy bedding of sandstone.

4.2.5 Interbedded Cross-bedded Coarse Limestone and Mudstone Facies (f 5):

Description: yellowish to greyish, trough cross bedded packestone- grainstone interbedded with thin layers of fine massive mudstone beds. This facies is only found in the eastern part of the study area (outcrops 1 & 2) (see the map in Figure 1.4) with a maximum thickness of 0.6 m at outcrop 2. This facies is underlying the stromatolite facies (f 3) in the upper part of section 2 with tepee structures (Figure 4.6A). In the middle of section 1, it's capped by planar cross–bedded skeletal oolitic grainstone (Figure 4.6B). The fine mudstone is mainly massive with some desiccation cracks. Otherwise, the coarse limestone is highly variable, with planar cross-bedded skeletal packstone and fine – grained oolitic grainstone that contain quartz grains and rain drop impressions at its top surface.

Interpretation*:* The same depositional conditions of previous facies (f 4) are represented here but with only minor siliciclastic sediments present. This rhythmic lithofacies was most probably deposited in an intertidal zone. The skeletal oolitic and oolitic packstone and grainstone, respectively, were deposited during the high energy periods of either tide or ebb currents whereas the fine muddy member was deposited in the current slack period. The V-shaped tepee structure denotes the peritidal depositional system and exposure (Kendall & Warren, 1987). The mud cracks and rain drop impressions indicate an intermittent subaerial exposure, while quartz grains existence reflects proximity to clastic shoreline.

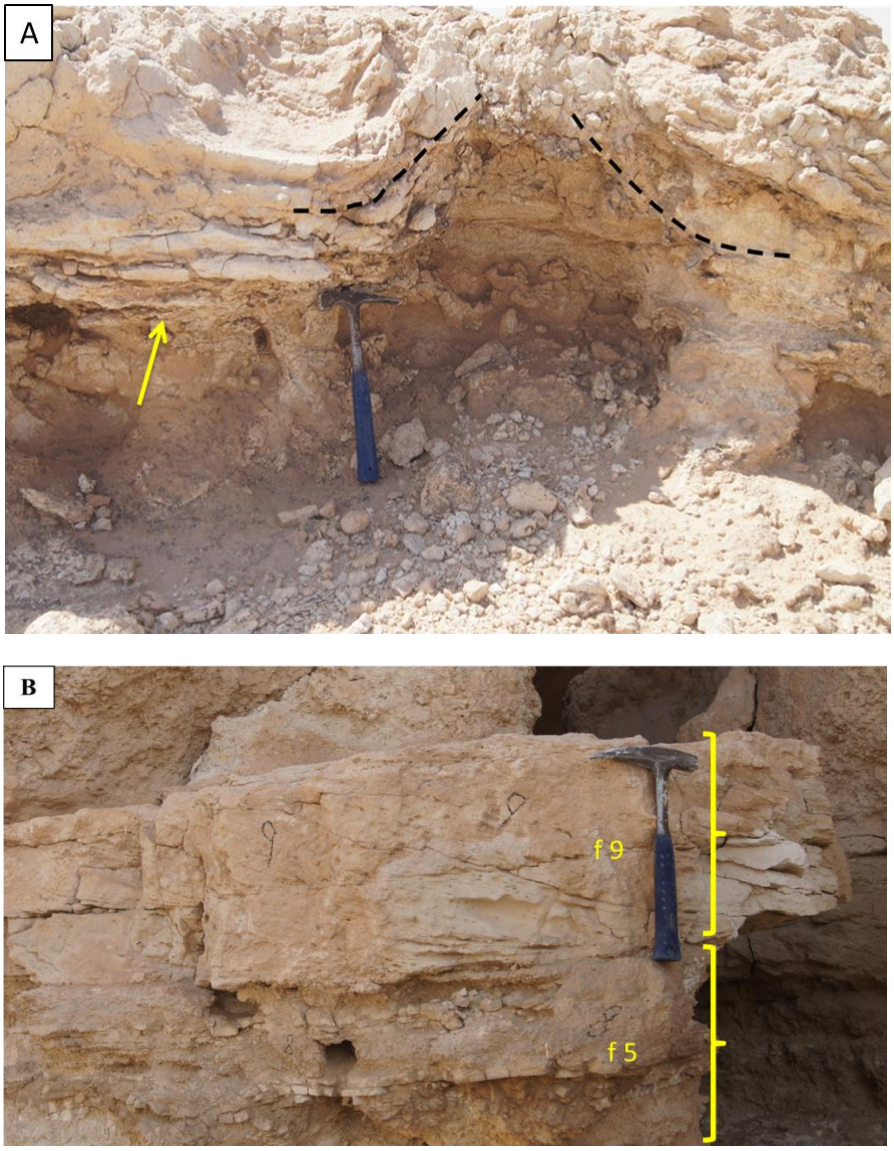

Figure 4.6: (A) Outcrop photograph of interbedded coarse Limestone – Mudstone interbedding facies (f 5) with tepee structure. (B) Skeletal oolitic grainstone (f 9) overlies (f 5).

4.2.6 Intra–formational Limestone Conglomerate (f 6):

Description: light grey to yellowish, 10 cm to 125 cm thick, consists of muddy pebbles (from f2) as well as skeletal oolitic grainstone pebbles (from f 9). The roundness of the pebbles ranges from well-rounded to sub rounded to angular (Figure 4.7A and 4.7B), and generally show a fining upward trend. This facies was found in all outcrops of the study area at different stratigraphic levels with distinctive erosional surface at the base.

Interpretation: the erosional surface at the base of this facies, and the intra-formational pebbles and their finning upward trend, indicates erosional process by storm event followed by re-deposition (tempestites) (Lasemi et al., 2012). This facies was found at different stratigraphic levels with different internal features that were interpreted as deposited within different depositional setting. In section 23, carbonate tempestites are interlayered with interbedded sandstone and mudstone rhythmites (f 4), which was mainly deposited in intertidal zone. Then, it is overlain by combination type of stromatolites and cut by estuarine channels. According to its stratigraphic location and its light brown muddy intraclasts that are similar to the underlying muddy layers, tempestites in section 23 are interpreted as supratidal to intertidal (Friedman, 1993). On the other hand, in section 8, tempestites are overlained by trough cross bedded oolitic grainstone which contains spherical type of stromatolite (f 11) and would be interpreted to be deposited most probably in the upper shore face zone. Consequently, tempestites were interpreted as been deposited within the lower shoreface (Friedman, 1993).

4.2.7 Trough Cross – Bedded Sandstone (f 7):

Description: greenish to yellowish grey, trough cross- bedded fine grained sandstone with erosive base (Figure 4.8A). This facies is only found in outcrops 16 and 19 (see the map in

Figure 1.4), with thicknesses ranging from 0.4 m up to 2.8 m. This facies shows some bioturbation features such as *Skolithos* and *Ophiomrpha* trace fossils (Figure 4.8B), as well as some calcite geodes.

Interpretation: The trough cross bedding structure indicates deposition under high energy conditions. Alternating between greenish and yellowish beds indicates oscillation between oxidizing and reducing conditions. *Ophiomorpha*, in addition to the previously mentioned features, indicates deposition in an upper shore face environment (Pemberton et al., 2012).

4.2.8 Herringbone Cross-Bedded Skeletal Oolitic Grainstone (f 8):

Description: yellowish grey to light grey, 0.1 to 0.6 m thick, bidirectional (herringbone) cross-bedded with mud drapes, reactivation surfaces (Figure 4.9 A, B and D) and keystone vugs (Figure 4.9 E), coarse grained skeletal oolitic grainstone. This facies observed throughout the entire study area. In some locations it shows planar cross bedding sets with reactivation surfaces between them. In the eastern part of the study area, this facies is associated with the interbedded cross-bedded coarse limestone and mudstone facies (f5). In thin-section ooids are the dominant components, although quartz grains, pelloids and aggregates also occur (Figure 4.9 C)

Interpretation: the observed associated physical sedimentary structures of this facies suggest that it formed within a tidal setting. The mud drapes on the cross bedding surfaces, the reactivation surfaces and the clear herringbone cross bedding are all diagnostic tidal deposit features (Eriksson and Simpson, 2004). Keystone vugs indicates periodic exposure and drying out of sediments. Previous observations in addition to the associated facies, suggest deposition in shallow water conditions, guided by flood and ebb tide currents in the intertidal zone.

Figure 4.7: (A) Intra–formational Limestone Conglomerate (yellow arrow) (f 6) with skeletal oolitic grainstone pebble. (B) Intra–formational Limestone Conglomerate (yellow arrow) (f 6) showing finning upward trend of mud pebbles.

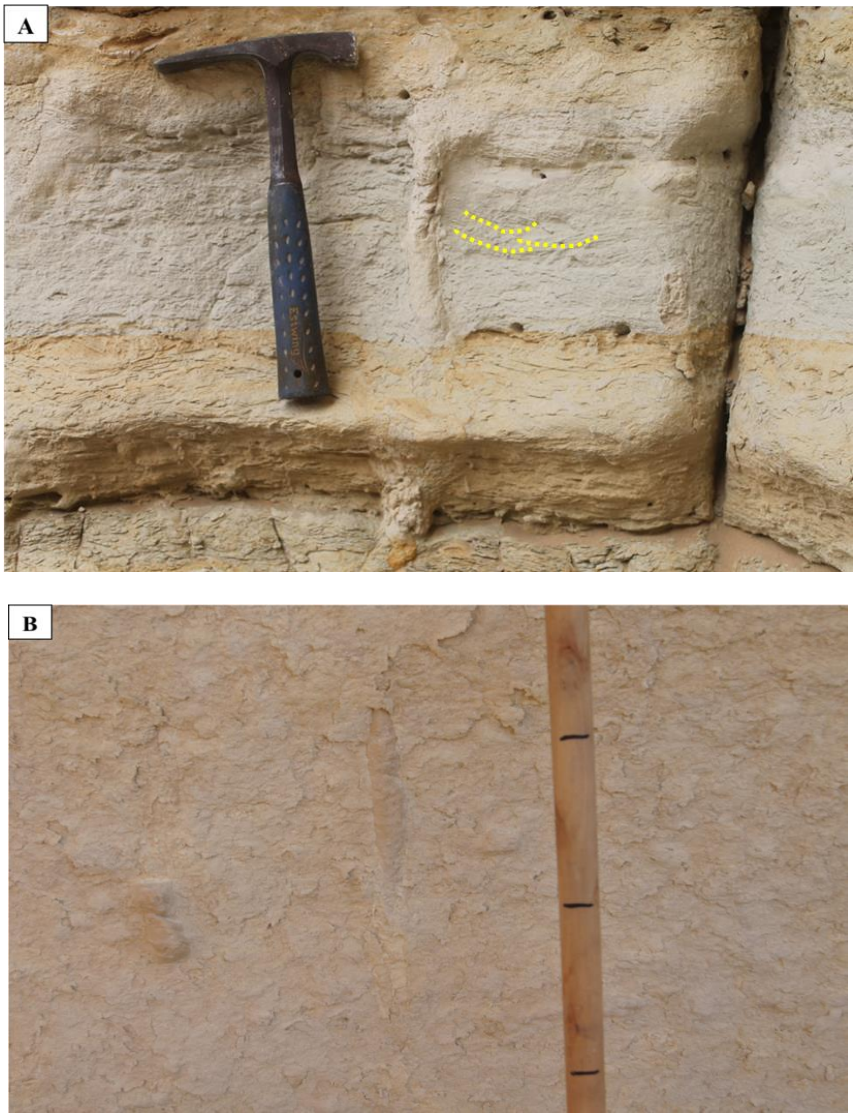

Figure 4.8: (A) Trough cross-bedded sandstone (f 7) with sharp erosive base and *Skolithos* trace fossil. (B) *Ophiomorpha* burrows in the trough cross bedded sandstone (f 7).

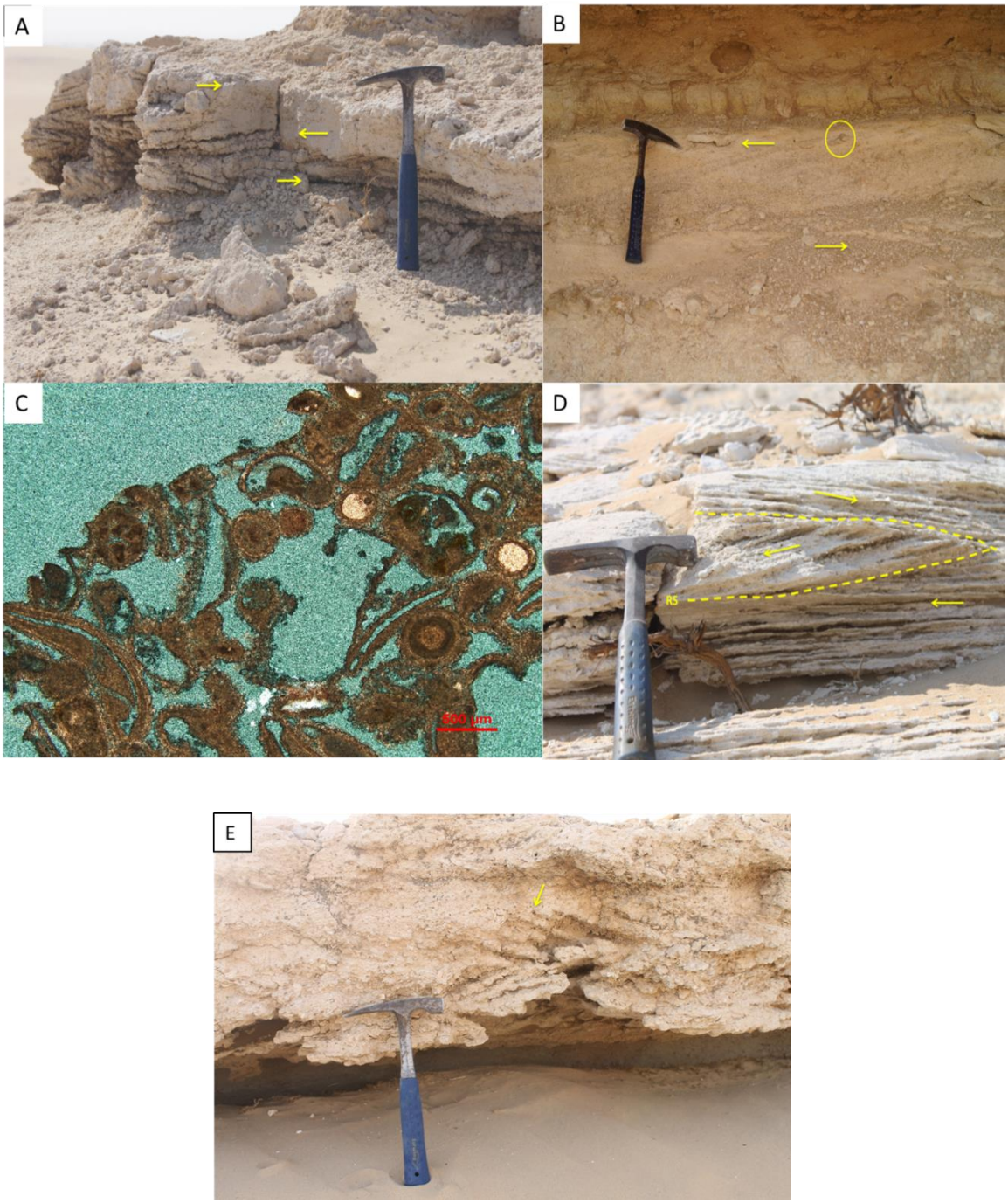

Figure 4.9: (A) Herringbone cross bedding (yellow arrows) in the middle of outcrop 2. (B) Mud drapes (yellow arrows) within the toughs. (C) Thin-section photomicrograph showing partially dissolved ooids, peloids and skeletal molds. (D) Reactivation surfaces (dotted line) at the lower part of outcrop 16. (E) Keystone vugs (yellow arrow) within (f 8) at outcrop 8.

4.2.9 Planar Cross – Bedded Skeletal Pelloidal Grainstone

Description: white to beige colored, planar cross-bedded with a variable thickness that ranged from 0.25m to 0.75 m. This facies has been observed in outcrops 1, 2 & 19 (see the map in Figure 1.4) in more than one stratigraphic position (Figure 4.10A). In some locations it shows mud drapes on the cross bedding surfaces, keystone vugs and tangential bottom sets (Figure 4.10 C). In thin-section it's dominated by skeletal grains (bivalves and foraminifera), peloids in addition to rare ooids (Figure 4.10B).

Interpretation: The planar cross bedding indicate a subaqueous deposition by the migration of straight-crested bedforms driven by unidirectional currents (Boggs, 2006). The fine grain size and the superficial scattered ooids suggest the presence of a medium strength transporting current. Keystone vugs suggest deposition under periodic subaerial exposure conditions. The association of interbedded heterolithic facies (f 5) and herringbone grainstone facies (f 8) suggest that this facies is most probably deposited in the lower intertidal zone (Lasemi et al., 2012).

4.2.10 Trough Cross-Bedded Aggregate Intraclast Oolitic Grainstones (f 10):

Description: light grey to yellowish color, trough cross–bedded with some flaser bedding (Figure 4.11A). Stromatolites were found in association with this facies in outcrops 8 and 19. It has a thickness range from 0.25 m up to 1.0 m, and occurs in outcrops 2, 8, 16 and 19 (see the map in Figure 1.4) in association with planar and herringbone cross-bedded grainstone facies (f 8 & f 9), carbonate conglomerates (f 6) and massive skeletal wackestone facies (f 13). Thin sections of this facies show a dominance of ooids and skeletal grain molds. Peloids and aggregates are also present but less common (Figure 4.11B).

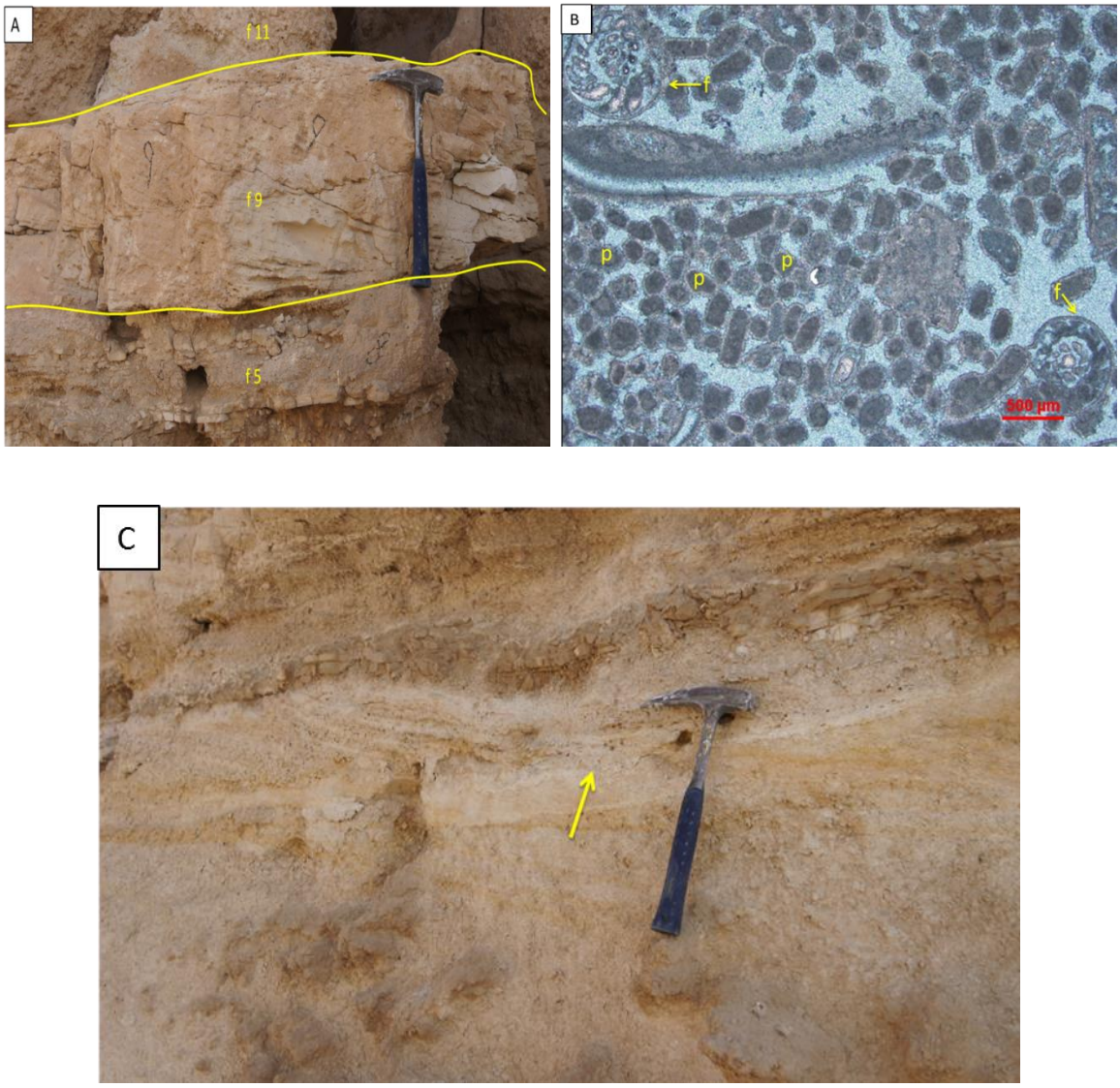

Figure 4.10: (A) Planar Cross-Bedded Skeletal Peloidal Grainstone facies (f 8) with high angle planar cross-bedding, and overlying (f 5) facies and underlying (f 11) facies. (B) Thin-section of Planar Cross-Bedded Skeletal Peloidal Grainstone (f 5) with dominance of peloids, and foram and bivalve molds. (C) Keystone vugs (yellow arrow) within (f 9) facies at outcrop 1.

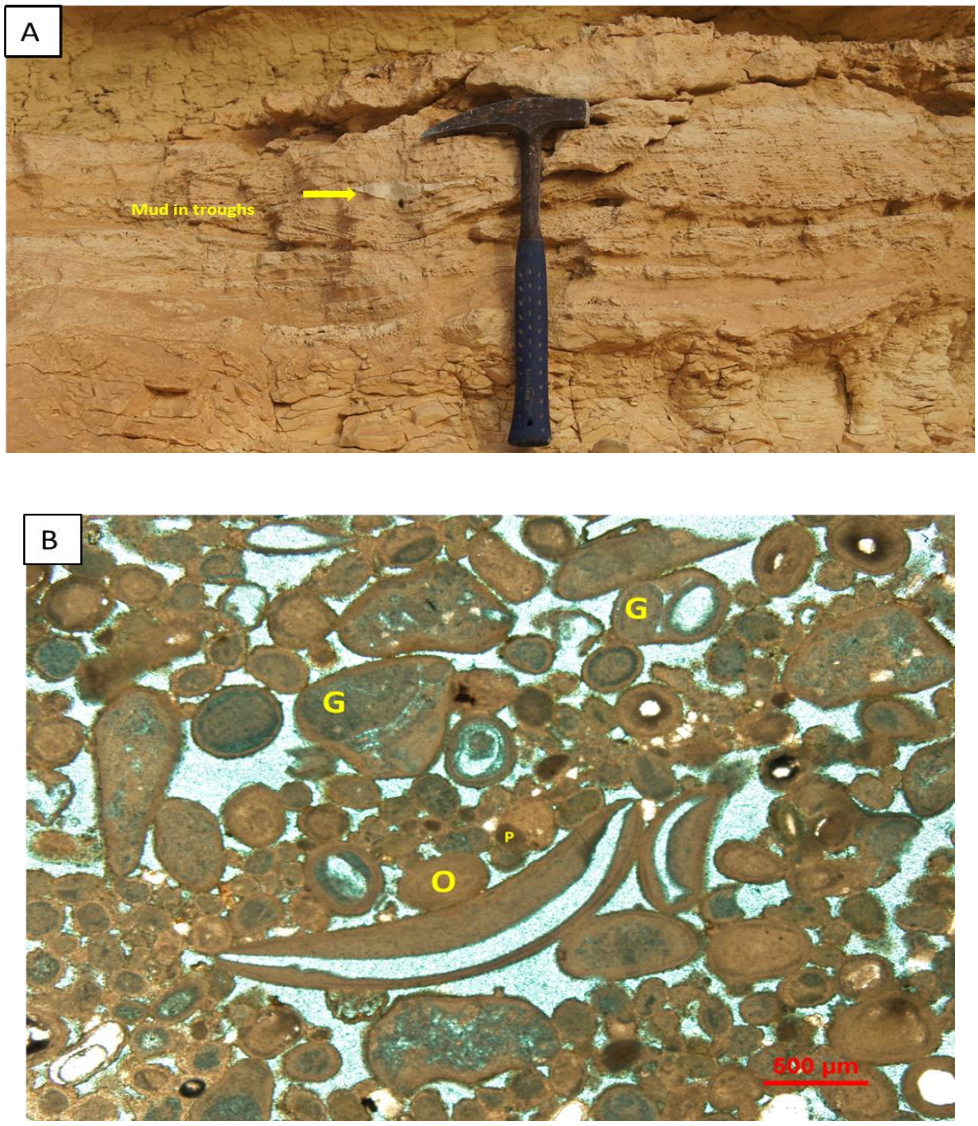

Figure 4.11: (A) Outcrop photograph for the Trough Cross-Bedded Aggregate Intraclast Oolitic Grainstones facies (f 10) showing trough cross-bedding and flaser bedding. (B) Thin-section photomicrograph of the same facies show the different components; G= grain aggregate, O= ooid, P= peloid.

Interpretation: the presence of ooids, intraclasts, and grain aggregates indicate deposition in a relatively high energy, shallow marine environment. The dominance of grain-supported texture, in addition the presence of ooids, peloidal packstone (f 11) intraclasts, and grapestones, infer a relatively high energy shallow marine depositional settings (Palma et al., 2007). The presence of this facies in association with subtidal skeletal wackestone and intertidal planar and herringbone cross bedded grainstones, in addition to previous observations, lead to the interpretation that this facies mainly represents subaqueous carbonate sand waves in upper shoreface depositional setting.

4.2.11 Massive Peloidal Skeletal Packstone (f 11):

Description: white to beige colored, 0.4 m thick, and contain some vugs, rich in skeletal grains. It was only found in the eastern part of the study area (outcrop 1 &2). This facies overlies the planar cross-bedded grainstone facies (f 9). Skeletal grains are dominated by mollusks (bivalves and gastropods) in the form of internal molds. It also contains coral fragment. This facies is intensively bioturbated by vertical and horizontal burrows (Figure 4.12A). Thin sections show the dominance of peloids and foraminifera, and dissolution of most of the skeletal grains forming moldic and vug porosity (Figure 4.12B).

Interpretation: the abundance of macro- and microfossils in this facies, beside the apparent absence of major physical current sedimentary structures would initially seem to suggest a skeletal bank (biostrome) depositional setting. However, the abundance of broken gastropods, bivalve and coral fragments, indicate that all components in this facies are allochthonous rather than autochthonous. The adjacent planar cross-bedded grainstone facies (f 9) (lower intertidal) in addition to the intensive bioturbation, which mainly had destroyed all previously existing sedimentary structures, point to a middle intertidal depositional environment (Rankey, 2012).

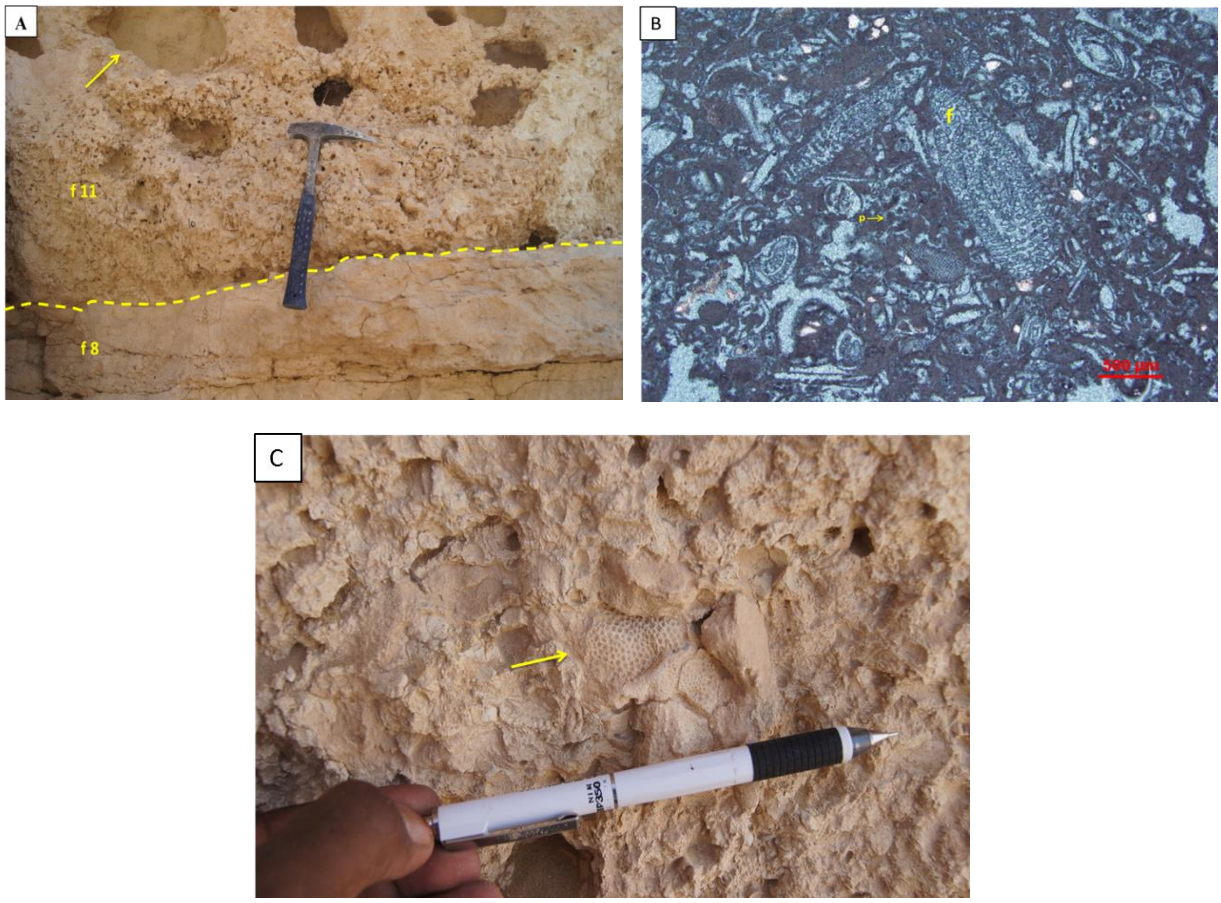

Figure 4.12: (A) Vertical and horizontal burrows (yellow arrow) within the Massive Pelloidal Skeletal Packstone facies (f 11). (B) Thin-section photograph of the same facies show the dominance of forams (f), and peloids (p) and dissolution of skeletal grains. (C) Coral fragment (yellow arrow) within (f 11) facies.

4.2.12 Channelized Planar Cross – Bedded Skeletal Oolitic Grainstone (f 12):

Description: yellowish grey to beige color, very coarse grained, planar cross-bedded grainstone that are 0.7m thick and 2.3 m width with erosive base that cut through planar cross-bedded grainstones (f 9) (Figure 4.13A). It was found only in outcrop-23. Thin-sections show good preservation of the ooids and skeletal grains (dominantly bivalves and foraminifera). The porosity is dominated by interparticle and intraparticle porosity (Figure 4.13B).

Interpretation: the coarse grain size of ooids, erosive base and planar cross bedding structures indicates deposition under high energy condition. This facies is interpreted as a tidal channel that cut through intertidal zone represented by (f 9) facies.

4.2.13 Massive Quartz Skeletal Pelloidal Wack-Packstone (f 13):

Description: white to light grey**,** bioturbated by vertical and horizontal burrows, 1.1 m to 3.5 m thick (the thickest and one of most dominant facies in the study area). It was found in outcrops 1, 2, 23, and 8 (see the map in Figure 1.4) with a thickness decreasing westward. It, always, stratigraphically overlies the interbedded mudstone-evaporite facies (f 2) with sharp surface separating them (Figure 4.14A). This facies, in some locations, contains zones of well-rounded muddy intra-formational pebbles that have a fining upward trend. Thin-sections contain pellets and dissolved skeletal grains as the main components, in a muddy matrix. Skeletal grains are represented by bivalves and foraminifera. Quartz grains are also present in thin-section (Figure 4.14B).

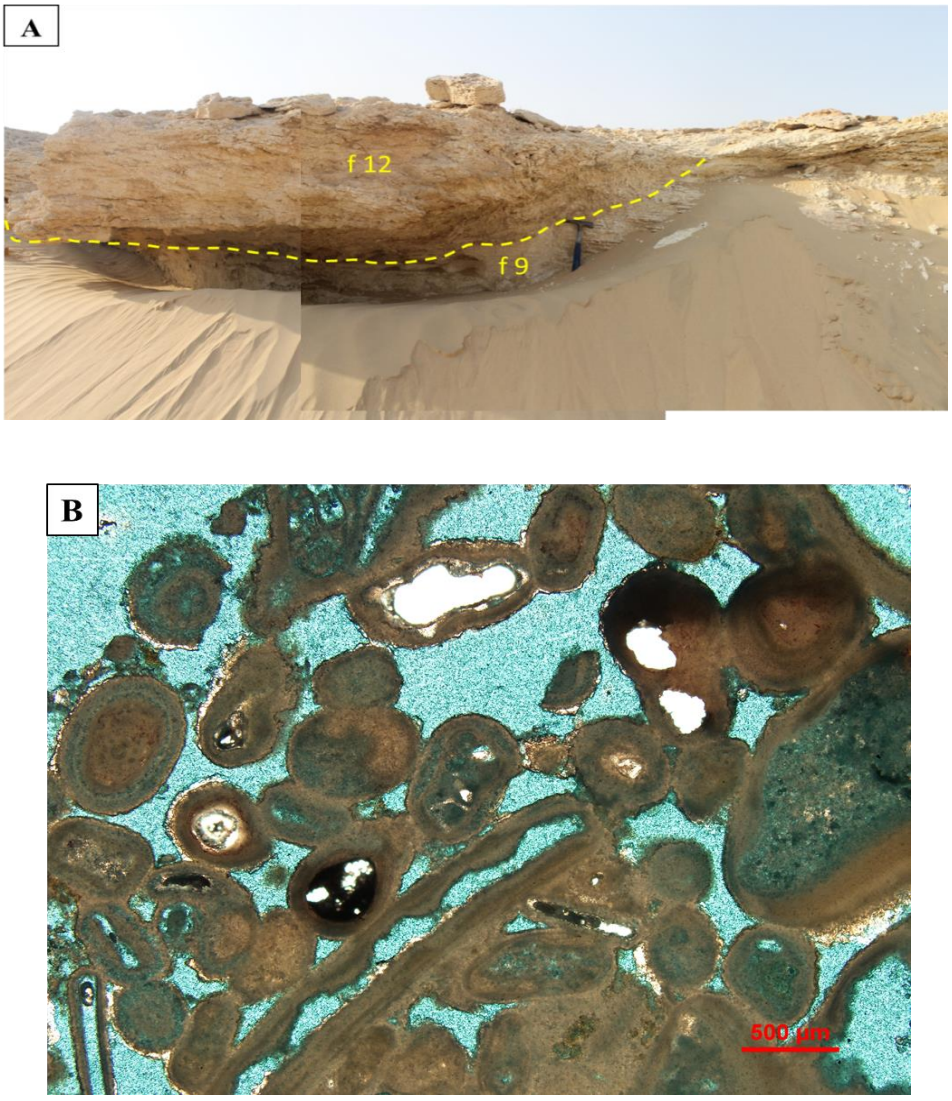

Figure 4.13: (A) Outcrop photograph for the Channelized Planar Cross-Bedded Skeletal Oolitic Grainstone (f 12) show the erosive base and planar cross-bedded grainstones (f 9). (B) Thin-section of the same facies show less dissolution effects on this facies and microbial encrustation.

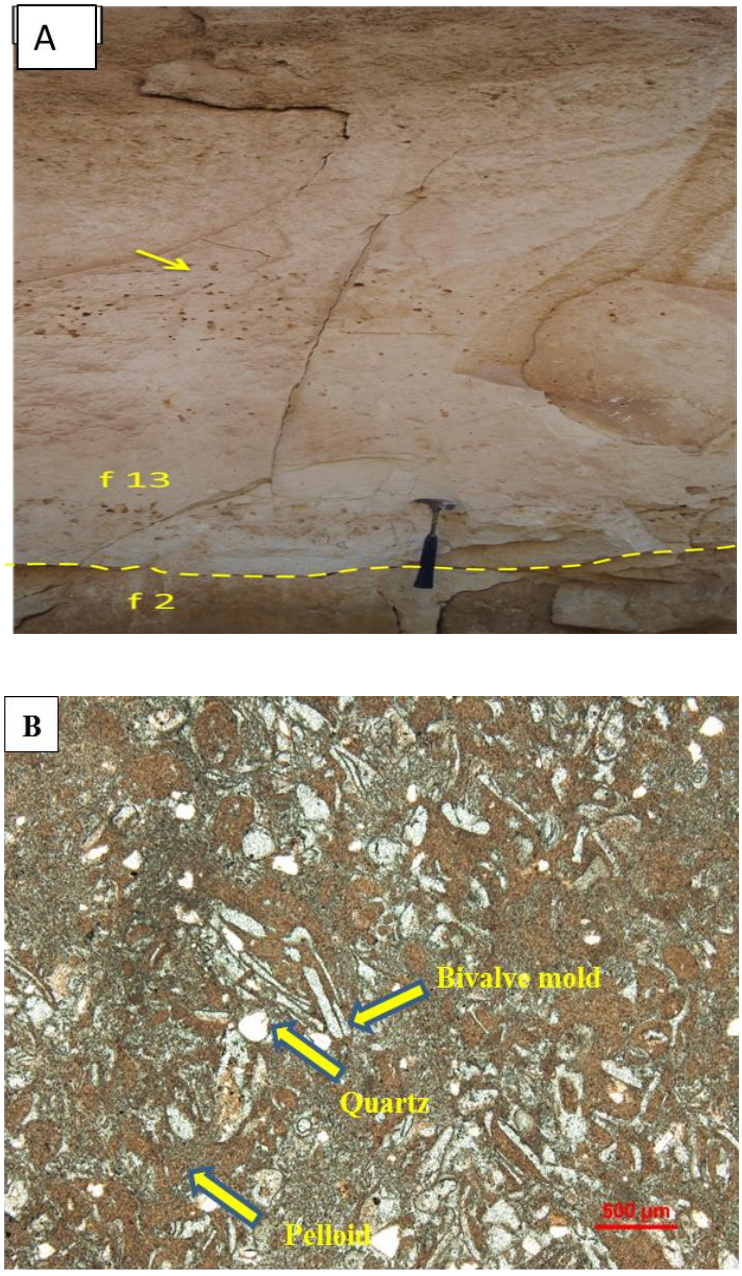

Figure 4.14: (A) outcrop photograph for the Quartz Skeletal Peloidal Wacke-Packstone facies (f 13) with the intra-formational clasts (arrow) overlying (f 2) facies with a sharp boundary. (B) Thin-section of the same facies (f 13) shows the dissolution of skeletal grains, and abundance of peloids and scattered quartz grains.

Interpretation: The abundant mud present in this facies, as well as its massive layers with the absence of physical current structures, suggest a general low energy environment in which sediments could settle out of suspension. The presence of abundant Peloids in this facies is a good indicator for shallow, low energy subtidal carbonate systems (Flügel, 2010). This facies, with the absence of exposure indications, was probably deposited below fair-weather wave base in the outer ramp zone. The intra-formational mud pebbles (at the base of this facies) are interpreted to have been deposited during short-lived storm events (Lasemi et al., 2012).

4.2.14 Massive Skeletal Wackestone (f 14):

Description: dark gray colored, massive, mound shaped, 2m width and about 1m thick, carbonate body. This facies cuts through massive skeletal packstone (f 11) and planar cross-bedded grainstones (f 8) (Figure 4.15A), and only occurs in outcrop 1. In thin section, it has wackestone texture, with skeletal (foraminifera & bivalves) grains as the dominant components. Most of these skeletal grains are dissolved (Figure 4.15B).

Interpretation: The dark color of the mud in this facies could be attributed to the high percentage of organic materials within it. Both the absence of current physical structures & bioturbation and the pure skeletal components, indicate an insitu skeletal build up. The domal architecture, the environmental indications of adjacent facies, the cross cutting relationship with these facies in addition to previous observations lead to the interpretation that this facies is most probably an inner – mid ramp skeletal mound (Flügel, 2010).

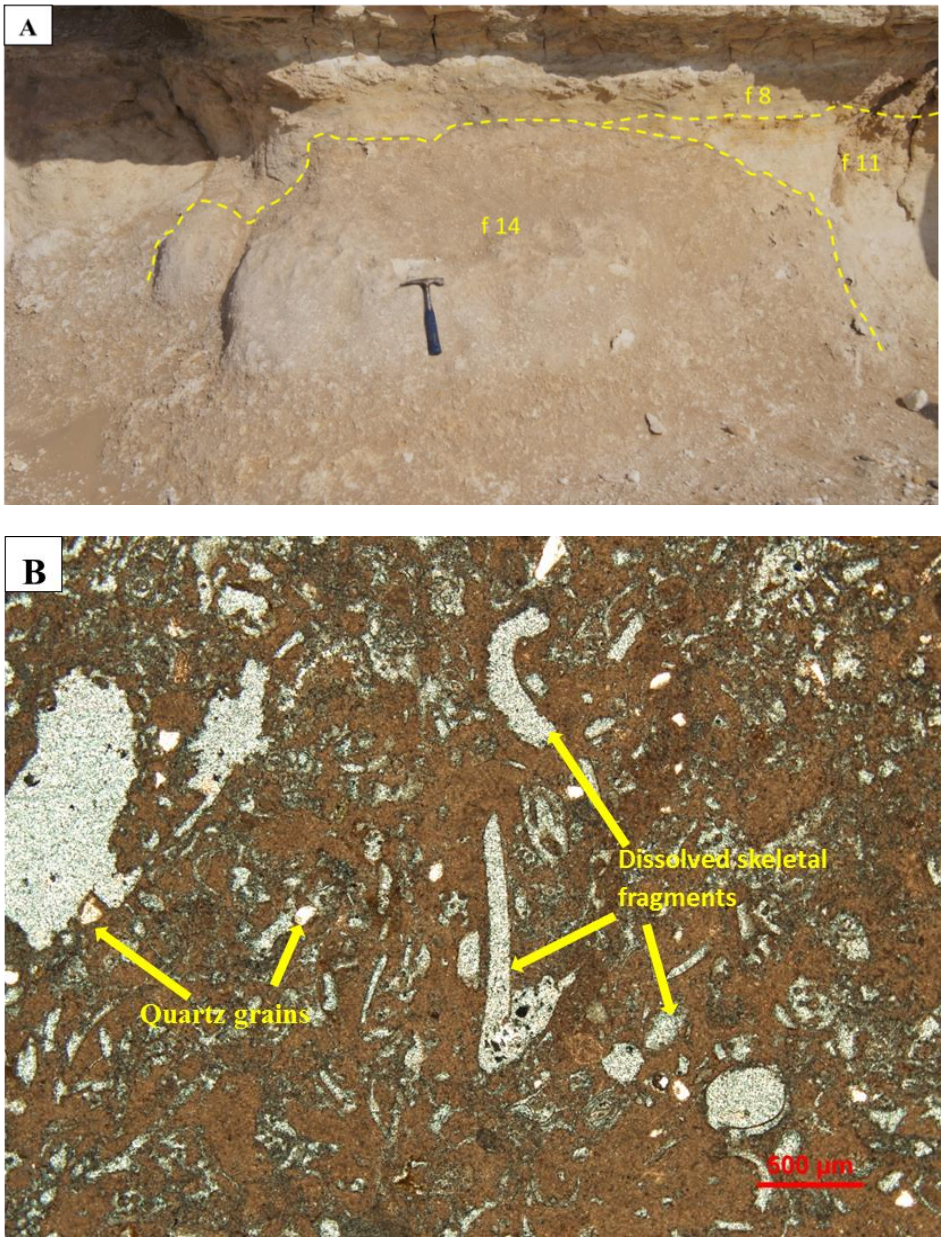

Figure 4.15: (A) Outcrop photograph show the mound shape of the Massive Skeletal Wackestone (f 14). (B) thin-section of the same facies shows dissolution of skeletal grains.

4.2.15 Dipping Planar Cross – Bedded Skeletal Oolitic Grainstone (f 15):

Description: creamy to white colored, 0.4 m thick with keystone vugs, internally laminated between ooid – and skeletal- dominated laminae (Figure 4.16A). The upper surface of this facies shows rain drop impressions (Figure 4.16B). This facies always overlies the trough cross-bedded grainstones (f 10) or herringbone cross-bedded grainstone (f 8). Thin-section of this facies shows grainstone texture, with dominance of pelloids, ooids, and skeletal grains (bivalves). The main porosity types are inter-granular, moldic and shelter porosity (Figure 4.16C).

Interpretation: The keystone vugs are most probably air pebbles that were trapped during deposition, indicating the shallowness and exposure of this facies. The rain drop impressions confirm this suggestion and, furthermore, give evidence of exposure. The parallel horizontal lamination, in addition to the fine grain size of this facies suggests a turbulent flow with high energy environment. Moreover, the existence of primary current lineation on the top of the layers indicates deposition in the upper flow regime, too. The early cementation, the adjacent facies, the good sorting of ooids, the shells accumulations in addition to previous observations strongly signify a surf \ swash foreshore beach deposition (Tucker, 2001).

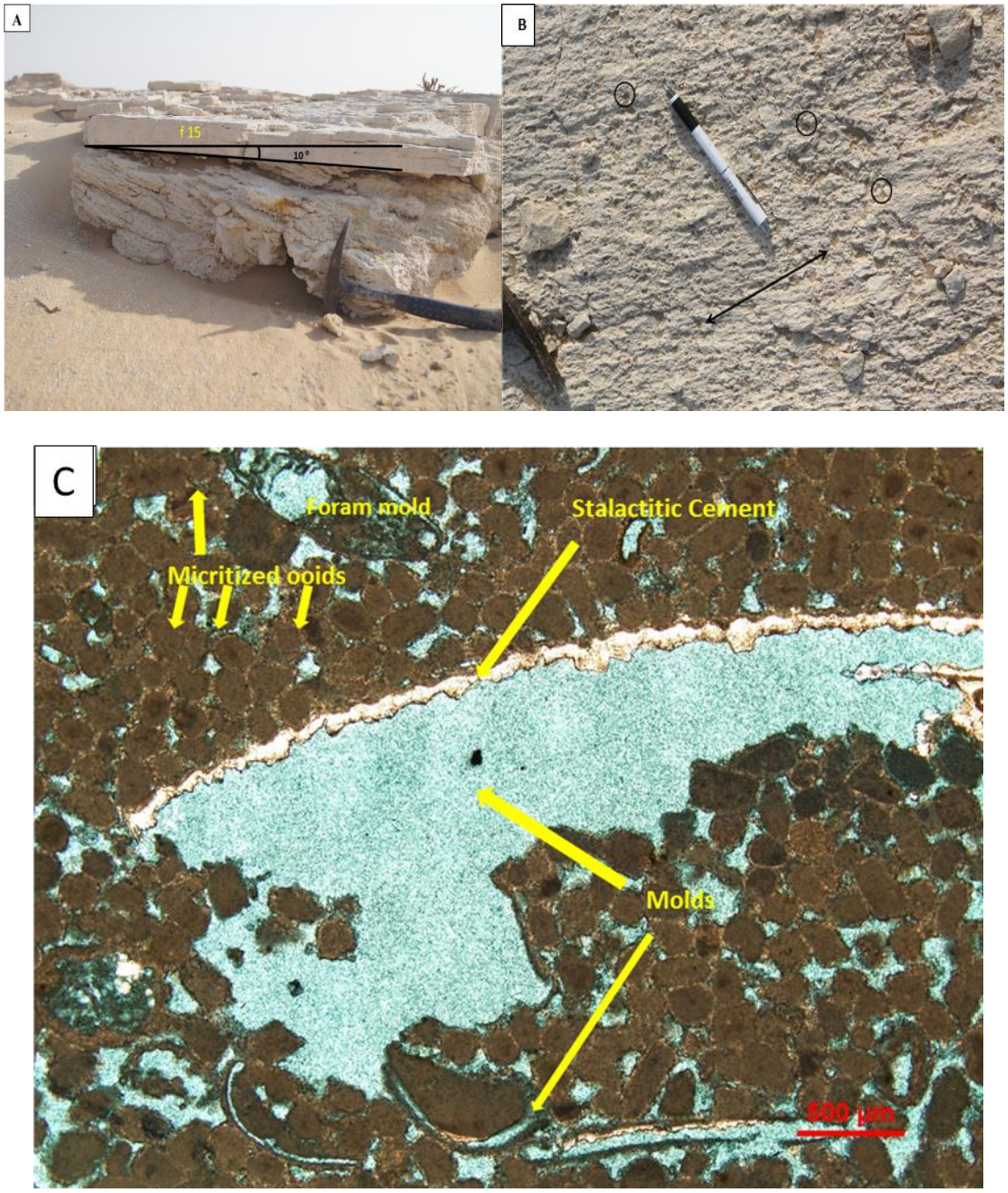

Figure 4.16: (A) Outcrop photograph of the Planar-bedded Skeletal Oolitic Grainstone facies (f 15). (B) Plan view of (f 15) showing rain drops (circles) and current lineation (arrow). (C) Thin-section of the same facies shows dissolution of the skeletal grains and micritization of ooids.

4.3 Depositional Environment

Fifteen lithofacies are defined within the Miocene Dam Formation in Al-Lidam area using the key features such as sediment color, bed thickness, bedding geometry, grain components, sedimentary texture, sedimentary structures, pore types, fossil content, and identified ichnofacies. Petrographic investigation included description of grain types, cement types and texture in order to determine the depositional facies and the diagenetic features. Distinctions between the carbonate facies are determined by grain types, sedimentary structures and the textural classification of (Dunham, 1962), as modified by (Embry & Klovan, 1971).

Base on spatial distribution of the identified lithofacies, a depositional model, that shows the different depositional environments, was proposed for the Miocene Dam Formation in the study area (Figure 4.17).

The Stratigraphic Sections for outcrop 2, 1, 23 and 8 are shown in Figure 4.18, 4.19, 4.20 and 4.21, respectively.

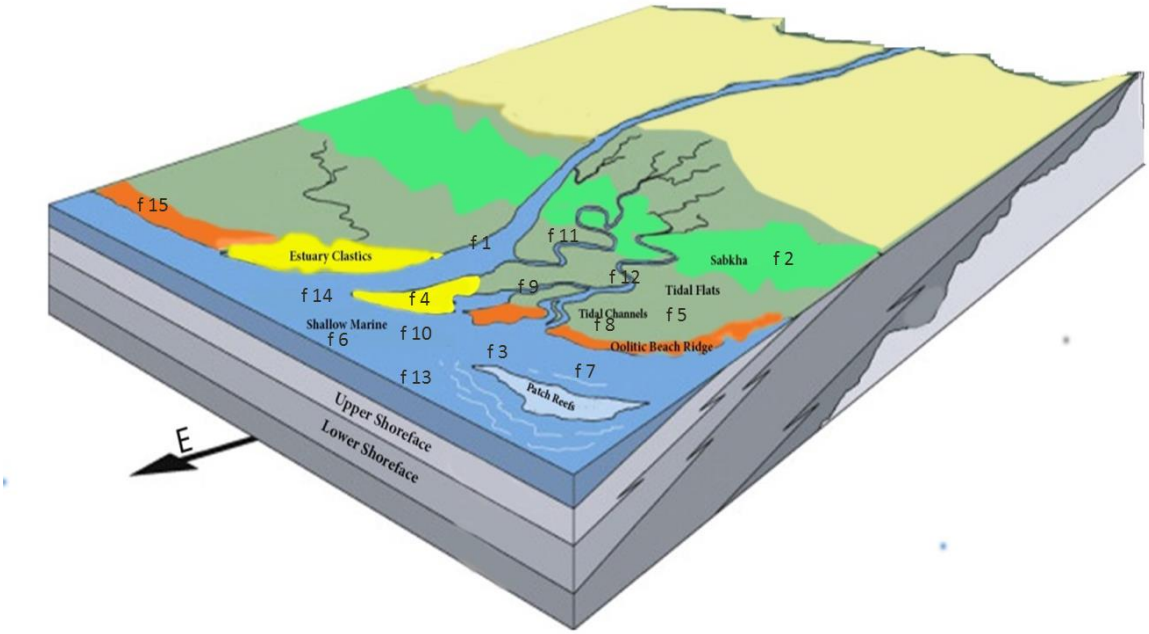

Figure 4.17: 3D Depositional model for the Miocene Dam Formation in Al-Lidam Area.

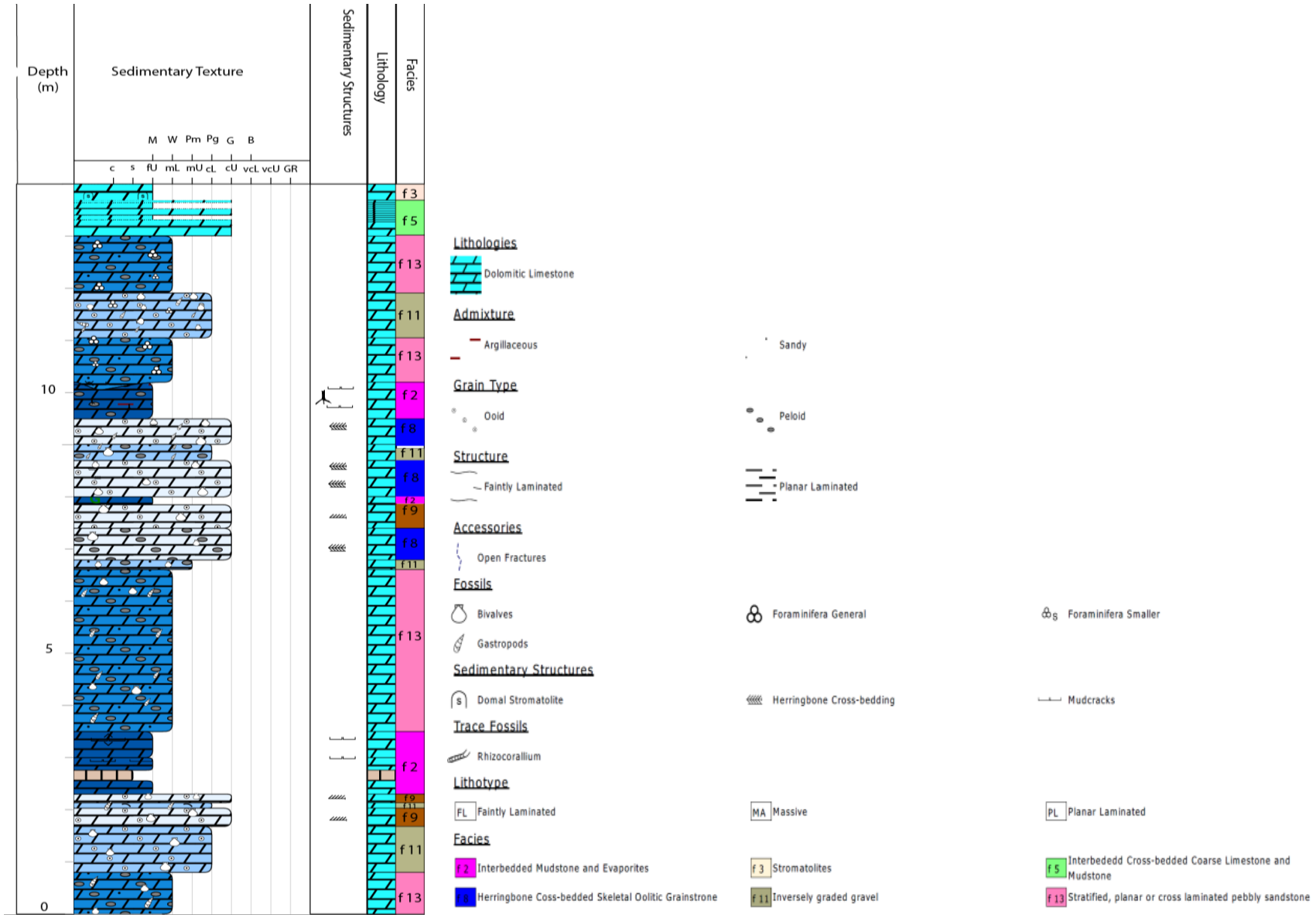

Figure 4.18: Vertical stratigraphic section of outcrop 2.

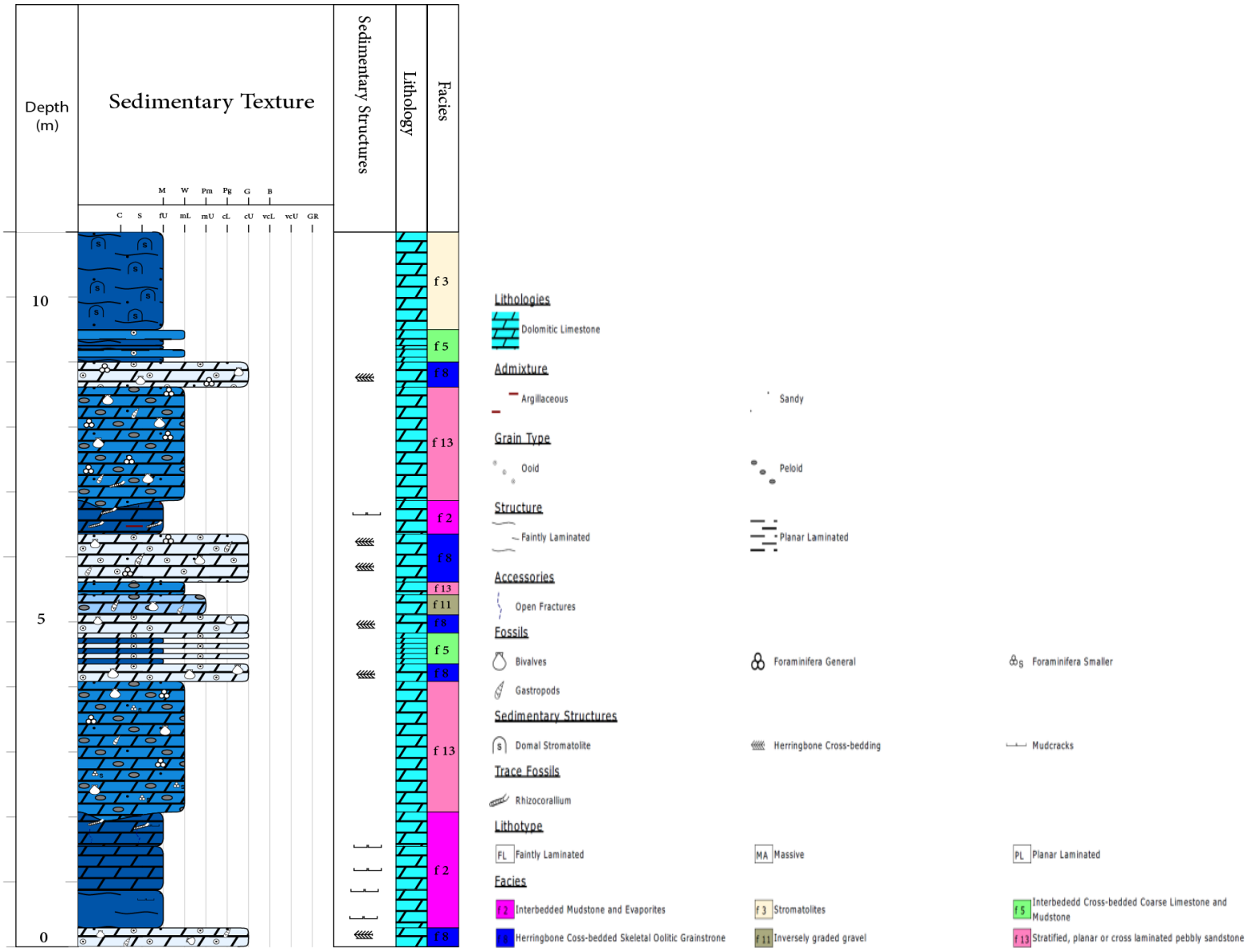

Figure 4.19: Vertical stratigraphic section of outcrop 1.

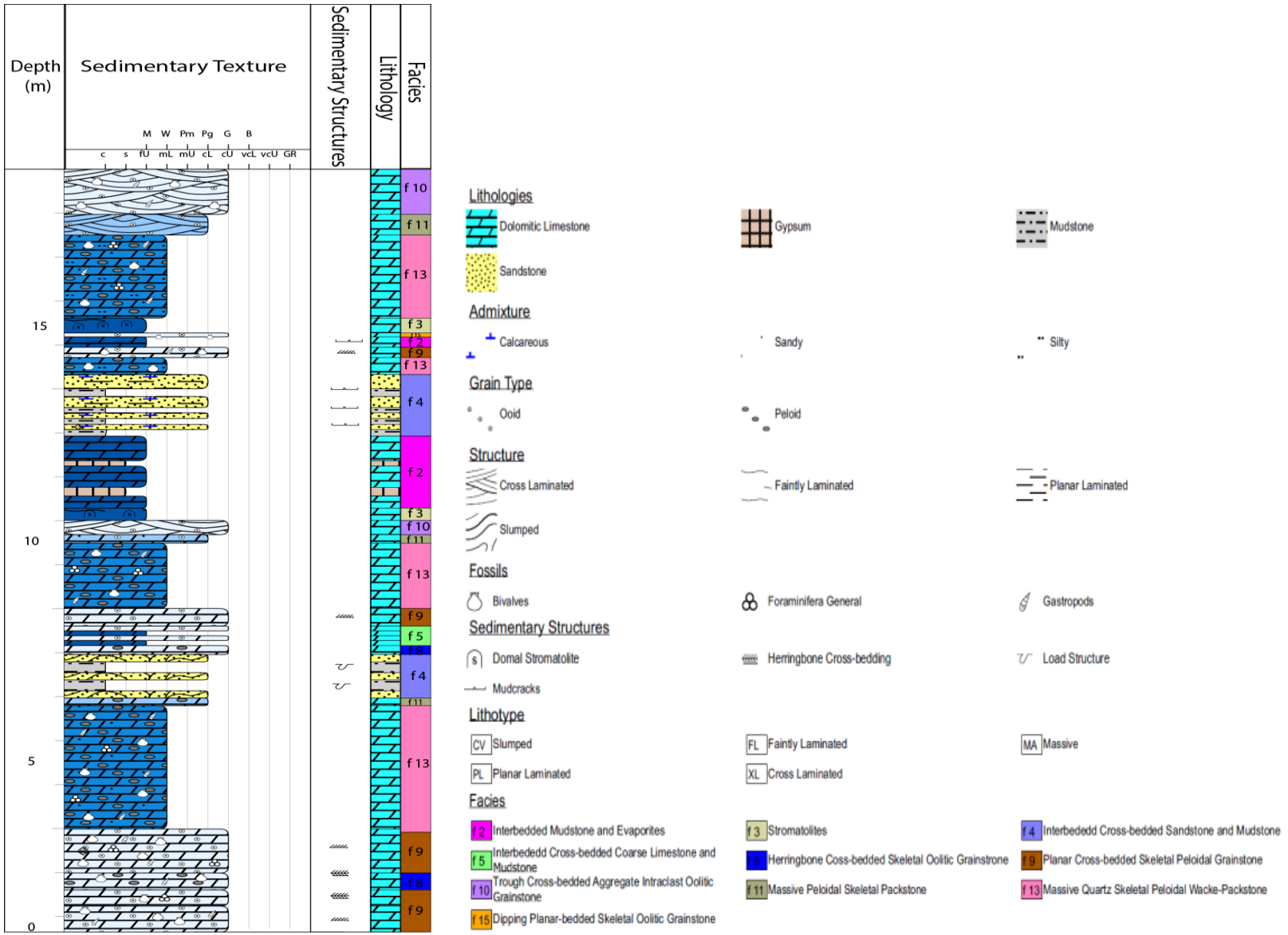

Figure 4.20: Vertical stratigraphic section of outcrop 23.

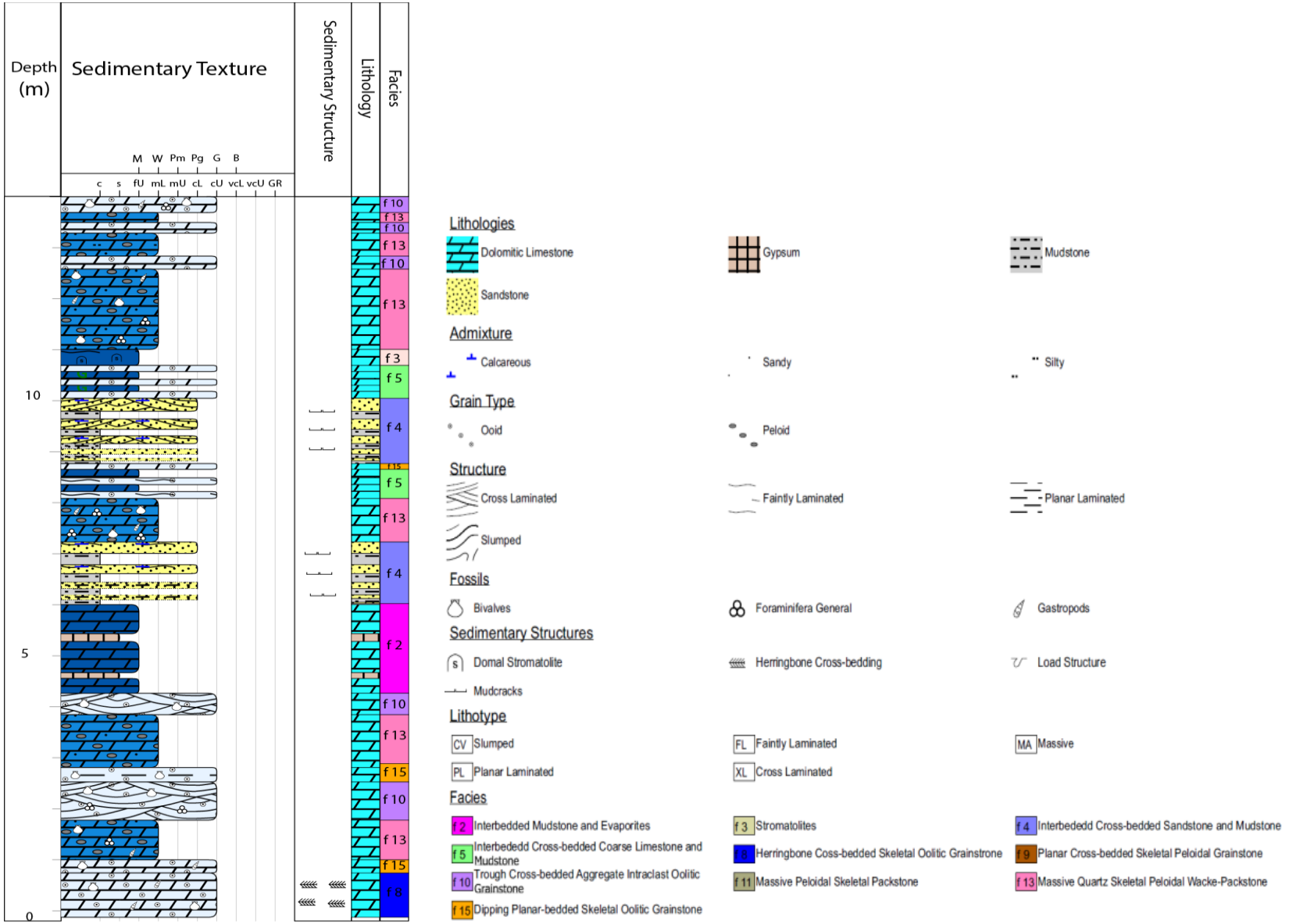

Figure 4.21: Vertical stratigraphic section of outcrop 8.

CHAPTER 5

CARBONATE DIAGENESIS

5.1 Introduction

"Diagenesis comprises all the natural changes in sediments occurring from the moment of deposition, continuing through compaction, lithification and beyond – stopping short of the onset of metamorphism. It is a continually active process by which sedimentary mineral assemblages react to regain equilibrium with an environment whose pressure, temperature, and chemistry are changing" (Ahr, 2008; Ali, Clark, & Dribus, 2010). Carbonate rocks, in comparison to siliciclastic, are more susceptible to these post-depositional processes, and are more affected by diagenesis. This high susceptibility, for diagenesis, of carbonate rocks can be attributed to two main factors; (1) the biological origin of most (90%) of carbonate rocks (Milliman, 1974; Wilson, 1975), (2) and the high chemical reactivity of carbonate minerals (Moore, 2013).

The major diagenetic processes that affect carbonate minerals are; dissolution, cementation, compaction, neomorphism, micritization and dolomitization (Flügel, 2010).

Dissolution: can be defined as the dissolution of carbonate grains and cements by under-saturated pore fluids (with respect to these grains and cements). This process can be easily observed in meteoric as well as in deep burial diagenetic environments (Longman, 1980; Moore, 2013). Depending on the mineralogy of the precipitated carbonate minerals and pore fluid chemistry, dissolution can be partial or complete.

Cementation: Include all processes that lead to mineral precipitation within the primary or secondary porosity. For cementation to occur, the pore fluids must be over-saturated with respect to precipitated minerals. Another factor that affects cementation is the volume of pore fluids that move through the sediments, with a greater volume of pore fluids typically leading to more cementation (Longman, 1980; Moore, 2013) . This process can be observed in meteoric, marine and burial diagenetic environments, but with different cement types and textures.

Compaction: Includes mechanical and/or chemical processes that act in response to increasing overburden stress. As a result of compaction, the grains move closer to their neighbors making distinctive grain-to-grain contact features. This process can be observed in shallow and deep burial diagenetic environments (Ali et al., 2010; Flügel, 2010).

Neomorphism: Includes al transformation taking place in the presence of water through dissolution-re-precipitation process between one mineral and itself or a polymorph (Flügel, 2010).

Recrystallization: Includes all changes in crystal lattice orientation, crystal shape and crystal size without change in mineralogy (Ali et al., 2010; Flügel, 2010).

Micritization: Micritization is a process by which carbonate grains are transformed into fine-grained calcite from their original form, usually removing their internal structure. Micritization may occur due to the action of endolithic algae and fungi which bore into bioclasts. The early stages of micritization lead to the formation of a micrite envelope, often with an irregular internal

surface. More intense micritization, however, can lead to the complete loss of internal structure of bioclasts (Reid & Macintyre, 2000).

Dolomitization: Is a process whereby limestone or its precursor sediment is completely or partly converted to dolomite by the replacement of the original CaCO3 by magnesium carbonate, through the action of Mg-bearing water (Flügel, 2010).

Diagenetic processes that have an influence on the petrophysical properties of carbonate reservoirs occur in different diagenetic environments (Tucker, 1993; Flügel, 2010). These diagenetic environments are: marine diagenetic environment, meteoric diagenetic environment, and burial diagenetic environment, with each one has its own characteristic features and processes.

Diagenesis of the Dam Formation was investigated for this study using different techniques including optical microscopy, X-ray diffraction (XRD), scanning electron microscopy (SEM) and cathodoluminescence (CL) microscopy. Diagenetic features and processes that were identified were classified according to their diagenetic environment in which they were interpreted to have formed (marine, meteoric and burial diagenetic environments).

5.2 Marine Diagenesis

Most carbonate rocks and sediments were originally deposited in marine water, and their diagenetic history starts there (Longman, 1980). In this stage, all of the pores were filled by marine water that is saturated with respect to calcium carbonate. Several distinctive features

indicative of marine diagenesis were observed in thin-section and SEM micrographs of the carbonate succession of the Dam Formation in the study area. These features include grain micritization, fibrous cementation by aragonite and magnesian calcite, and polygonal sutures. Each one of these features will be discussed below separately.

5.2.1 Micritization

This process occurred on the seafloor or just below by boring on the grain margins by micro-organisms such as endolithic algae, fungi and bacteria (Figure. 5.1). The holes were then filled with fine grain cement or sediments (Reid & Macintyre, 2000), forming a micrite envelope; micrite envelopes occur commonly throughout the Dam Formation in the Al-Lidam area (f 8, f 9, f 10, f 11, f 12 and f 15 facies) (Figure. 5.2A and 5.2B). This micrite envelope played a role in preservation of the grain shapes, even in cases where the grain has been completely leached away. Due to their relative resistance to dissolution (Flügel, 2010), micrite envelopes play a role in preservation of porosity by preventing the grains from being destroyed by compaction or dissolution during later diagenetic processes, (Figure. 5.3A, 5,3B and 5.3C). Micrite envelopes are more common in the Dam grainstone facies, especially in the beach and upper shoreface grainstone facies, but are rare or absent in the packestone, wackestone and mudstone facies. In some cases (such as in facies 12 and 15), micritization has been extensive, leading to destruction of the original microarchitecture of grains (Figure. 5.4A and 5.4B).

Abundant micrite envelopes as well as extensive micritization were attributed to the high microbial activity within the upper shoreface as well as in the beach environments. In addition, the high water movement rate at these environments also played an important role in micritization, by allowing large volumes of water to pass through the microbial-bored holes leading to precipitation within these holes (Longman, 1980).

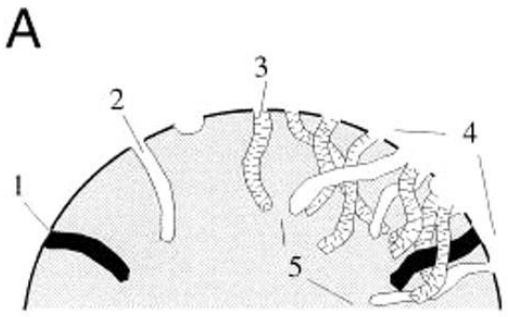

1. live endolith
2. empty bore holes (common)
3. fringe cement
4. incomplete grain margins
5. irregular edge of micritic rim

Figure 5.1: Micritization process by endolithic micro-organisms boring within grain margins (modified from Reid & Macintyre, 2000).

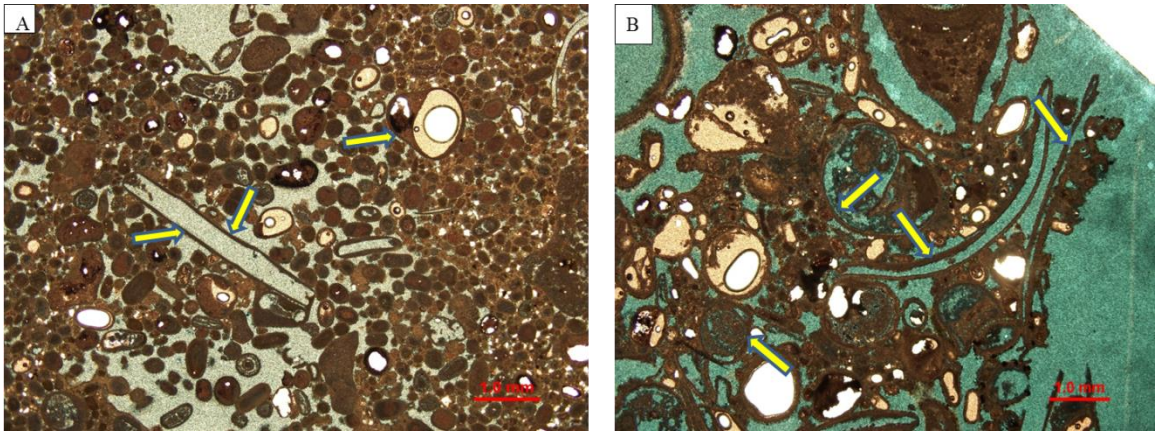

Figure 5.2: (A) Thin-section photomicrograph showing a micrite envelope (yellow arrows) developed on a leached grain in the trough cross bedded aggregate intraclast skeletal oolitic grainstone facies (f 10). (B) Thin-section photomicrograph showing several micrite envelopes (yellow arrows) surrounding leached grains in the planar cross bedded skeletal peloidal grainstone facies (f 8).

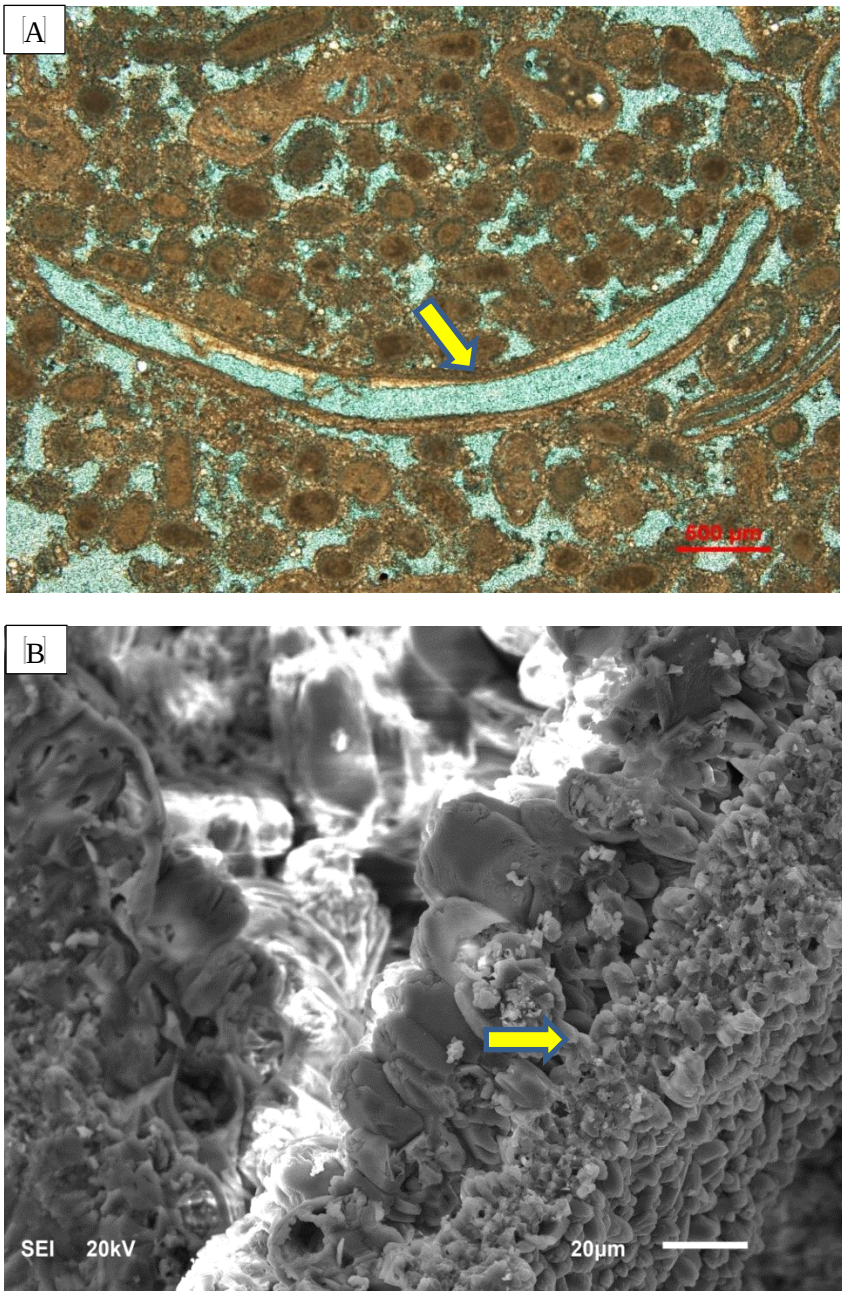

Figure 5.3: (A) Thin-section photomicrograph showing a micrite envelope (yellow arrow) preserving the original shape of a dissolved bivalve fragment. (B) SEM photomicrograph showing a micrite envelope (yellow arrow) preserving the pore shape of dissolved grains.

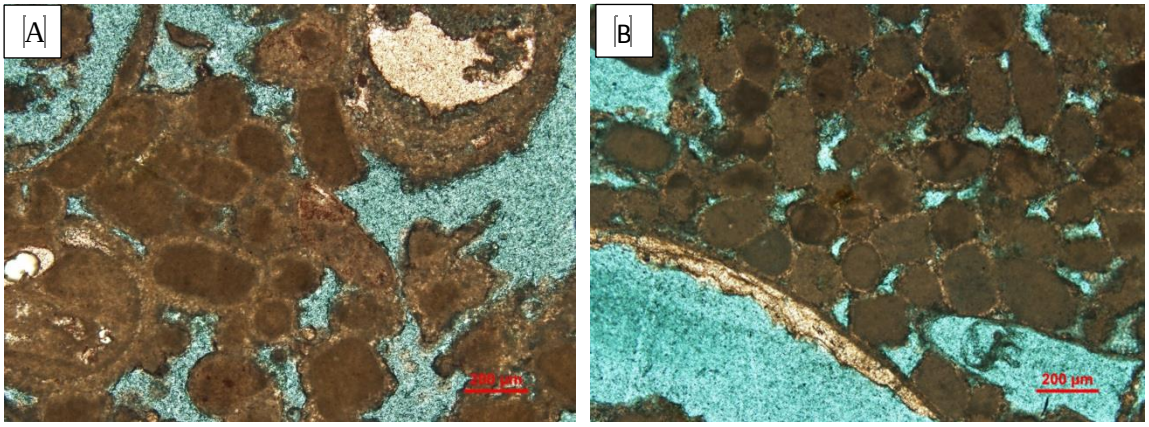

Figure 5.4: Thin-section photographs shows micritization obscuration of the original texture of ooids of the (A) Channelized Planar X-bedded Skeletal Oolitic Grainstone (f 12), and (B) Dipping Planar X-bedded Skeletal Oolitic Grainstone (f 15).

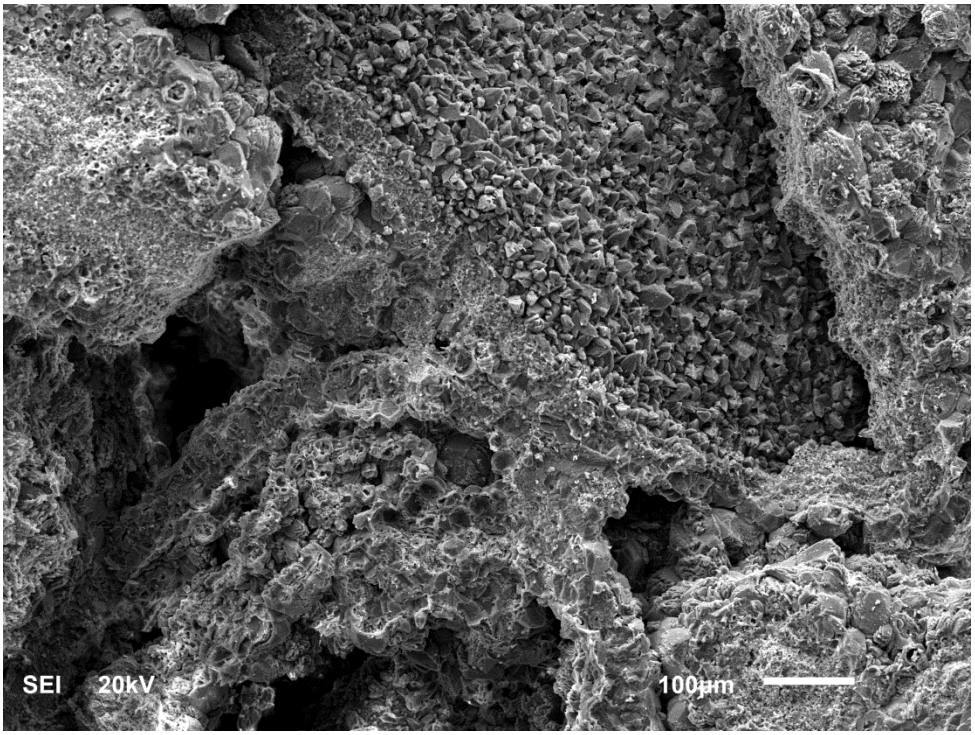

Figure 5.5: SEM microphotograph shows high-magnesium calcite cementation on the skeletal fragments of the intertidal grainstone facies (f 9).

5.2.2 Marine Cementation

The marine environment in tropical shallow water carbonate environments is characterized by pore fluids that are supersaturated with respect to the most of the common carbonate minerals (aragonite and calcite). Therefore, the marine environment is potentially the site of porosity destruction by marine cementation (James & Choquette, 1983; Land & Moore, 1980).

Folk (1974) suggested a model to relate the different calcite cement morphologies to the Mg/Ca ratio of the precipitating fluid. His model is based on the concept of the sidewise poisoning of the growing calcite crystal by the substitution of the Mg ion for Ca. The smaller ionic radius of the Mg ion, relative to the Ca ion, causes lattice distortion at the edge of the growing crystal, stopping growth at the edge, and ultimately leading to the elongation of the crystal in the C-axis direction (Figure. 5.6A). Therefore, the marine water (which have high Mg/Ca ratio (Moore, 2013)) tends to precipitate bladed and elongate cements, while meteoric water, with low Mg/Ca ratio, tends to precipitate more equant cement (Figure. 5.6B).

Fibrous aragonite and acicular, isopachous calcite cement has been observed in the Dam Formation in the Al-Lidam area. These cements were precipitated as high-magnesium calcite (Figure 5.5) as well as fibrous aragonite (Figure 5.7A), on the outer surfaces of the skeletal and non-skeletal grains. Generally, high-Mg calcite and aragonite cementation was not found through the packstone and wackestone facies. However, it was more restricted to the grainstone facies, especially the intertidal and beach grainstone facies (f 8) and (f 15).

The presence of fibrous aragonite and isopachous high-Mg calcite suggests a precipitation in marine phreatic environment.

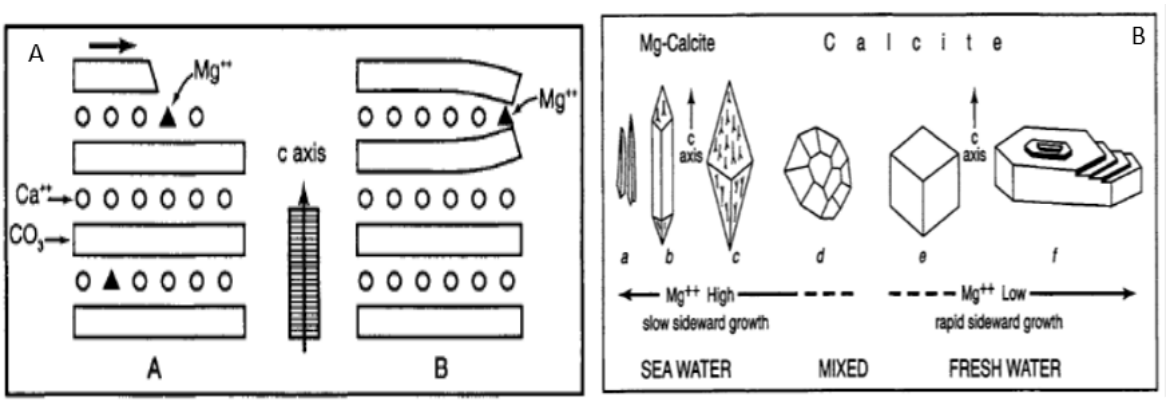

Figure 5.6: (A) Morphology of calcite crystals as controlled by selective Mg-poisoning. (B) Calcite crystal growth habit as a function of Mg/Ca ratio (Folk, 1974).

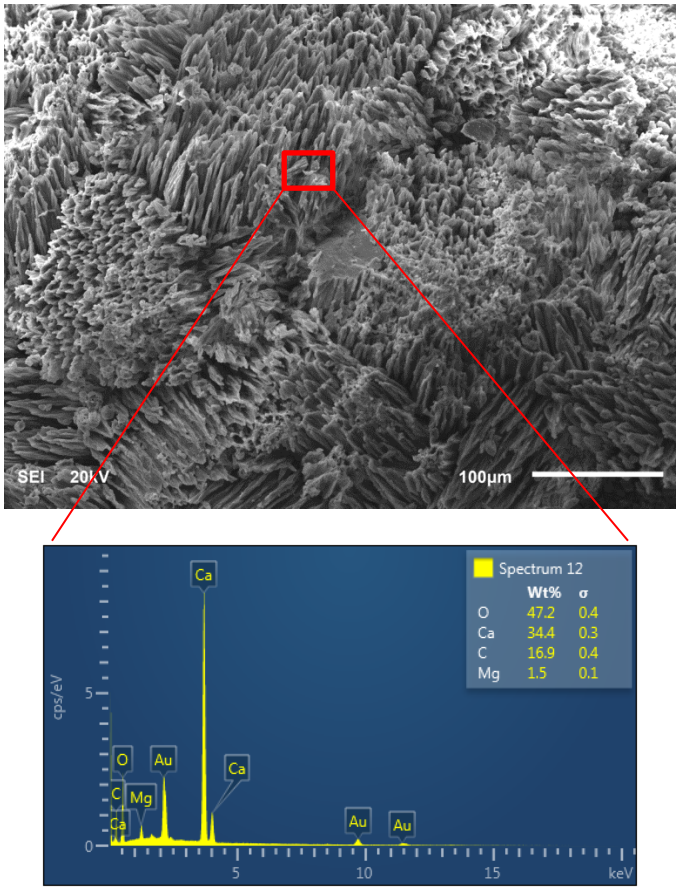

Figure 5.7: SEM microphotograph (A) shows the fibrous, originally, aragonite cement that has altered to low magnesium calcite as shown by EDS (B).

These cements were interpreted to have precipitated from pore fluids that are supersaturated with respect to aragonite and magnesium calcite (marine water) and then to have been altered to low magnesium calcite as indicated by SEM and Energy Dispersive X-ray Spectroscopy (EDS) (Figure. 5.7A and 5.7B) (Longman, 1980).

The rare and infrequent presence of marine cementation through the packstone and wackestone facies is attributed to two reasons: (1) either the marine fibrous and isopachous cements were not precipitated due to low energy condition (slow pore fluids movement), or (2) it was precipitated and then dissolved or altered to meteoric equant calcite cements. On other hand, the high rate of marine water movement, by tidal activity, through the porous and permeable grainstone facies was the main factor that triggered the marine cementation in these facies.

In addition to the high rate of pore fluid movement, carbon dioxide CO_2 degassing by photosynthesis and tidal pumping , also played a role in marine calcite and aragonite cementation (Longman, 1980; Moore, 2013; Tucker and Wright, 1990).

5.3 Meteoric Diagenesis

The meteoric diagenetic environment is one of the most important diagenetic settings relative to the development and evolution of carbonate porosity (Moore, 2013). Meteoric waters are chemically dilute, and typically undersaturated with respect to most carbonate minerals (aragonite and magnesian calcite). Thus, meteoric waters are strongly aggressive toward metastable carbonate minerals and have ample opportunity to dissolve these minerals. This strong aggressiveness is attributed to the fact that meteoric waters have access to large CO_2 reservoirs that are present in the atmosphere as well as in the vadose zone as the waters percolate downward toward the meteoric phreatic zone (Morse & Mackenzie, 1990). The Pco_2 of soils can often reach concentrations of 10^{-2} atm, two orders of magnitude higher than atmospheric Pco_2 ($10^{-3.5}$ atm) (Matthews, 1974). The carbonates dissolved by these aggressive fluids then become available as cement as the fluids transport them and reach, at later stages, the saturation phase with respect to the precipitated carbonate minerals. The low Mg/Ca ratios and salinities found in most meteoric waters generally favor the precipitation of calcite (Longman, 1980).

The meteoric diagenetic environment consists of two important sub-environments, the vadose zone and the phreatic zone. The meteoric vadose diagenetic environment is unique because it is a two-phase system, air and water. This system is reflected in the distributional patterns and unusual morphology of the cements precipitated in this environment. Such cements are most common at grain contacts; and they exhibit microstalictitic and meniscus fabrics (Longman, 1980; Moore, 2013). The meteoric phreatic diagenetic environment is the most important meteoric environment relative to porosity modification because of the large volume of water available for dissolution and precipitation. Moldic porosity and abundant pore-filling circumgranular calcite cements are common in the phreatic zone (Moore, 2013).

In the study area, the Dam Formation reveals several stages of subaerial exposure as indicated by desiccation cracks of the fine grained mudstone facies (f 2), and rain drop impressions that occur on the top of beach grainstone facies (f 15). As a result of these exposure events, the whole carbonate succession was affected by pervasive meteoric diagenesis. Phreatic meteoric diagenetic features are more prominent than those of the vadose diagenetic environment. Vadose diagenetic features are represented by meniscus cements that partially fill the pore spaces between grains, and are especially common in the grainstone facies. Phreatic meteoric diagenetic features are represented by extensive dissolution of the skeletal and non-skeletal grains, and by equant calcite cementation on the grain margins and within dissolved grains.

5.3.1 Meteoric Vadose Diagenesis

In this zone, the pore spaces are filled by both air and water (Figure. 5.8), and the pore fluids are undersaturated with respect to the calcium carbonate which has led to dissolution of some of the metastable carbonate minerals (aragonite and magnesian calcite). Dissolution in the vadose zone is balanced by cement precipitation. As a result, most of depositional porosity is preserved without significant changes (Moore, 2013).

Since cements are concentrated at the pore throats, permeability is significantly reduced at this zone (Halley & Harris, 1979).

The paleoclimate at the time of deposition of the Dam Formation in the study area was semi-arid climate as inferred by the presence of thin evaporite beds interbedded with the mudstone facies (f 2). Subsequent evaporite cementation (Figure. 5.9A and 5.9B) also indicates arid to semi-arid conditions during deposition. Another characteristic feature that indicates vadose diagenesis under semi-arid climate is the development of tepee structures (Tucker, 2001), within the

interbedded carbonate –mudstone facies (f 5) (Figure. 4.5A). As a result of this environment, no evidence of extensive karstification was observed in the study area.

Because pores in the vadose zone are not completely water filled, any water that is present tends to be held between grains by capillary forces or under grains as pendant drops (Longman, 1980). As a result of this inhomogeneous water distribution, meniscus cementation occurred as bridge - like calcite cement that precipitated between non-skeletal grains (ooids) (Figure. 5.10A and 5.10B). This meniscus cementation can also be seen in SEM (Figure. 5.11). Since they precipitate as a bridge at the pore throat between grains without filling the whole pore space, meniscus cementation served to reduce permeability significantly.

5.3.2 Meteoric Phreatic Diagenesis

The meteoric phreatic diagenetic environment is the most important diagenetic environment in term of porosity evolution. Since the basic fuel for diagenesis is water, and pore spaces in the meteoric phreatic zone are completely filled with meteoric water, diagenetic processes are more intense and efficient in the meteoric phreatic environment than in the vadose zone above (Moore, 2013).

Features indicative of meteoric phreatic diagenesis observed within the carbonate succession of the study area are dominated by grain dissolution and equant calcite cementation. All depositional textures (grainstone, packstone, wackestone and mudstone) of the Dam Formation in the study area were affected by meteoric dissolution that led to great enhancement of the original porosity.

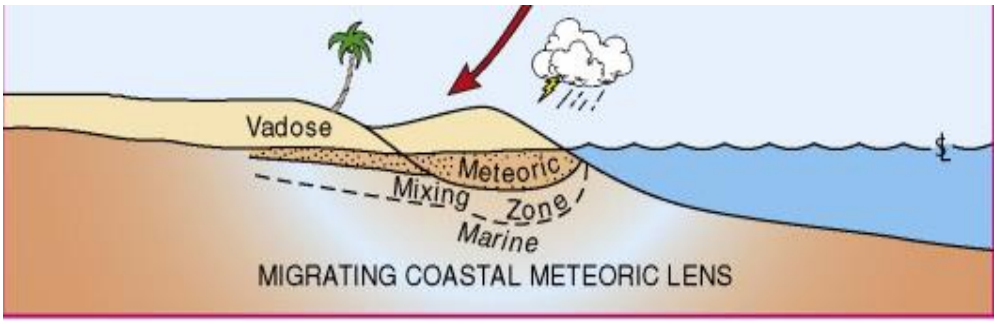

Figure 5.8: Sketch diagram show the vadose diagenetic environments at the top of the phreatic diagenetic environment (from Moore, 2013).

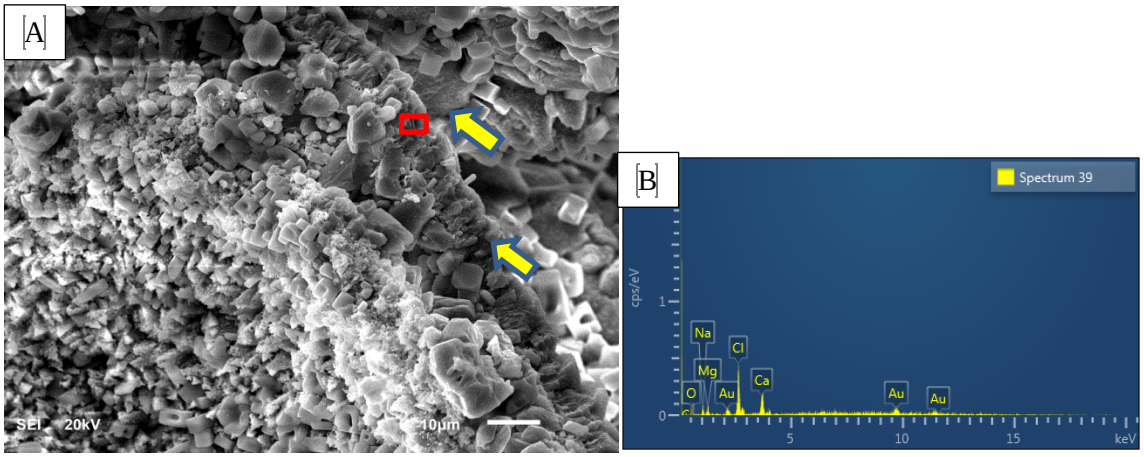

Figure 5.9: Evaporite (halite) cementation (yellow arrows) at the grain margins as shown by SEM photomicrograph (A) and EDS analysis (B).

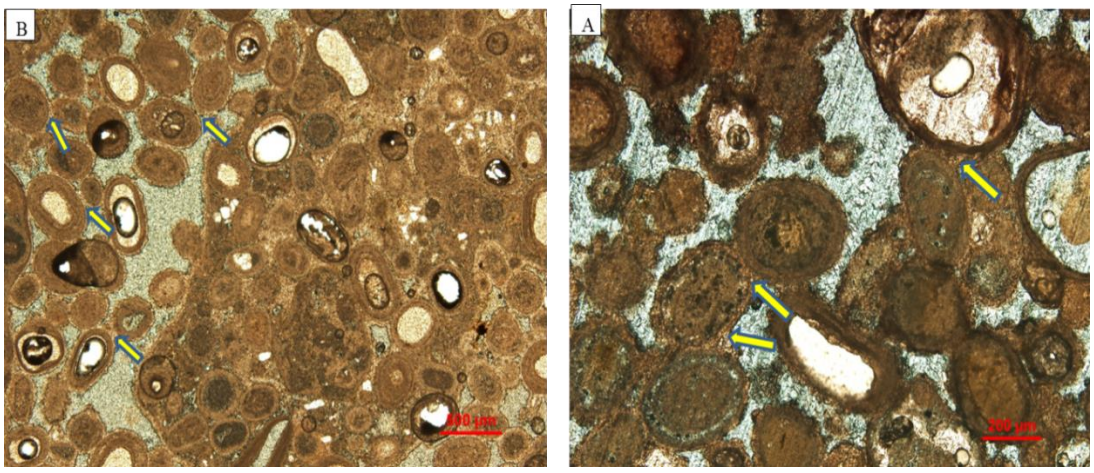

Figure 5.10: (A) Thin-section micrograph shows meniscus cementation (yellow arrows) present as bridge-like cement between ooids within trough cross bedded oolitic grainstone (f 10), and (B) Intertidal grainstone (f 9).

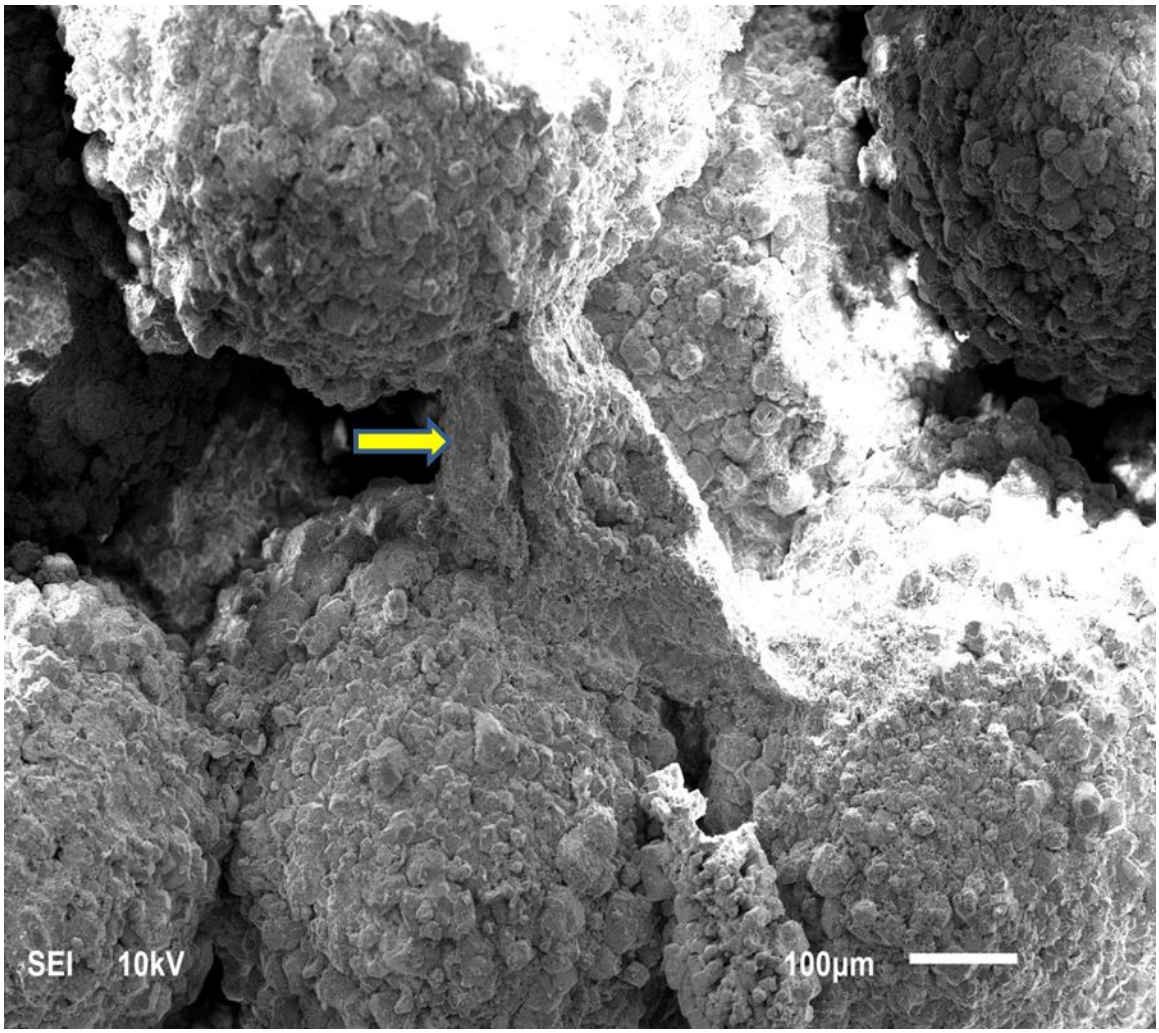

Figure 5.11: SEM photomicrograph shows the meniscus cement between two ooids (arrow).

5.3.2.1 Grain Dissolution

Almost all skeletal grains in the study area were dissolved and now occur as molds (Figure. 5.12A and 5.12B). The dissolution of the skeletal and non-skeletal grains is more prominent in the planar cross-bedded skeletal grainstone facies (f 8) at outcrop 2, and skeletal packstone facies (f 11) at outcrop 1 (Figure. 5.13A and 5.13B), where they underlie the interpreted exposure surface. This extensive dissolution led to generation of abundant secondary moldic and vug porosity. The beach grainstone facies (f 15) shows minor dissolution of the non-skeletal grains, but complete dissolution of the skeletal grains (Figure. 5.14A and 5.14B). Some forams such as miliolids and rotalids were preserved (Figure. 5.15A and 5.15B) and they were not affected by this dissolution.

Skeletal grains in the study area are dominated by bivalves, gastropods and foraminifera. Since the original mineralogy of these skeletal grains was composed of aragonite (Sellwood et al., 1985), the extensive dissolution of these allochems suggests that they were dissolved by undersaturated water with respect to aragonite, which suggests dissolution by meteoric water.

This preferential dissolution of skeletal grains is due to the fact that the original mineralogy of these grains (bivalves and gastropods) is dominated by aragonite, while the non-skeletal grains are cemented, during marine cementation, by high magnesium calcite that was, perhaps, altered to low magnesium calcite which was more resistant to meteoric dissolution.

Dissolution resistance of the observed forams is attributed to their original calcite mineralogy (Armstrong & Brasier, 2005).

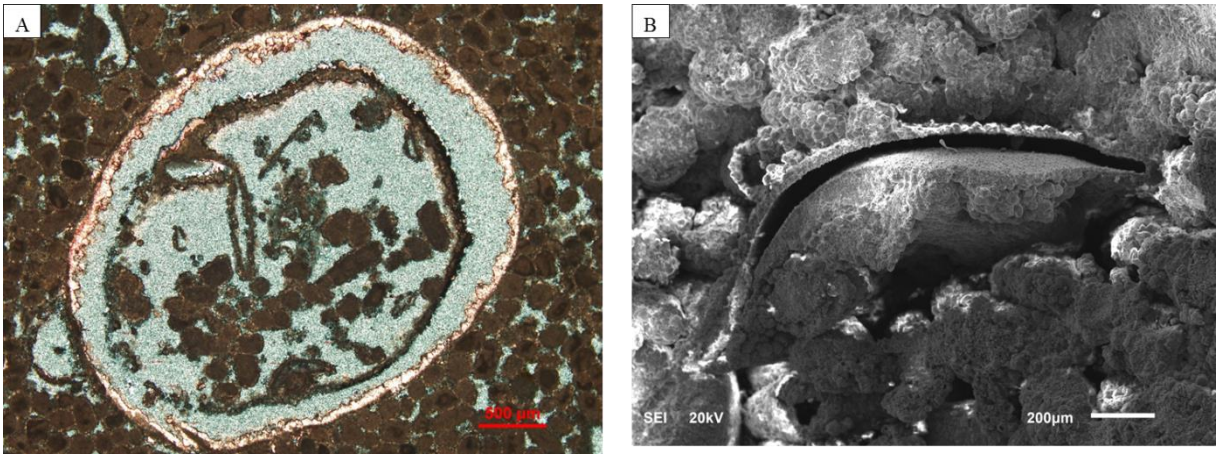

Figure 5.12: (A) Thin-section photomicrograph shows completely dissolved bivalve grain within beach grainstone facies (f 15). (B) Dissolved bivalve grain present as mold within peloidal grainstone facies (f 8).

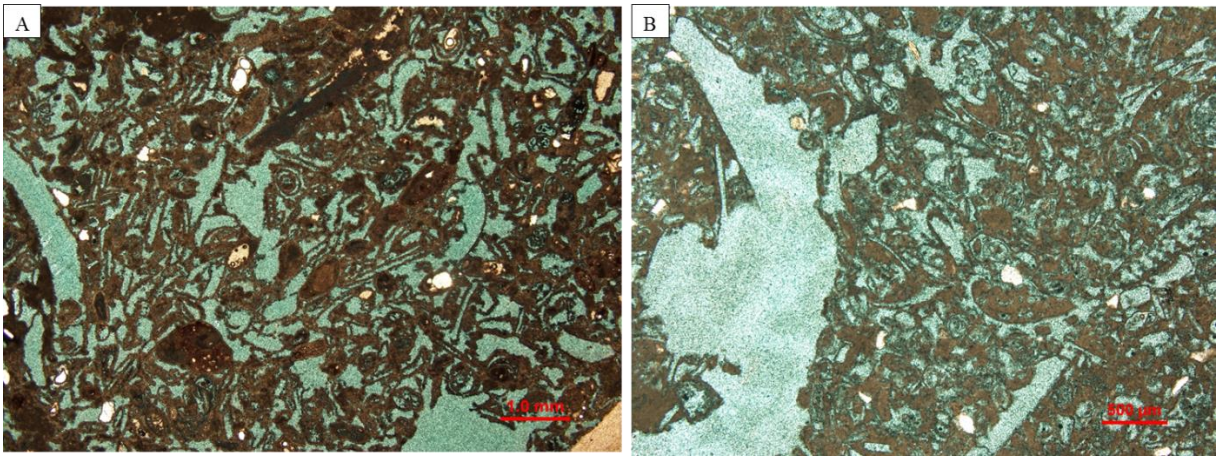

Figure 5.13: Extensive meteoric phreatic dissolution of the skeletal and non-skeletal (ooids) grains of (A) planar X-bedded grainstone (f 8), and (B) skeletal packstone facies (f 11).

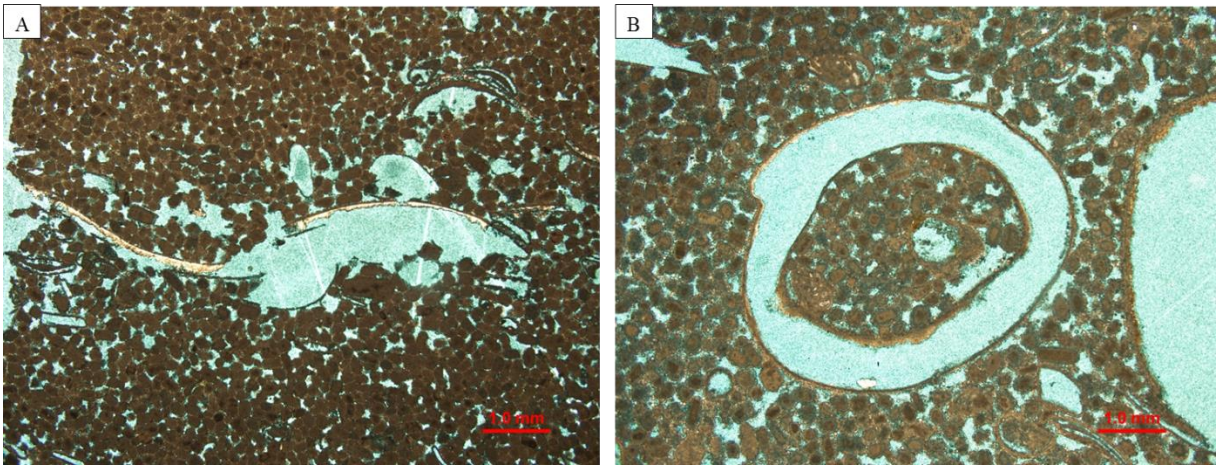

Figure 5.14: Preferential dissolution of skeletal grains (bivalves here) by meteoric waters forming moldic secondary porosity within the beach grainstone facies at outcrop 8 (A) and outcrop 23 (B).

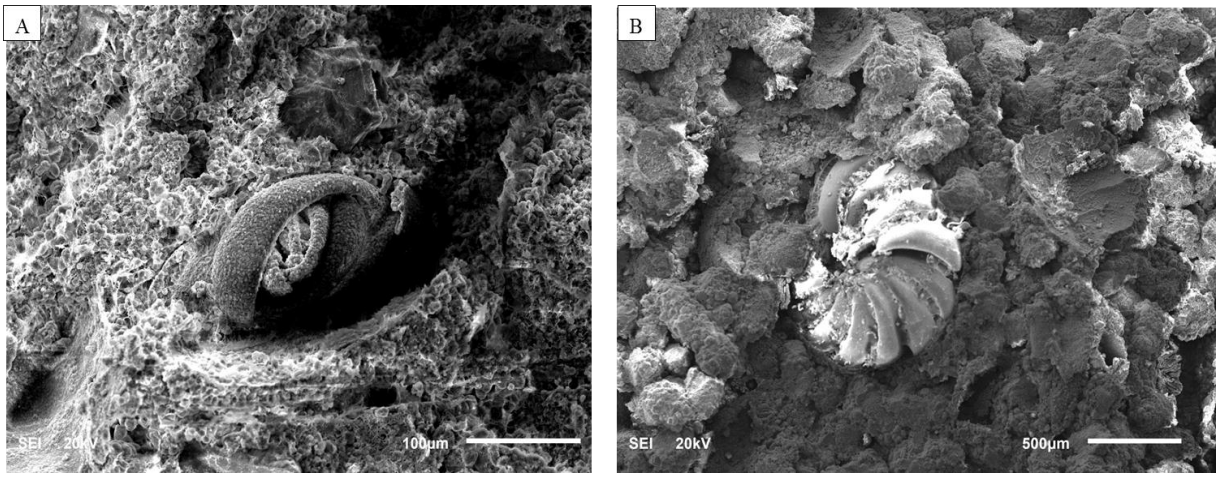

Figure 5.15: (A) Preserved calcitic miliolids foram within the massive quartz skeletal pelloidal wackestone facies (f 13). (B) Preserved calcitic rotalid within the beach grainstone facies (f 15).

5.3.2.2 Equant Calcite Cementation

As the dilute meteoric waters passed through the carbonate succession they dissolved most of the metastable carbonate minerals forming moldic and vuggy porosity that enhanced the original porosity. Moving downward, the meteoric water became more saturated with respect to calcium carbonate, and started to precipitate equant calcite cement on the grains as well as within the molds occluding both the original inter-granular and secondary moldic porosity (Longman, 1980; Moore, 2013).

Most of the grainstone facies (f 8, f 9, f 10, f 12, and f15) were affected by this cementation (Figure. 5.16A and 5.16B), while the wackestone - packstone facies (f 11, f 13 and f 14) shows infrequent equant calcite cementation either on the grains or within the molds (Figure. 5.17A and 5.17B). In the beach grainstone facies (f 15), equant calcite cement was precipitated within the skeletal molds (Figure. 5.18).

The rare precipitation of equant calcite within wackestone - packstone facies can be attributed to the low permeability of this facies that hindered the movement of $CaCO_3$-oversaturated solution through the open pore spaces and precipitate the cement. In addition to low permeability, most of the packstone and wackestone lithofacies are far from the interpreted exposure surface, which suggest less influence of meteoric water.

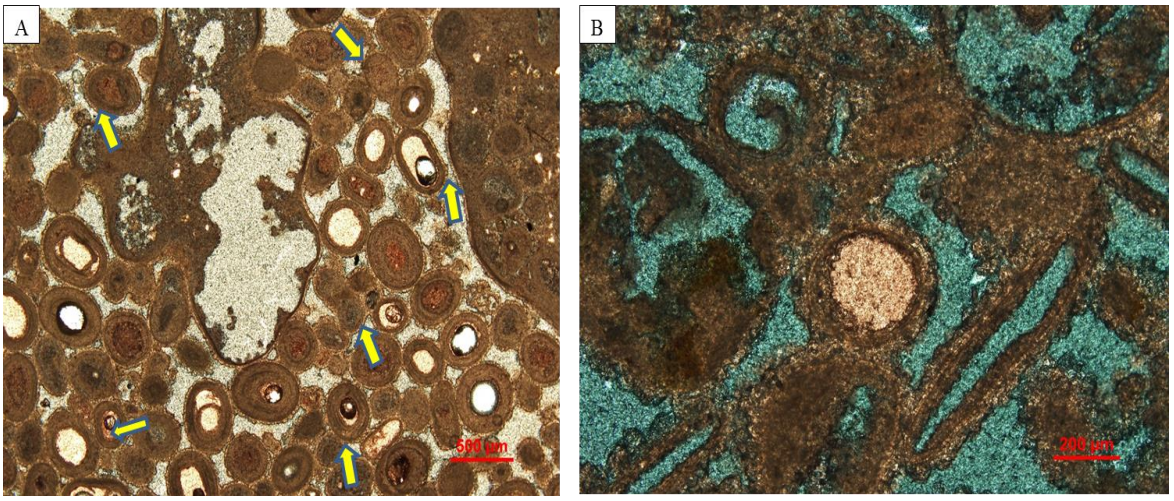

Figure 5.16: Thin-section photomicrograph shows equant calcite precipitation (arrows) on ooids surfaces as well as within oomoldic pores of (A) aggregate oolitic grainstone facies (f 10), and (B) herringbone skeletal oolitic grainstone facies (f 8).

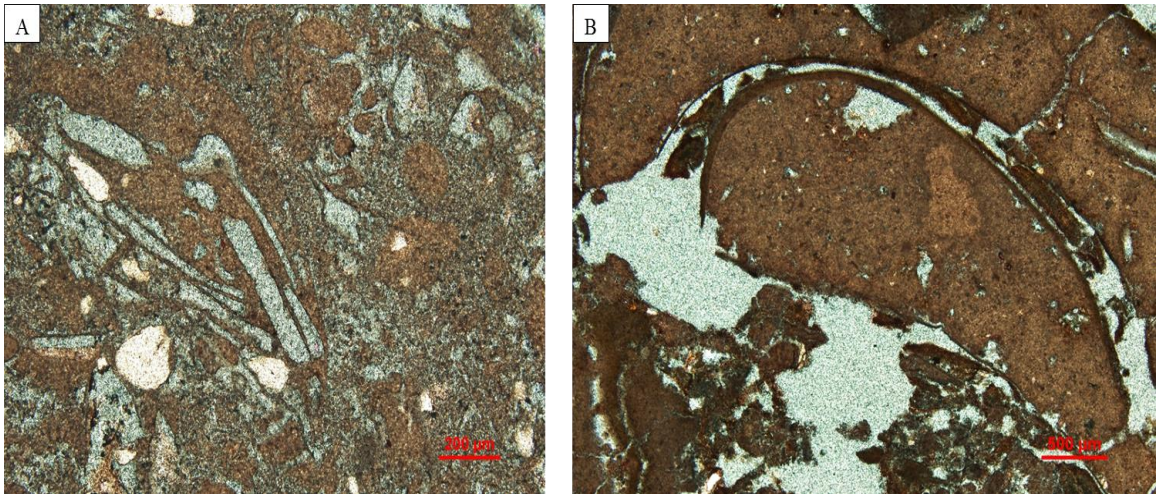

Figure 5.17: Thin-section photomicrograph shows no precipitation of equant calcite within the skeletal molds of (A) quartz pelloidal wackestone (f 13), and (B) Peloidal skeletal packstone.

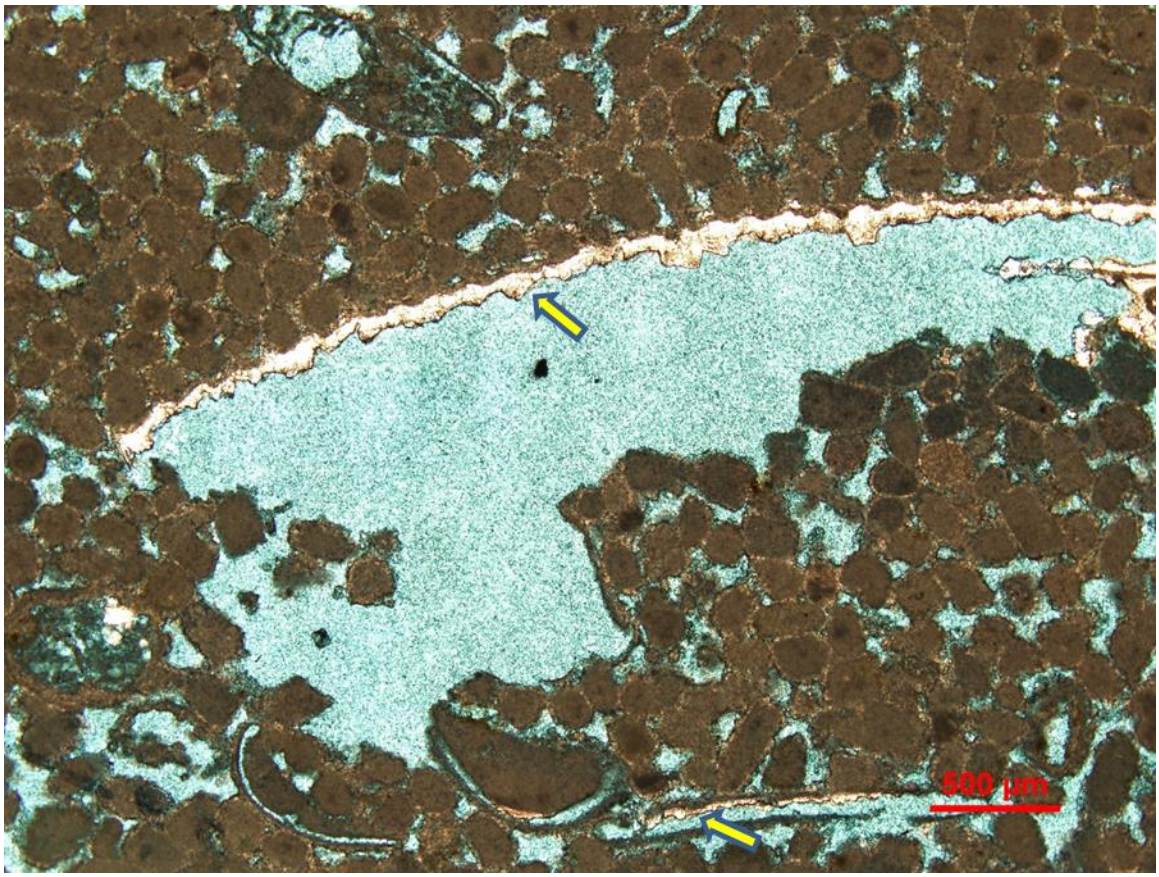

Figure 5.18: Thin-section photomicrograph showing equant calcite cement crystals precipitated in a bivalve mold of beach grainstone facies (f 15).

5.4 Burial Diagenesis

Most burial diagenesis processes lead to the destruction of porosity (Tucker, 1993). These processes include burial cementation, compaction, pressure solution and fracturing. Burial of non-cemented carbonate sediment under increasing overburden results in compaction and pressure solution (Flügel, 2010). The major burial diagenetic processes that affected the Dam formation in the study area are mechanical compaction and fracturing.

In the grainstone facies, mechanical compaction is represented by different grain contact textures. The beach grainstone facies (f 15) shows no features of mechanical compaction. This can be attributed to the early cementation that prevented the grains from compaction. In the lower parts of the section (outcrop 2, 23, and 16), mechanical compaction is represented by tangential grain contacts. In addition to tangential contact, sutured contacts were also observed between the ooids of the herringbone x-bedded skeletal oolitic grainstone facies (f 8) (Figure. 5.19A), that reduced the intergranular porosity. Another mechanical compaction feature was observed, in the upper part of outcrop 16, as concavo-convex contact between the skeletal grains (Figure. 5.19B) which indicates a higher grade of compaction regime (Flügel, 2010). Fracturing of carbonate matrix and grains was also found in the study area, but this was restricted to the wackestone and packestone facies (Figure. 5.20A). This can be attributed to the fact that the grainstone facies were subjected to calcite cementation, which prevented the grains from being crushed during burial, more than the mud-dominated facies (Shinn, 1983; Moore, 2013). Or could be a result of greater preserved interparticle porosity in the grainstones that allowed for grain re-orientation during burial, to accomodate increasing overburden stress.

These fractures were partially filled with evaporites (halite), as indicated by SEM-EDS, during later diagenetic processes (Figure. 5.20B).

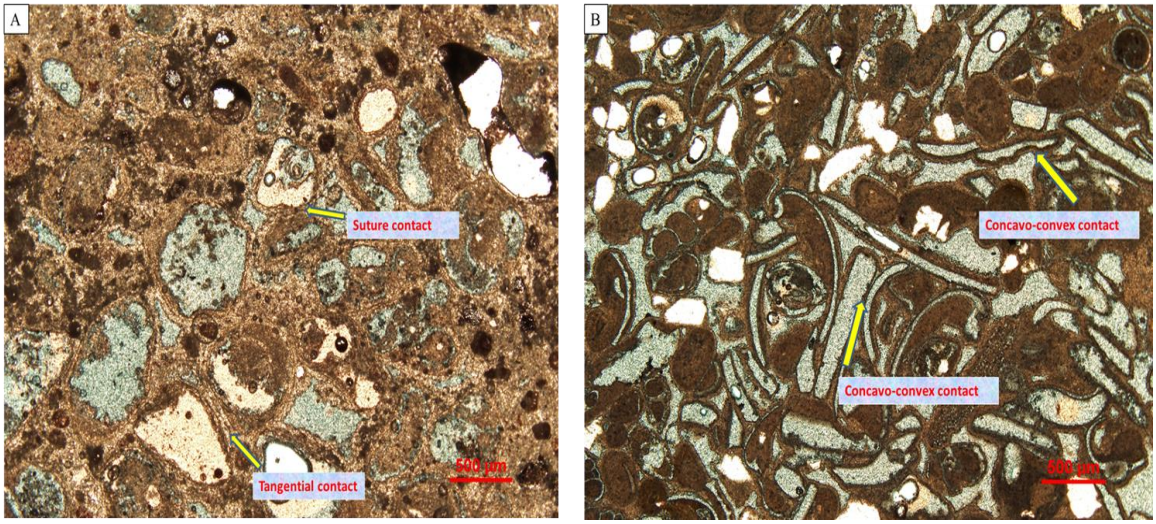

Figure 5.19: Thin-section photomicrographs show several mechanical compaction features observed at grain contacts including (A) tangential and sutured contacts, and (B) concavo-convex grain contacts.

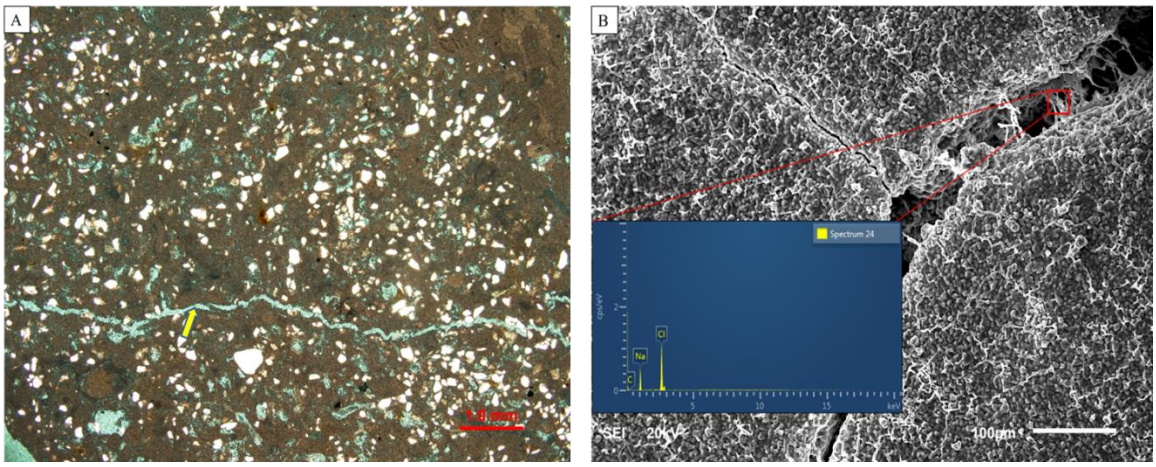

Figure 5.20: (A) Thin-section photomicrograph showing the burial fracturing that occurs in the quartz wackestone facies (f 13). (B) SEM photomicrograph shows the partial filling of the fracture by halite as indicated by EDS.

5.5 Dolomitization

Dolomite is a complicated mineral in terms of its crystal structure and should precipitate from seawater but it does not. Dolomite rocks are typically porous and represent about 50% of carbonate hydrocarbon reservoirs worldwide (Warren, 2000), thus they are a target in petroleum exploration (Tucker & Wright, 1990b).

The most important factors in dolomite precipitation are; source of magnesium Mg^{2+}, and the process by which the dolomitizing fluid is pumped through the carbonate succession (Tucker, 1993). Although seawater is supersaturated with respect to the dolomite, it does not commonly precipitate directly from seawater due to kinetic obstacles (Tucker & Wright, 1990b). The most important of these are; the high ionic strength of the seawater and the fast carbonate precipitation rate, hydration of Mg^{2+} ions and the low activity of CO_3^- ions (Tucker & Wright, 1990b). Dolomite is a highly ordered mineral, hence the simple structural minerals such as aragonite and high-magnesium calcite precipitate preferentially from seawater (Tucker & Wright, 1990b).

Most dolomite rocks in the geological record are of two types; (1) the relatively abundant, dolomite of replacement origin, and (2) the rare primary dolomite of direct precipitation (Hsu, 1967; Tucker & Wright, 1990b).

Replacement dolomite crystals form in different textures that range from euhedral to anhedral, with terms xenotopic, idiotopic and hypidiotopic referring to the mosaic (Fig. 5.21) (Gregg & Sibley, 1987).

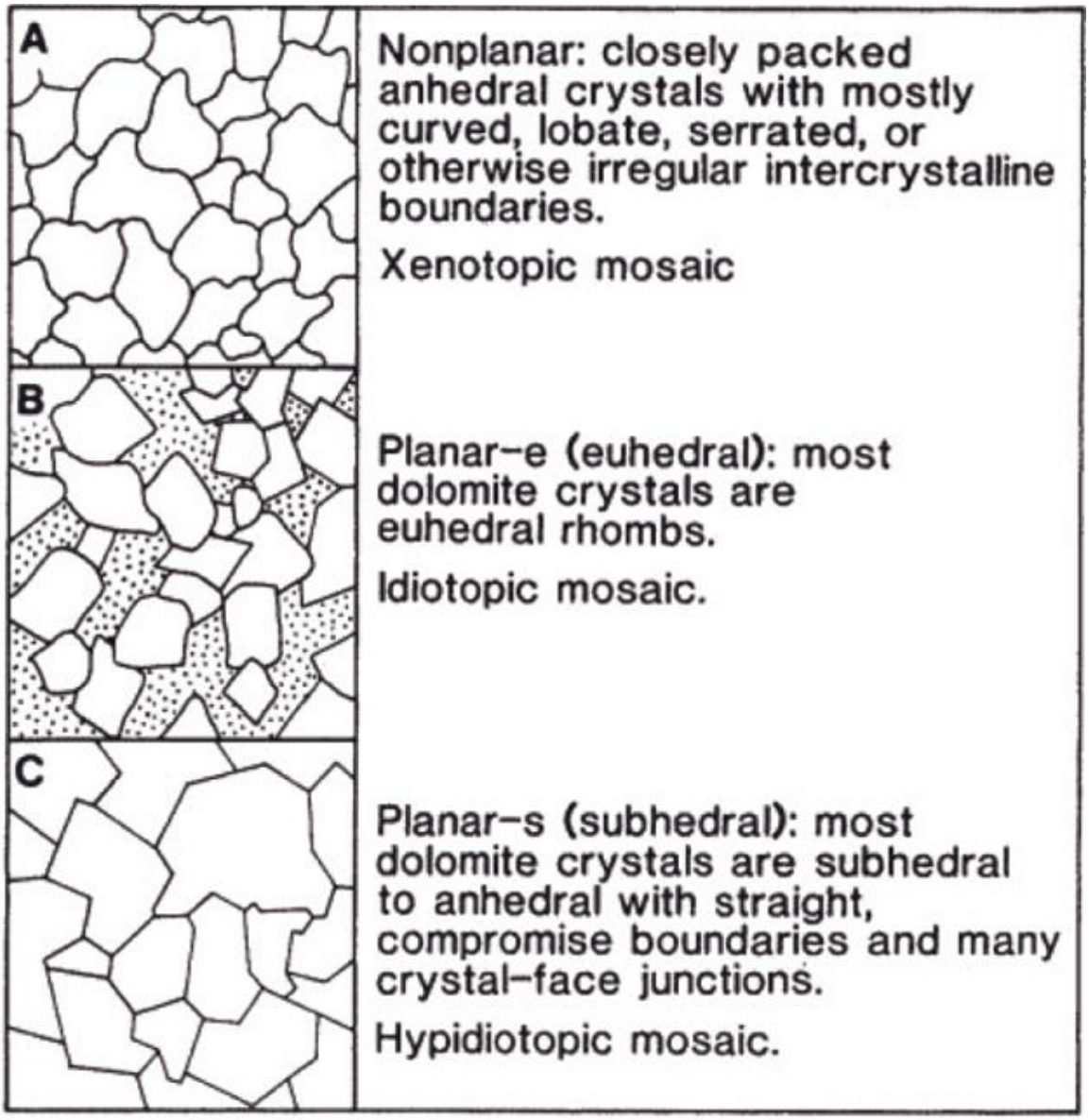

Figure 5.21: Three common dolomite textures. (A) Non-planar crystals in a xenotopic mosaic. (B) Planar-e crystals (e for euhedral) in idiotopic mosaic. (C) Planar-s crystals (s for subhedral) in hypidiotopic mosaic. (From Gregg & Sibley, 1987).

Replacement of calcite by dolomite can be fabric retentive or destructive, depending on the grain original mineralogy, crystal size, timing and nature of dolomitizing fluids. High-Mg calcite and aragonite grains can be dolomitized with good fabric retention, relative to low-Mg calcite grains (Tucker & Wright, 1990b).

Dam Formation carbonates in the Al-Lidam area are pervasively dolomitized with good fabric retention as indicated by optical microscopy, X-Ray Diffraction (XRD) and Scanning Electron Microscopy (SEM). These dolomites have textures that range from fine grained crystalline dolomite to coarsely crystalline dolomite (Lumsden & Chimahusky, 1980 classification).

Most bivalves and gastropods are replaced by mimetic dolomite, while the ooids nuclei are replaced by medium to finely crystalline dolomite (Figure. 5.22A, B and D).

In the more grainy facies, the skeletal and non-skeletal grains are dolomitized with good fabric retention due to their original mineralogy (aragonite and high magnesium calcite) (Land & Epstein, 1970; R. C. Murray, 1960). The mudstone facies is preferentially dolomitized, as indicated by XRD, with retention of sedimentary structures which resulted in fine grained dolomite replacement of the precursor calcite (Figure. 5.22C). Similar cases of lime mud dolomitization is documented from modern supratidal dolomites (Shinn, 1983).

Dolomite also occurs as cement between the dolomitized skeletal and non-skeletal grains as well as cement that fills the dissolved skeletal molds (Figure. 5.23A). It also occurs as single isopachous layer of large (> 20 μm) anhedral rhombs lining the molds of bivalves grains (Figure. 5.23B).

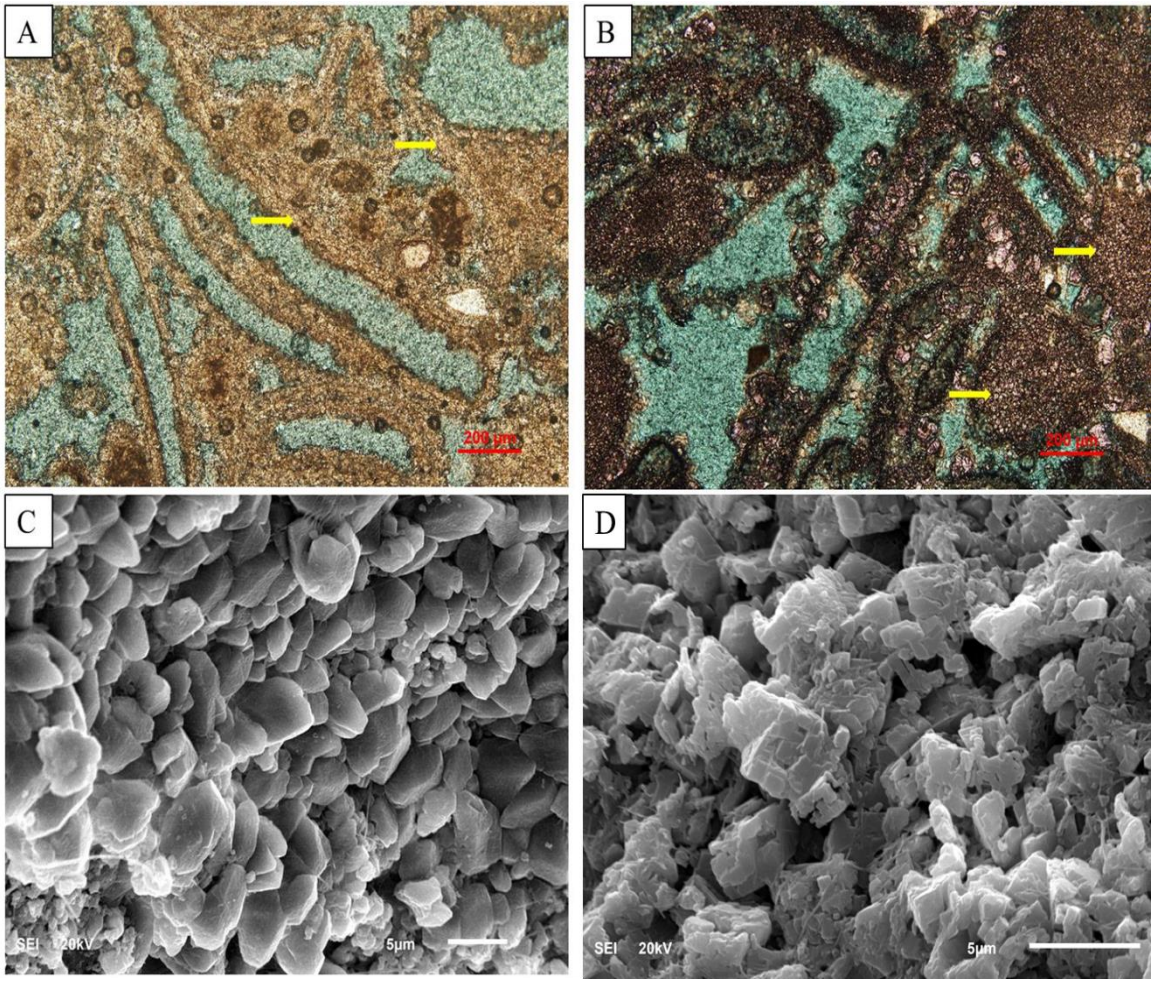

Figure 5.22: Thin-section photomicrographs show coarsely crystalline dolomite (arrows) in a xenotopic mosaic within skeletal grains (A) and ooids (B) of skeletal oolitic grainstone f 9 with good fabric retention. (C) SEM photomicrograph shows anhedral finely crystalline dolomite crystals of dolomitized mudstone lithofacies. (D) SEM photomicrograph shows subhedral finely crystalline dolomite crystals of skeletal oolitic grainstone lithofacies (f9).

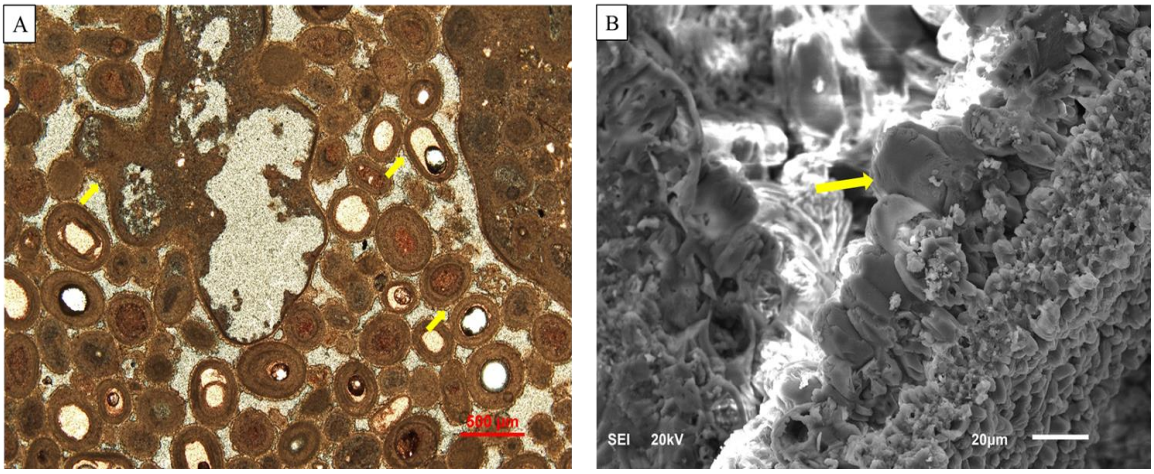

Figure 5.23: (A) Thin- section photomicrograph shows isopachous dolomitic cement coating the ooids of the skeletal oolitic grainstone lithofacies f 9. (B) SEM photomicrograph shows anhedral coarsely crystalline dolomite growing toward the center of the interparticle pores and lining the oomolds of the same lithofacies (f 9).

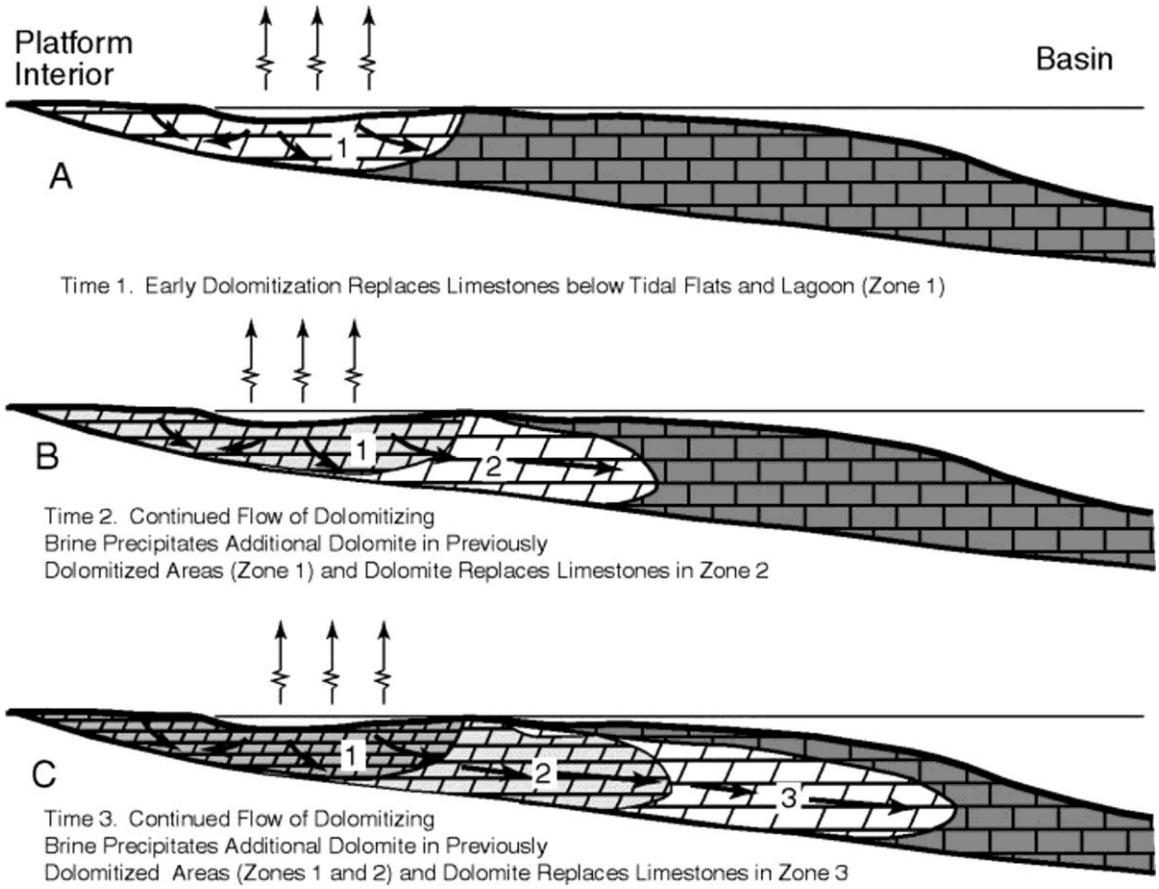

Figure 5.24: Proposed Sabkha–Evaporative dolomitization model for the Dam Formation dolomites in the Al-Lidam area (from Saller and Henderson, 2001).

The association of the study area's dolomites with evaporite minerals (gypsum, anhydrite and halite) as in f 2 suggests that dolomitization could have occurred as a result of evaporation and increasing Mg/Ca ration in descending pore fluids, as proposed by the evaporative-sabkha dolomitization model of Tucker & Wright (1990b) (Figure 5.24).

In this model, water is mainly supplied to the supratidal flats by high tides and storms. During summer seasons, intense heat over sabkha results in evaporation of seawater and precipitation of evaporite minerals; gypsum ($CaSO_4$. $2H_2O$) and anhydrite ($CaSO_4$). This process consumes the available Ca^{2+} ions and increases the Mg^{2+}/Ca^{2+} ratio in the pore fluids, which triggers the dolomitization process. Another related factor facilitating dolomitization is that evaporite minerals precipitation served to reduce the sulphate content of the pore fluids by incorporating SO_4^{2-} ions in the crystal lattice of gypsum and anhydrite. The remaining pore fluids with high Mg^{2+} and lower SO_4^{2-} content can then become powerful dolomitizing agents as they descend downward through underlying carbonate layers.

Relics of coccoid microbial fossils were also found under SEM (Figure 5.25), which also support the sabkha dolomitization model. These microbial fossils represent a type of cyanobacteria that can survive under sabkha conditions(Maliński et al., 2009).

Using XRD data, the ordering degree and stoichiometry of dolomites in the study were noticed to generally increase westward from outcrop 2 in the east toward outcrop 16 in the west (Figure 5.26) which also support the dolomitization by sabkha evaporative model

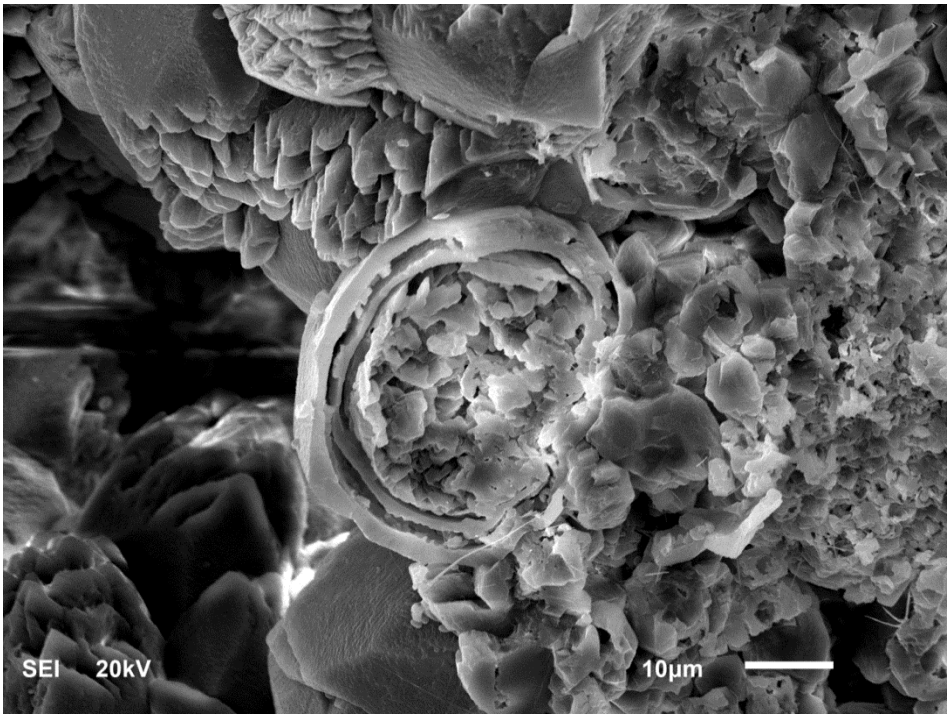

Figure 5.25: SEM photomicrograph shows a relic of coccoid microbial fossil as indicative for sabkha environment.

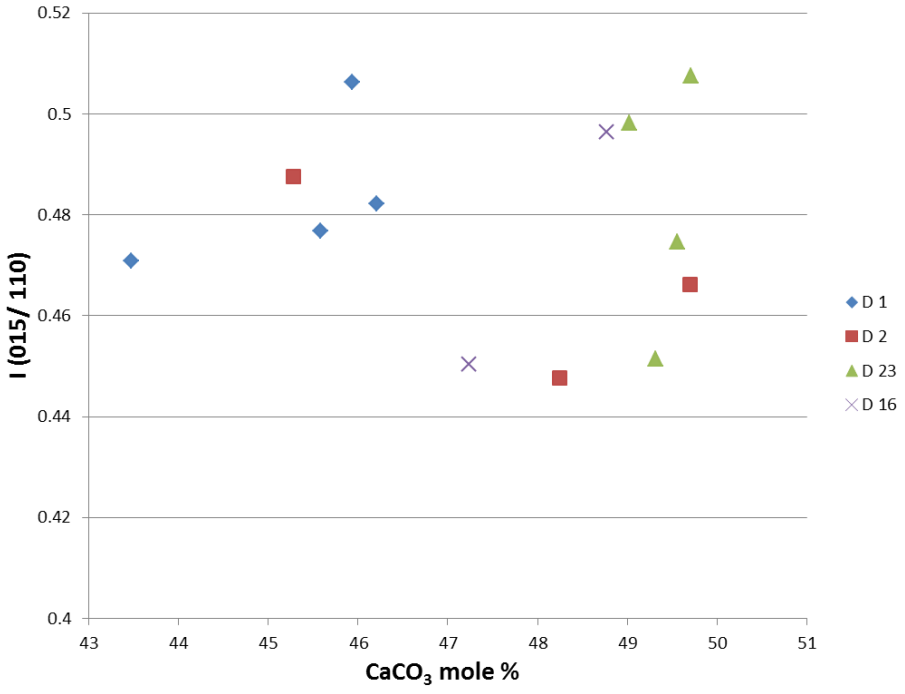

Figure 5.26: Stoichiometry and ordering of representative dolomite samples showing general increasing westward (From outcrop 2 (D 2) in the east toward outcrop 16 (D 16) in the west)

5.6 Clay Minerals Precipitation

Clay minerals including palygorskite and illite were observed in the study area and occur as pore filling phases. These minerals were observed, from SEM, in the massive quartz skeletal wackestone (f 13). Palygorskite was also noticed, from XRD, within the intertidal oolitic grainstones (f 8 and f 9) (Figure 5.27C). The presence of palygorskite, illite and kaolinite in some Paleogene formations of Saudi Arabia and Bahrain have been reported by Shadfan et al. (1985) and Çağatay (1990).

Palygorskite has also been reported from subsurface Neogene strata of Kuwait (Mishra et al. 2012). In the study area, palygorskite occurs as interwoven fibrous mats that fill the pore spaces or bridge between the grains (Figure 5.27A). Illite occurs as fibers that coat the calcite grains and grows into the pore spaces (Figure 5.27B) to significantly reduce permeability.

The origin for these minerals precipitation is interpreted as the dissolution of potassium K-feldspar, which was also observed from SEM (Figure 5.28), by meteoric waters to provide source of aluminum and silicate (Bjørlykke, 1998); dissolution of dolomite from the skeletal grains is suggested to be the source of magnesium for palygorskite.

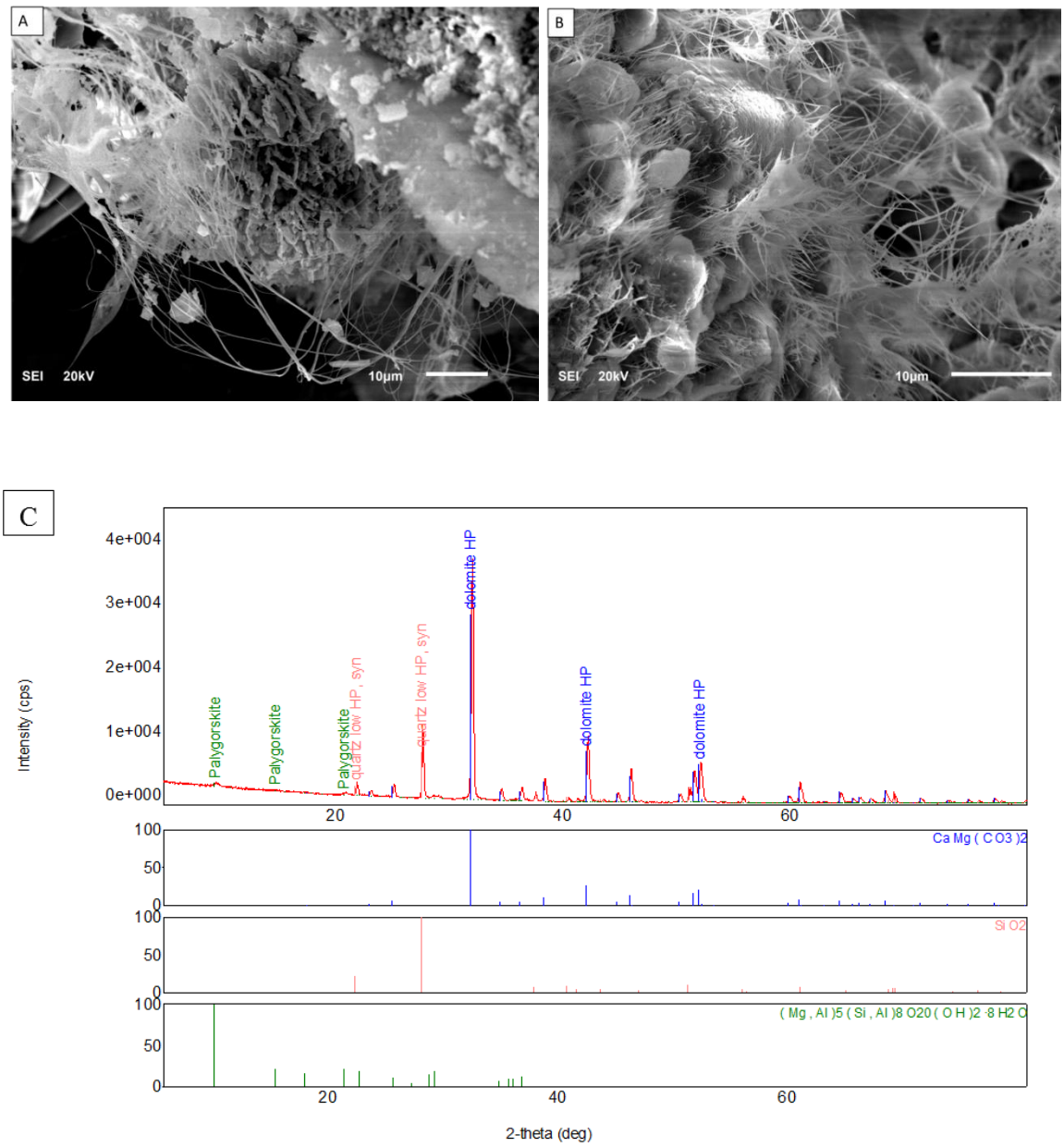

Figure 5.27: SEM photomicrograph shows (A) palygorskite mineral occurrence as fiber mats that fill the pore space, and (B) fibrous illite coating the calcite crystals and bridge between the grains. (C) XRD diffractogram shows the presence of palygorskite within the intertidal grainstone lithofacies (f 8).

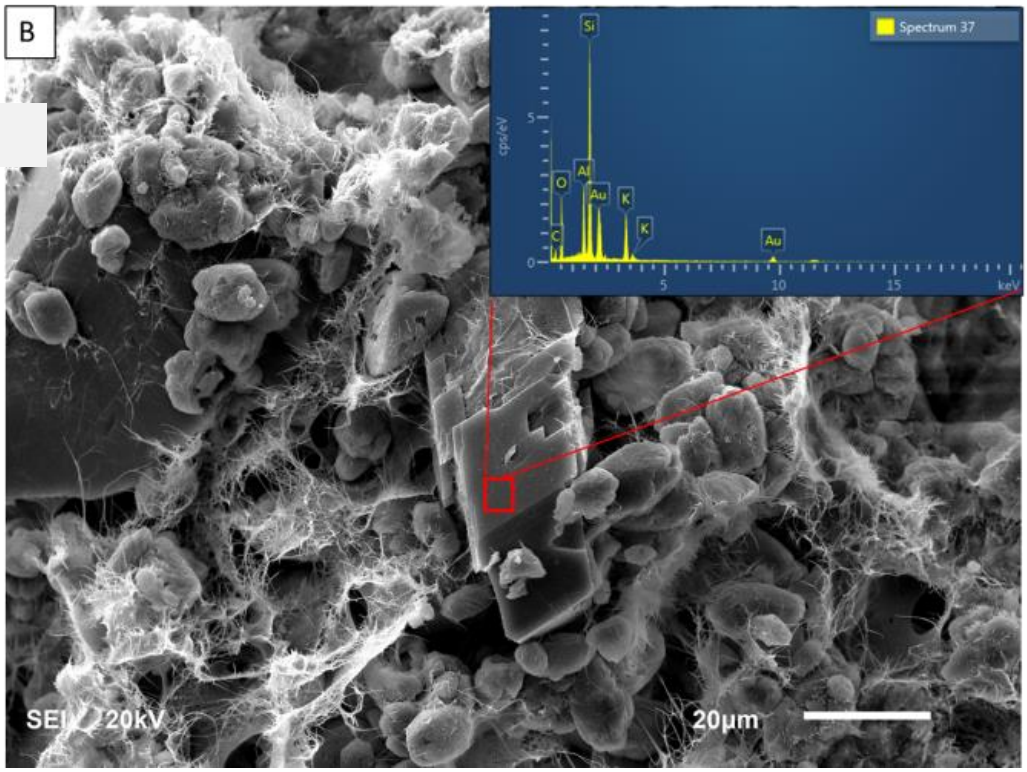

Figure 5.28: SEM photomicrograph showing K-feldspar crystal, and SEM-EDS elemental analysis, with some partial dissolution.

5.7 Paragenetic Sequence

The paragenetic sequence is the sequence in which the different diagenetic events occurred and altered the sediments. The sequence of diagenetic events in a carbonate system depends on factors such as the sediment itself, grain size and texture, mineralogy, nature of pore fluid and climate (Tucker and Wright 1990; Tucker 1993; Flugel 2004). Based on petrographic characteristics and geochemical results, the diagenetic processes that occurred in the Dam Formation in the Al-Lidam area are shown in (Figure 5.29).

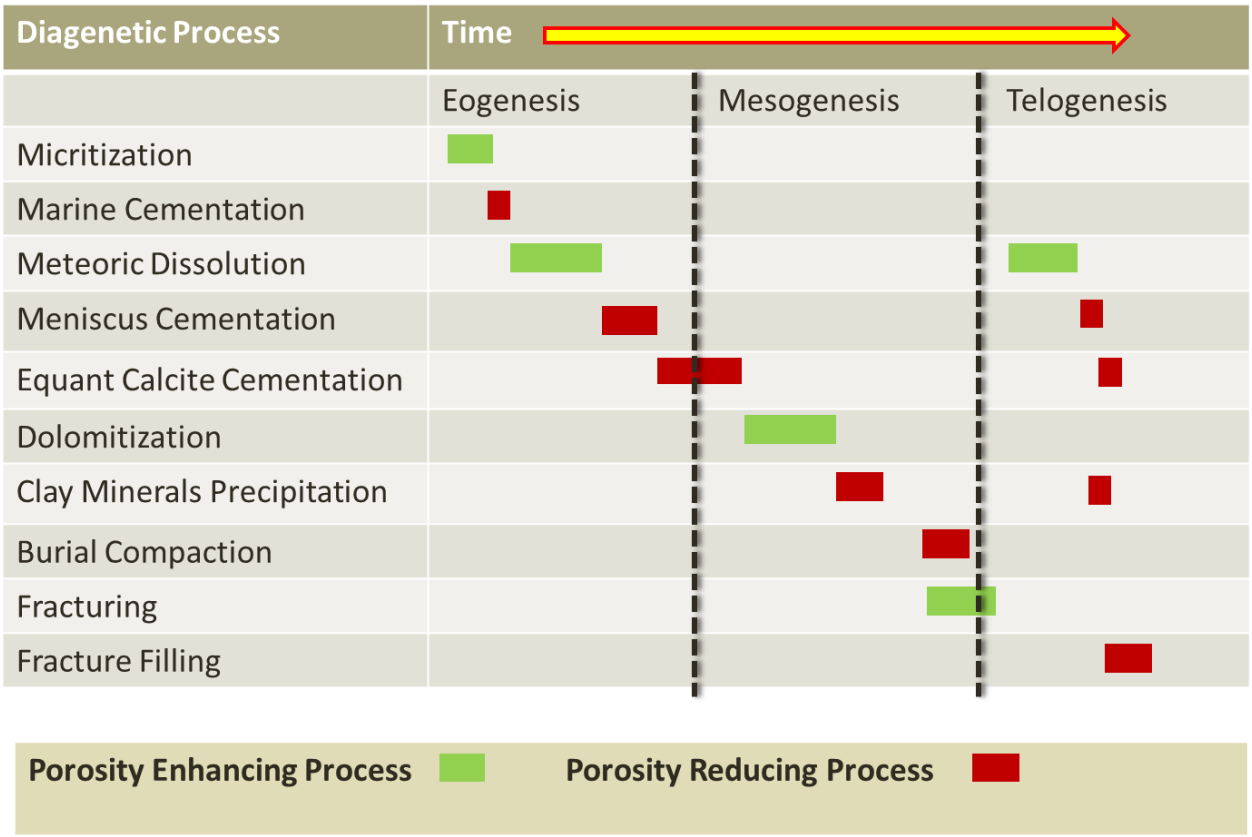

Figure 5.29: The paragenetic sequence of the Miocene Dam Formation in the Al-Lidam area.

CHAPTER 6

LINKING CARBONATE DIAGENESIS TO SEQUENCE STRATIGRAPHY

6.1 Introduction

Carbonate diagenesis is controlled by a series of complex, interrelated parameters. These are tectonic setting, depositional facies, original mineralogy of sediments and the paleo-climatic conditions (Morad et al., 2000; Worden & Morad, 2003).

Changes in relative sea- level drive changes in pore fluid chemical composition, as well as the duration of subaerial exposure, which in turn control the early mineralogical stabilization and porosity evolution. Therefore, carbonate diagenesis can be linked to the sequence stratigraphic framework (Tucker, 1993; Morad et al., 2013).

Using sequence stratigraphic models, sedimentary facies distribution and their original porosities and permeabilities can be predicted (Van Wagoner et al., 1990; Posamentier & Allen, 1999).

Putting carbonate diagenesis into sequence stratigraphic framework facilitates a better understanding of diagenetic patterns in limestone successions and permits a degree of prediction (Tucker, 1993).

6.2 Sequence Stratigraphy Concepts

Sequence stratigraphy is a framework of genetically related facies and their bounding surfaces that are used to determine depositional setting and to improve understanding of how stratigraphic units, facies tracts, and depositional elements relate to each other in time and space within sedimentary basins. The sequence stratigraphy approach can be applied to well logs, core or outcrop data and the interpretation can depend on different sets of data, but, the basic geometrical criteria for interpretation remain the same (Catuneanu, 2006).

The strength of this technique lies in its potential to predict facies within a chrono-stratigraphically constrained framework of unconformity-bound depositional sequences. The main procedure for constructing a sequence stratigraphic framework is to identify and delineate the bounding and subdividing surfaces (which are produced by accommodation changes). The changes in relative sea level make the sediments precipitate with different stacking patterns depending on the accommodation space available for accumulation. These various stacking patterns form the basic building blocks or units (parasequences, sequences and system tracts) of the sequence stratigraphy, with each one having its own distinctive stacking pattern and features.

These building units of the sequence stratigraphy framework will be briefly defined in the following context;

6.2.1 Sequence

A sequence was defined initially by Sloss (1949, 1963) as stratigraphic unit that is bounded by unconformities. This definition was modified by Mitchum (1977) who described the sequence as a genetically related stratigraphic succession that is bounded by unconformities and their correlative conformities.

6.2.2 Parasequence

A parasequence is a relatively conformable succession of genetically related beds or bed sets bounded by marine flooding surfaces and their correlative surfaces. In addition to these defining characteristics, most parasequences are asymmetrical shallowing-upward sedimentary cycles (Van Wagoner, 1995).

6.2.3 System Tract

A system tract is depositional systems formed in the same period of time and subdivides a sequence (Brown and Fisher 1977). Every system tract is characterized by its stacking pattern of strata and its position within the sequence and surfaces bounding it. Description of system tracts is as follow:

6.2.3.1 Lowstand System Tract (LST)

Is restricted between the lower sequence boundary (SB) and the transgressive surface (TS). Its sediments accumulate since the start of relative sea level to drop till the onset of transgression (Catuneanu, 2006).

6.2.3.2 Transgressive System Tract (TST)

Is bounded by transgressive surface (TS) and the maximum flooding surface (MFS), and its sediments accumulate from the onset of sea transgression till its maximum transgression; just before regression (Catuneanu, 2006).

6.2.3.3 Highstand System Tract (HST)

Is represents the top of the sequence and bounded by the maximum flooding surface (MFS) at the bottom and capped by the sequence boundary (SB) (Catuneanu, 2006).

6.2.4 Sequence Stratigraphy Surfaces

Sequence stratigraphic surfaces mark changes in stratal stacking pattern. They are surfaces that can serve, at least in part, as systems tract boundaries. These surfaces can be defined as follow;

6.2.4.1 Sequence Boundary (SB)

The SB is subaerial unconformity and/or its correlative conformity. Where it is an unconformity, it is represented by surface of subaerial exposure and erosion. In places, an unconformity may be marked by obvious erosion, such as a major incised channel or a beveling of structurally tilted underlying strata. It overlies the HST and underlies the LST (Posamentier and Allen 1999).

6.2.4.2 Maximum Flooding Surface (MFS)

The MFS marks the change in trend from a fining upward trend below to a coarsening upward trend above, and from deepening – upward to shallowing upward trend. It overlies the TST and underlies the HST (Posamentier and Allen 1999).

6.2.4.3 Transgressive Surface (TS)

The transgressive surface represents the first major flooding surface to follow the sequence boundary and is usually distinct from the relatively minor flooding surfaces that separate parasequences in the lowstand systems tract. It overlies the LST and underlies the TST (Posamentier and Allen 1999).

There are four main types of sequence models in sequence stratigraphy in practice. These are Exxon/van Wagoner et al. (1988), Embry (1993), Hunt & Tucker (1992), modified by Helland-Hansen and Gjelberg (1994) and Posamentier & Allen (1999) sequence model (Figure 6.1).

In this study, the sequence stratigraphic framework is established by another contemporaneous study (Bashari, 2015) using Posamentier & Allen (1999) sequence model.

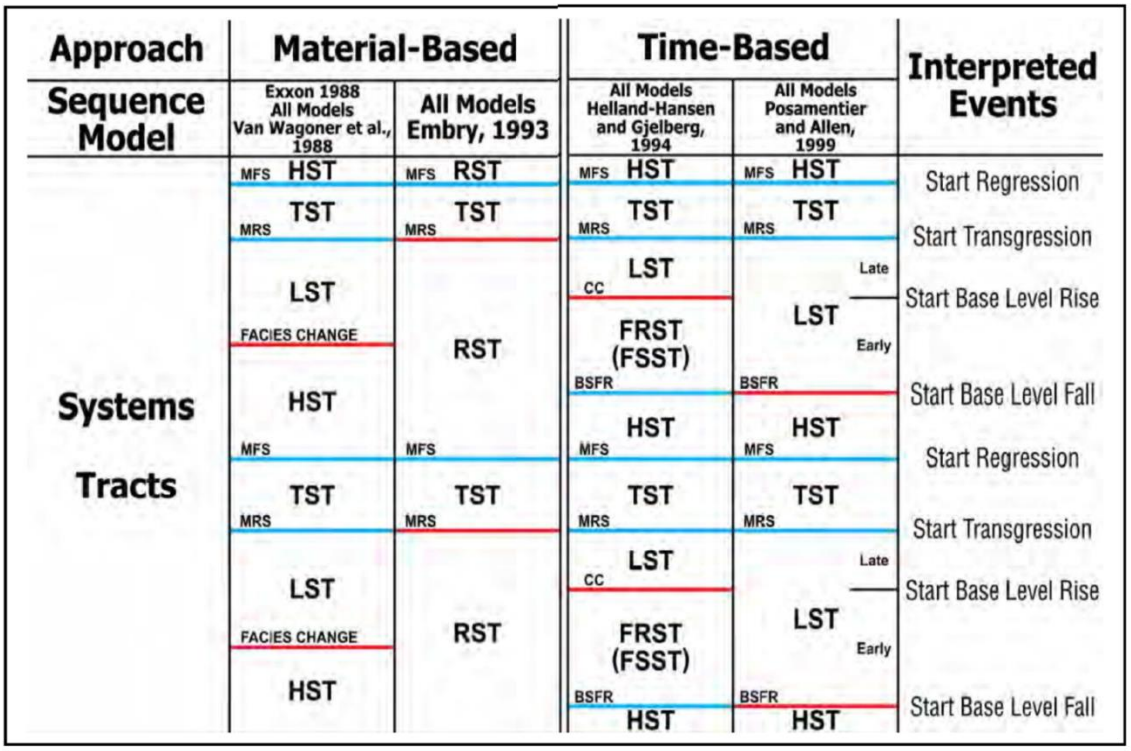

Figure 6.1: Schematic of different sequence models, with red lines represent sequence boundaries (after Catuneanu, 2006).

6.3 Sequence Stratigraphy of the Study Area

The Dam Formation lies within a tectonostratigraphic mega sequence (TMS AP 11) (Sharland, et al., 2001). This TMS lies between two unconformities marking both the onset of the Red Sea opening and the collision initiation between Eurasia and the Arabian Plate as lower boundary (Beydoun, 1993), and the present topographic surface as top boundary. This TMS also includes major geologic events; subsidence occurred in the eastern part of the plate due to the Zagros imbricated thrust sheets loading, while the western parts were uplifted thermally. This resulted in gradual change in the foredeep basin sedimentology from carbonates to continental clastics. The Dam Formation has been interpreted as a 3rd order sequence and carbonates near its base are correlated to MFS Ng20 (Sharland et al., 2001).

In the study area, three major 4th order sequences were recognized within the exposed outcrops of the upper Dam Formation, these are, from bottom to top; DLS 1, DLS 2 and DLS 3. The upper sequence DLS 3 and the lower sequence DLS 1 are not bounded at the top and bottom, respectively, by a sequence boundary. The only complete sequence in all studied sections is the middle one DLS 2 which is bounded at the bottom by sequence boundary (SB 1) and at the top by sequence boundary (SB 2). The two sequence boundaries are associated with subaerial exposure markers in addition to the depositional facies change from shallow to deeper water setting. Such markers are indicators for relative sea level changes.

In all the studied outcrops, the lower sequence boundary (SB 1) is associated with deposition of sabkha evaporites and mud (Figure 6.2A). In addition to sabkha deposits, rhizoliths were also found as an indicator for subaerial exposure (Figure 6.2B). These deposits are underlain by the coarser, oolitic and skeletal grainstones of shallow marine setting, indicating change in the depositional trend as well as in the relative sea level.

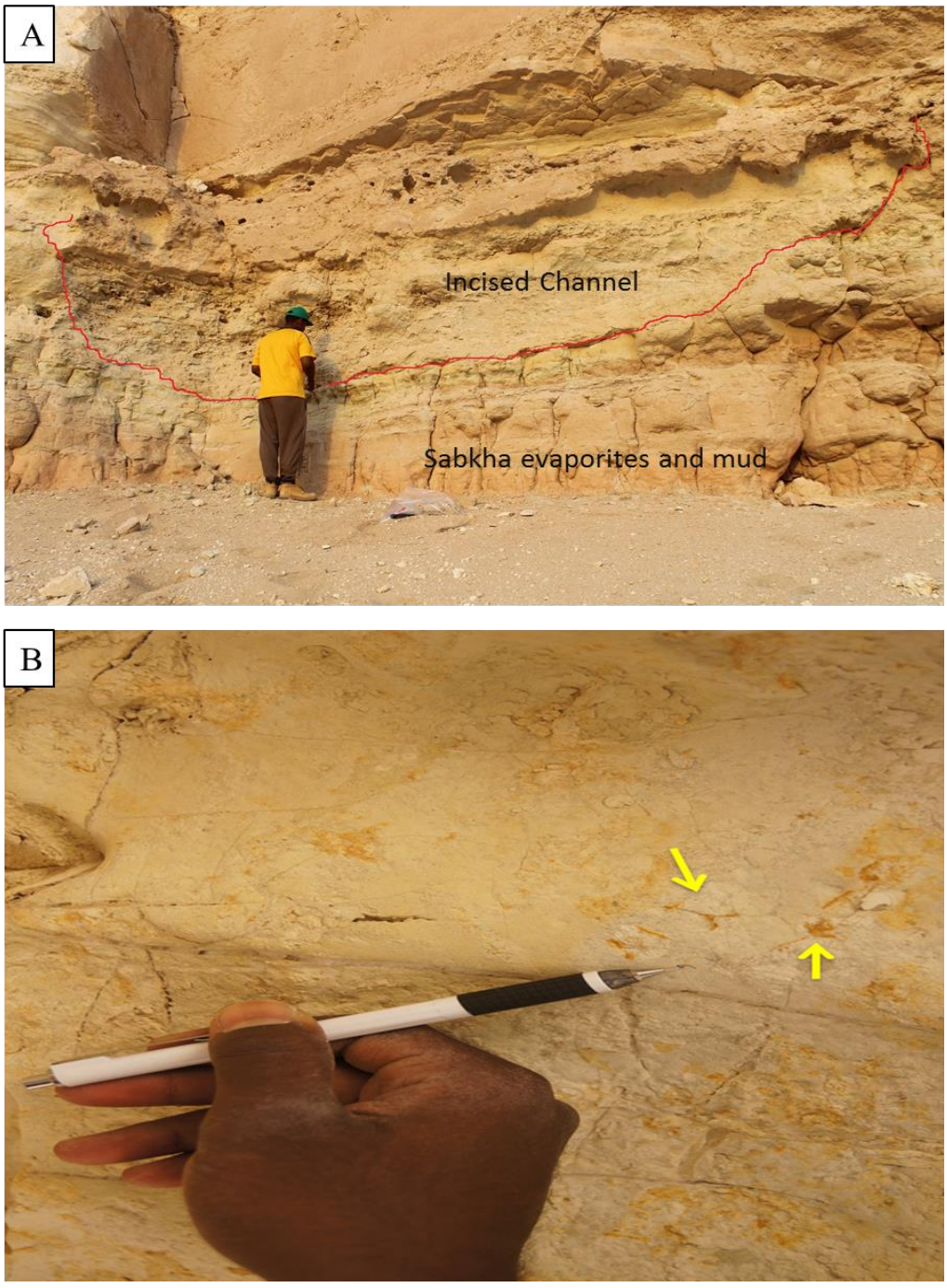

Figure 6.2: Sequence Boundary (SB 1) indicators. (A) Sabkha deposits and incised channel indicates drop in relative sea level. (B) Rhizolith (arrows) in the mud of mud-evaporite facies as indicator of exposure.

In outcrop 23, SB 1 is associated with incised channel which is filled by fine grained, extensively bioturbated silty sandstone (Figure 6.2A). The presence of incised channel suggests drop in the relative sea level. The incised channel and the mud-evaporite lithofacies represent the earliest stage of the low stand system tract (LST 2) where the relative sea level was at the lowest point.

The late (LST 2) shows evidences of relative sea level rising with the deposition of intertidal siliciclastics (f 4). This stage reaches in a depth wise, in outcrop 16, subtidal upper shoreface sandstone facies (f 7) conditions. The intertidal mud-sandstone interbedding show three thickening upward sequences, which goes parallel with the proposed increase in the accommodation space, and is typical to the late LST (Catuneanu et al., 2011).

Going upward stratigraphically, thick, fine carbonate wacke-packstone (f 13) with erosive sharp base (Figure 6.3A), sometimes with intra-formational pebbles, mainly of mud clasts and locally of stromatolites (Figure 6.3B), was deposited. This change, from supratidal sabkha deposits and intertidal interbedded siliciclastics to subtidal lower shoreface wacke-packstone facies indicates increase in the accommodation space.

Consequently, the erosive base was interpreted as the transgressive surface (TS 2), and the thick wacke-packstone facies represents the transgressive system tract (TST 2). The maximum flooding surface (MFS 2) is represented in the middle of thickest layer of the wacke-packstone facies (which is regarded as the deepest facies in the whole succession).

The highstand system tract (HST 2) is dominated by shallowing, thinning upward carbonate parasequences. This HST is characterized initially by the wacke-packstone facies and is then followed by different skeletal peloidal/oolitic grainstone shallower facies deposited in upper shoreface, foreshore and intertidal zones (f 8, f 9, f 10, f 11, f 14, f 15).

Figure 6.3: Transgressive surface with erosive base (arrows) above the mudstone of LST 1(A) and ravinement surface with stromatolite clasts (B) (arrow).

Thinning upward indicates a decrease in the accommodation space upward, which goes parallel with properties of the HST (Catuneanu et al., 2011).

At the top of the HST 2 facies, thin supratidal mud flat facies (probably part of f 2) is found containing mud cracks (Figure 6.4A). In addition to mud cracks, rain drop impressions were also observed in the skeletal oolitic grainstones at the top of HST 2 (Figure 6.4B). Both of these features are indicators of subaerial exposure and they suggest that a sequence boundary SB 2 immediately overlies them.

Immediately overlying the supratidal mud facies is a transgressive ravinement surface. This surface represents the TS 3 of the upper sequence while the thin mud bed underlying TS 3 can be interpreted as the LST 3. Although this upper sequence is not complete and its upper boundary has been eroded away, but we can still delineate the MFS 3 in it because its parasequences show the gradual thinning and shallowing upward character of the HST. The MFS 3 could be put in the middle of the deepest bed (f 13) at the beginning of the sequence. The lower sequence DLS 1 doesn't show anything other than thinning & shallowing upward shallow carbonate parasequences similar to those representing the HST in the lower and the upper sequences.

6.4 Carbonate Diagenesis within a Sequence Stratigraphic Framework

6.4.1 Sequence DLS 1

As discussed earlier, the base of this sequence is not observed in the studied outcrops. Nevertheless, the HST of this sequence is observed in outcrops 2, 1, 23 and 8.

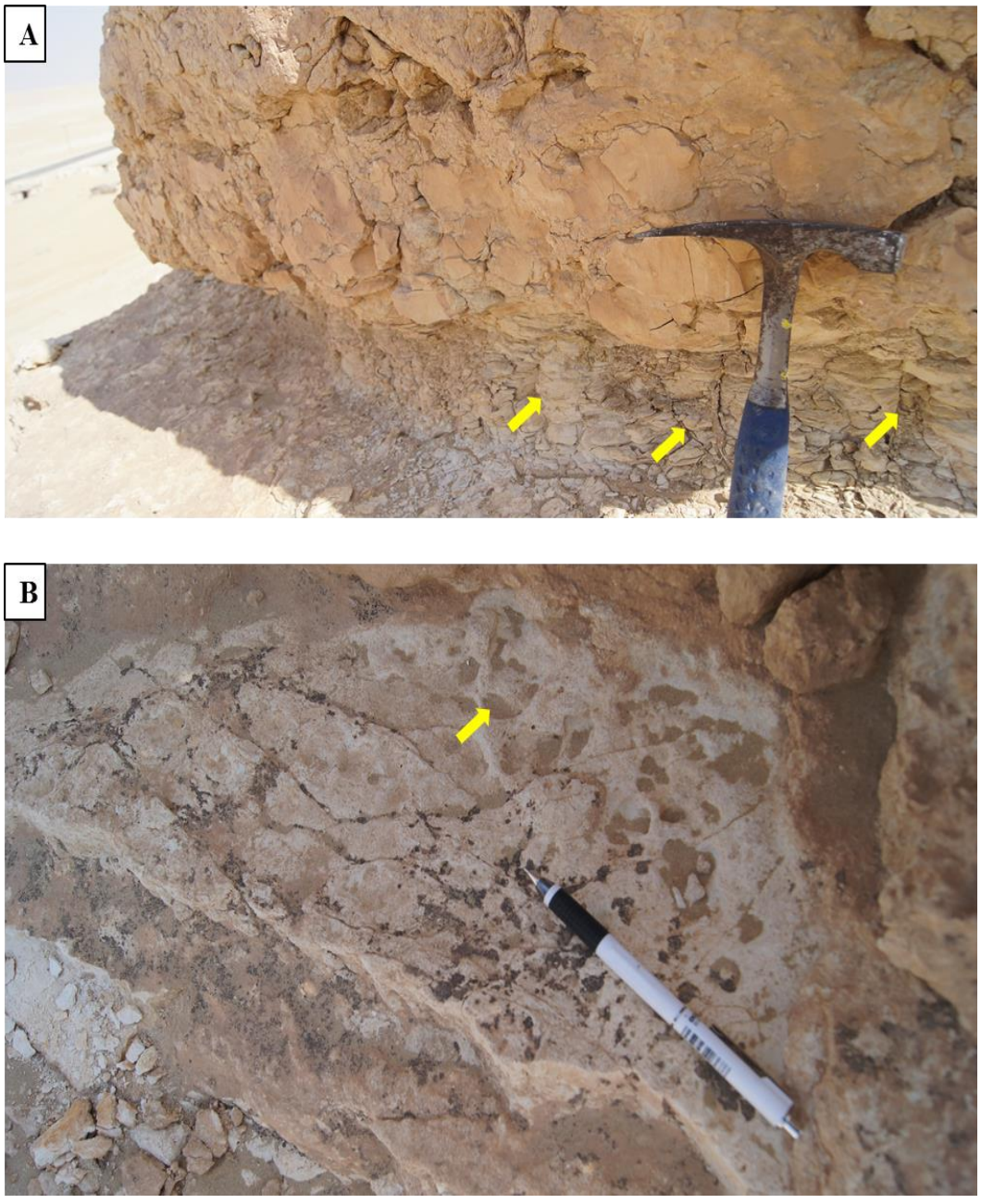

Figure 6.4: Subaerial exposure indicators at the top of HST 1; (A) mud cracks (arrows), and (B) rain drop impressions (arrows).

HST 1 is dominated by dolomitized skeletal/ oolitic grainstones that thin upward toward the sequence boundary (SB 1) with decreasing in accommodation space.

Most of these grainstones show extensive dissolution, as most of the skeletal (gastropods and bivalves) and non-skeletal grains (ooids) are dissolved and leached and occur as molds. In some parts, this dissolution is associated with inter-particle as well as intra-particle equant calcite cement which is interpreted as being precipitated when the pore spaces were filled by meteoric water during the relative sea level fall, during the exposure period associated with SB 1. This meteoric water was the reason behind the extensive dissolution, as it is more aggressive toward the calcium carbonate. This extensive dissolution increases upward toward the sequence boundary SB 1 (Figure 6.5A).

Partial dolomitization is also observed and increases toward the upper part of the HST 1, leading finally to massive dolomitization immediately below the sequence boundary SB 1 (Figure 6.5B). This dolomitization is associated with and underlies the interbedded mudstone-evaporites lithofacies of LST 2 of the next sequence DLS 2. The dolomitization was interpreted as evaporative-sabkha dolomitization as discussed earlier.

Slight compaction evidences were also noticed in HST 1 in form of suture contacts (Figure 5.19A), between ooids, which indicates shallow burial condition.

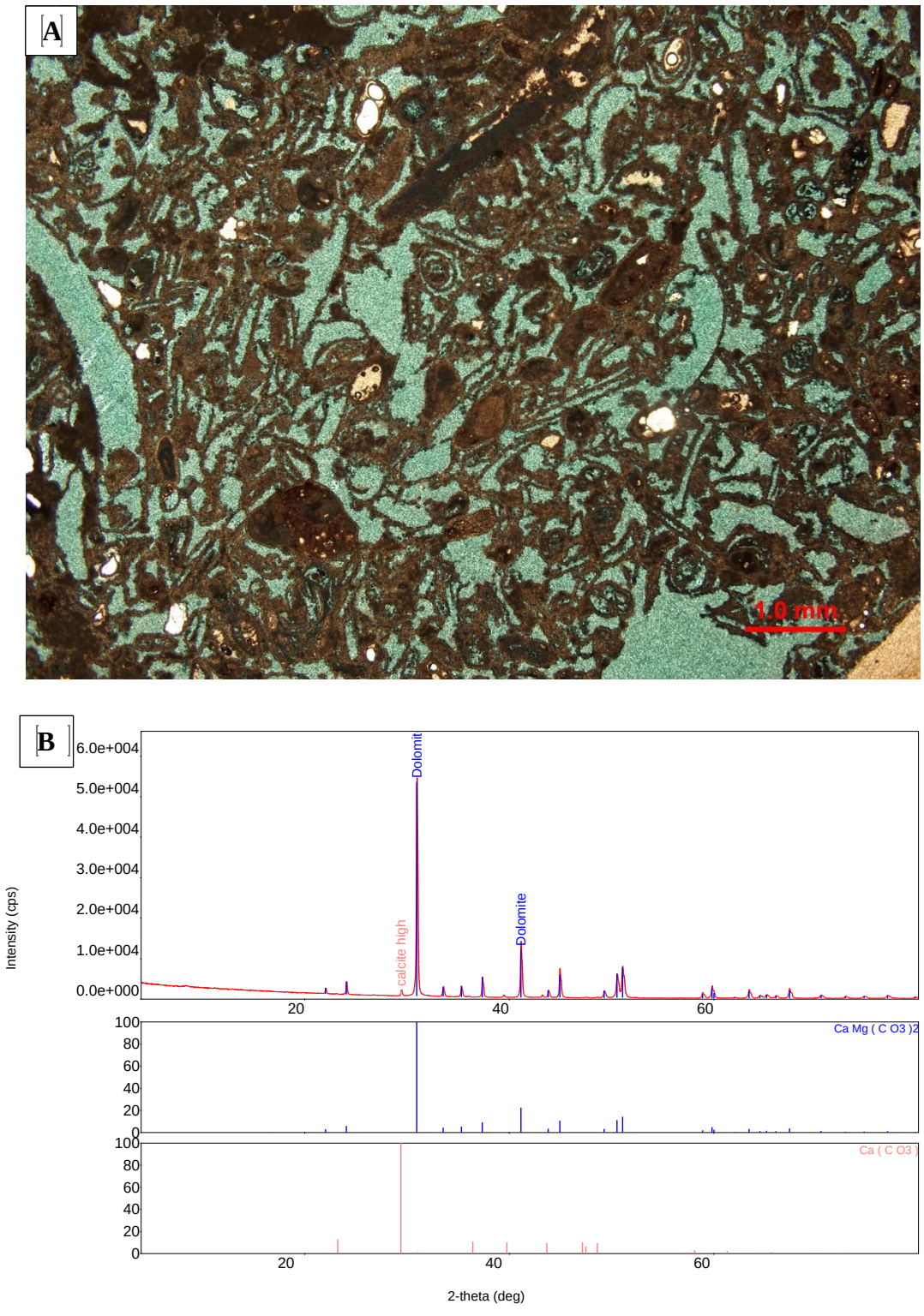

Figure 6.5: (A) Extensive dissolution, and (B) Massive dolomitization (as shown by XRD) at the top of the HST of the lower sequence DLS 1.

6.4.2 Sequence DLS 2

As discussed previously, the base (SB 1) of this sequence DLS 2 is overlain by interbedded mudstone-evaporite sabkha deposits, and rests on the intertidal grainstones of the highstand system tract (HST 1) of the underlying sequence DLS 1.

The lowstand system tract (LST 2) is composed of interbedded mudstone-evaporite lithofacies in all studied outcrops. In outcrop 23, LST 2 is represented by sabkha deposits as well as by an incised channel sandstone (Figure 6.2A) that cuts through the underlying HST 1. In outcrops 23 and 8, LST 2 is also composed of intertidal interbedded sandstone-mudstone lithofacies.

The interbedded mudstone-evaporite lithofacies shows vertical mud cracks, which are filled by gypsum. XRD analysis shows partial dolomitization as well as clay minerals (palygorskite) precipitation (Figure 6.6A). The friable sandstone of the incised channel shows extensive bioturbation in addition to clay minerals (illite and kaolinite) precipitation.

The transgressive system tract (TST 2) of this sequence DLS2 is dominated by subtidal dolomitized quartz wackestone-packstone lithofacies.

TST 2 shows bioturbation that increases upward toward the maximum flooding surface (MFS 2) (Figure 6.6 B). The lower parts of the TST 2 show some compaction indicators, such as hairline-thick fractures, especially in the muddier parts. As we go upward in TST 2, skeletal grains content increases and is associated with increasing grain dissolution (Figure 6.7A) as well as dolomitization. Dissolved skeletal grains occur as molds that play a major role in porosity enhancement of this unit. Clay minerals, such as kaolinite and palygorskite, were also noticed from SEM within the TST 2 (Figure 6.7B), and play a role in a permeability reduction.

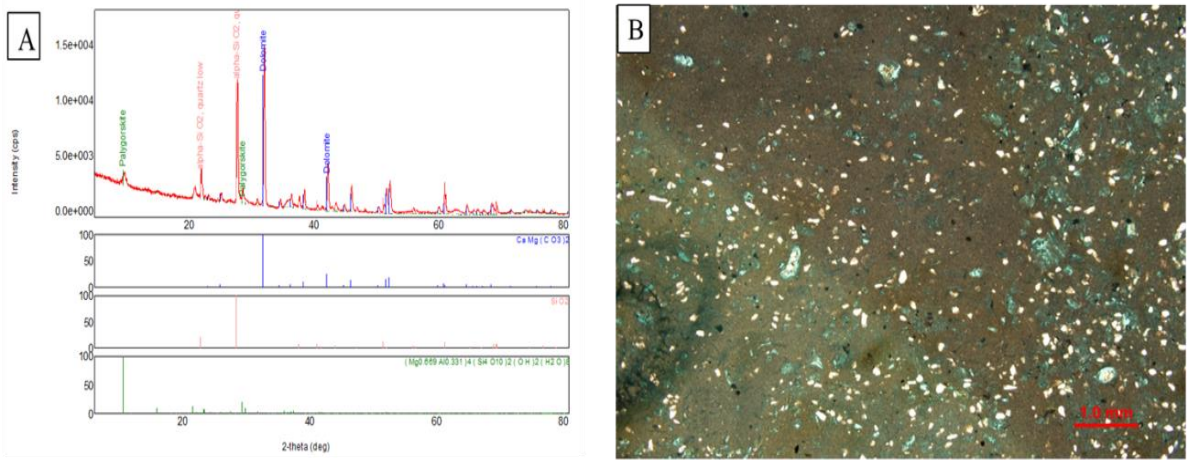

Figure 6.6: (A) XRD analysis shows dolomitization of the LST 2 interbedded mudstone-evaporite lithofacies with occurrence of palygorskite. (B) Thin-section photomicrograph shows bioturbation of the quartz wackestone-packstone lithofacies at the top of TST 2.

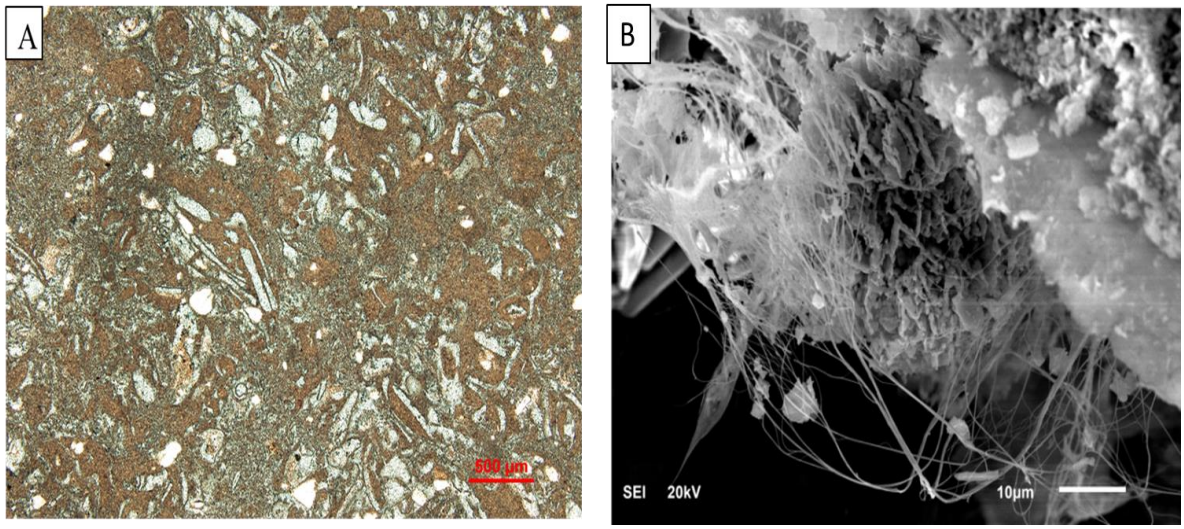

Figure 6.7: (A) Thin-section photomicrograph shows dissolution of the skeletal grains within the dolomitized quartz wackestone-packstone lithofacies at the upper part of TST 2. (B) SEM photomicrograph shows palygorskite clay mineral within the same lithofacies in TST 2.

The high stand system tract (HST 2) of this sequence DLS 2 is dominated by herringbone cross bedded, dolomitized skeletal, peloidal and oolitic grainstones and packstone that overlies the maximum flooding surface (MFS 2), which in turn overlies the dolomitized quartz wackestone-packstone of the underlying transgressive system tract (TST 2).

From a diagenesis point of view, similar to HST 1 of the underlying sequence (DLS 1), HST 2 is characterized by dissolution of most of the skeletal grains as well as non-skeletal grains (ooids). This grain dissolution increases upward toward the sequence boundary (SB 2), leading to moldic and vuggy porosity and enhancing overall porosity as a result of subaerial exposure during the relative sea level fall (Tucker, 1993). In addition to grain dissolution, equant calcite cementation as well as meniscus cementation were also observed in the (HST 2) which also indicate meteoric diagenetic condition (Figure 6.8A) (Longman, 1980).

Dolomitization was also observed as increasing upward leading to massive dolomite below the sequence boundary (SB 1) (Figure 6.8B). This dolomitization effectively enhanced the porosity of the (HST 2) by creating intercrstalline porosity between the dolomite crystals.

6.4.3 Sequence DLS 3

As discussed earlier, the upper boundary of this sequence is not observed in the study area.

In the eastern part of the study area the lowstand system tract (LST 3) is dominated by 30-45 cm of mud cracked dolomitized mudstone. In comparison to LST 2, the mudstone of LST 3 does not show any occurrence of evaporites in outcrop, but XRD analysis shows occurrence of gypsum and anhydrite.

In the western part of the study area (outcrop 8), in addition to the dolomitized mudstone, LST 3 is also contains interbedded sandstone-mudstone that thickening upward with increase in accommodation space, and suggest late stages of LST (Posamentier and Allen, 1999).

The transgressive system tract (TST 3), similar to TST 2, is composed of quartz dolomitized wackestone-packstone, but with higher content of quartz grains.

Bioturbation was observed in TST 3 to increase upward toward the maximum flooding surface (MFS 3). Bioturbation is present in mud-supported deposits in the transgressive and in the regressive systems tracts, suggesting that it is independent of sea-level fluctuations.

Dolomitization was also noticed, from XRD analysis, in TST 3 with general decrease in dolomitization relative to TST 2, suggesting that the dolomitizing fluids are decreasing upward toward the clastics of overlying Hofuf Formation.

Marine cementation was also observed in the lower part of TST 3 in outcrop 8, as aragonite needles coating the skeletal grains and some ooids (Figure 6.9A), which may formed during relative sea level rise when the pore spaces were filled by marine waters. Hairline fractures are also occurs at the muddier parts of the TST 3 (Figure 6.9B) which indicates influence of compaction.

The high stand system tract (HST 3) of this sequence (DLS 3) is dominated by dolomitized skeletal oolitic grainstones and packstones with more quartz content.

Similar to HST 1 and HST 2, HST 3 is also affected by meteoric dissolution of the skeletal and non-skeletal grains which increases upward in the all studied outcrops forming moldic and vuggy porosity (Figure 6.10A). This could be attributed to subaerial exposure and the action of meteoric water during the relative sea level fall of the overlying (predicted) sequence boundary.

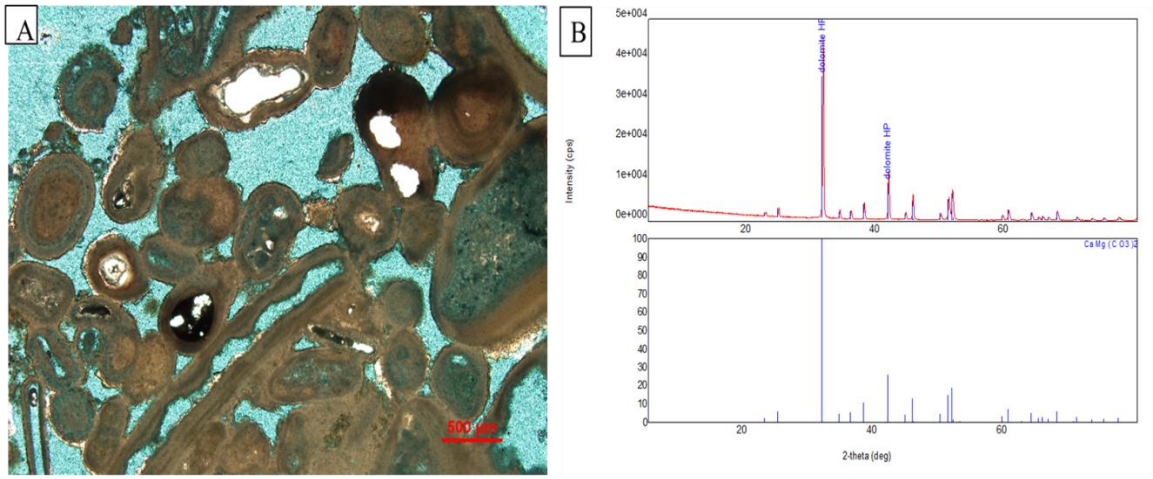

Figure 6.8: (A) Thin-section photomicrograph shows the partial grain dissolution and meniscus calcite cement precipitation in the upper parts of HST 2. (B) XRD diffractogram shows massive dolomitization of the pelloidal oolitic grainstone lithofacies below the sequence boundary (SB 1).

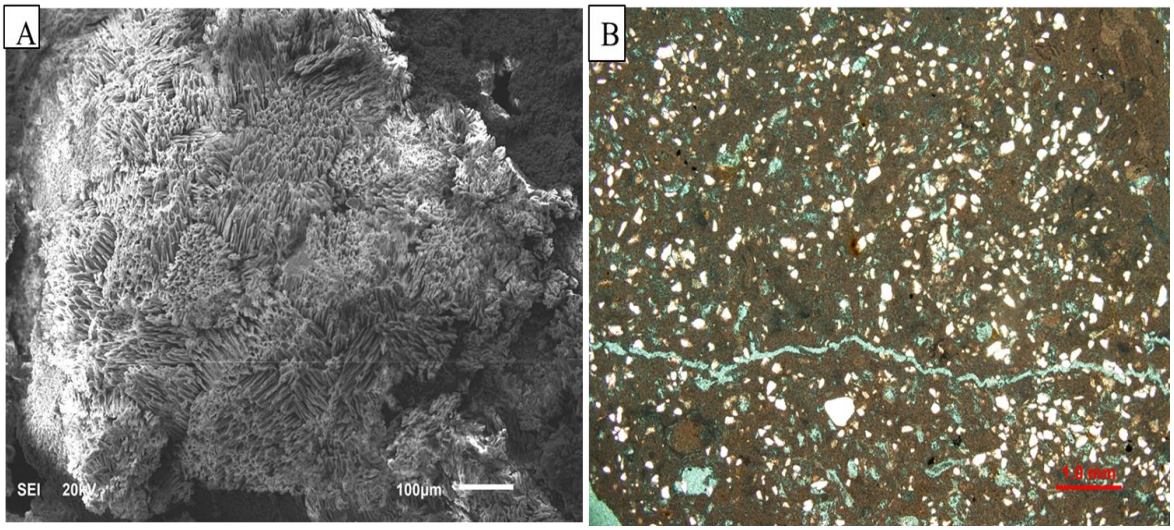

Figure 6.9: (A) SEM photomicrograph shows aragonite needles on the surface of ooids within the TST 3. (B) Thin-section photomicrograph shows hairline fracture within the dolomitized quartz wackestone-packstone lithofacies of the TST 3.

Dolomitization was also observed from XRD and SEM which also increases upward toward the (predicted) sequence boundary. Dolomitization and grain dissolution played a major role in porosity enhancement of the HST 3.

Burial compaction was noticed from the western part of the study area (outcrop 16), where the grains are compacted against each other forming concavo-convex contacts (Figure 6.10B).

Stratigraphic Sections with the diagenetic features of all studied outcrops are shown in the next figures; Figure 6.11, 6.12, 6.13 and 6.14 for outcrop 2, 1, 23 and 8, respectively.

A correlation has been made between the studied outcrops base on the system tracts and sequence subdividing time surfaces as shown in (Figure 6.15)

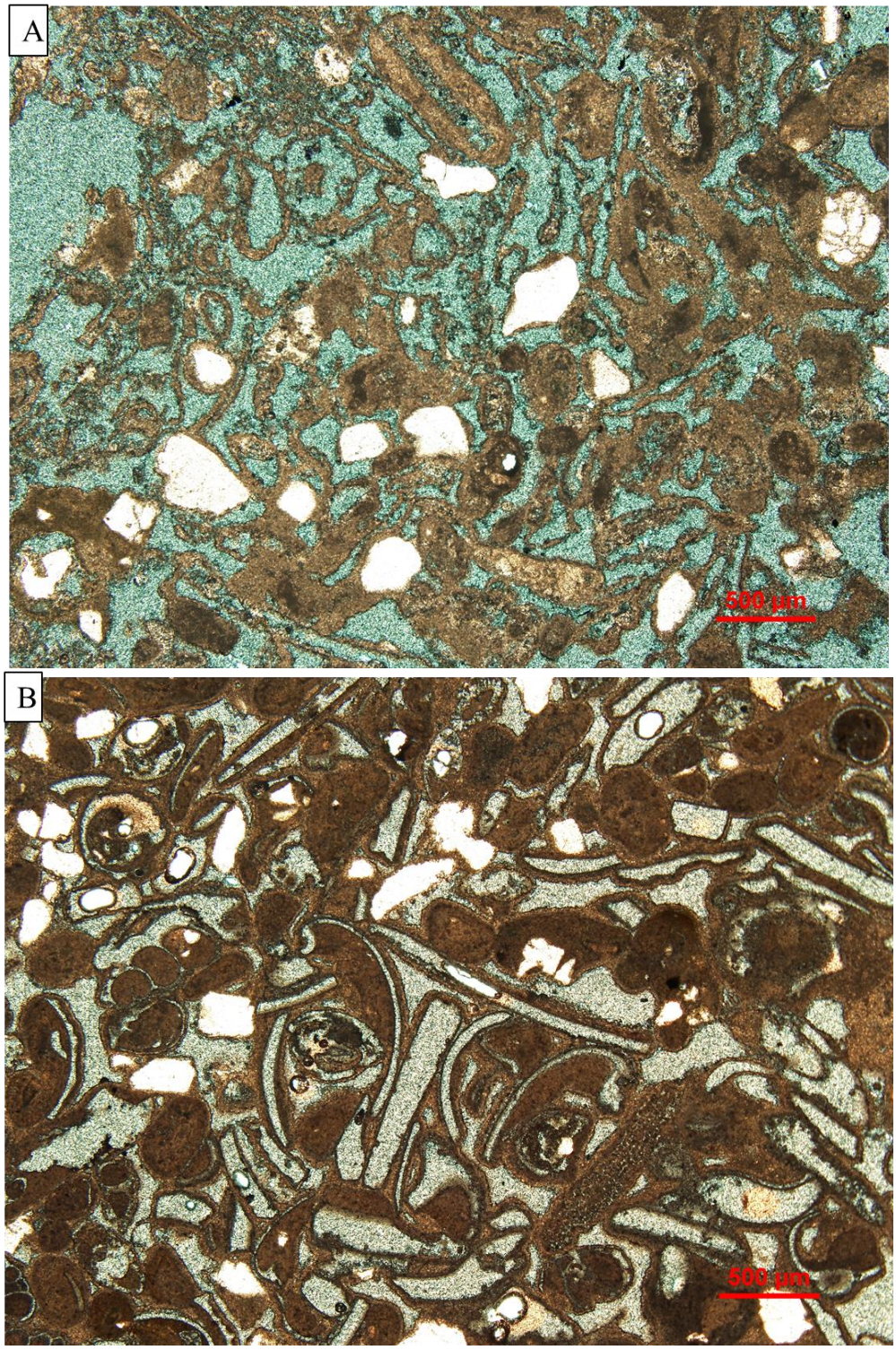

Figure 6.10: (A) Thin-section photomicrograph shows grain dissolution by meteoric water in the upper part of (HST 3) at outcrop 1. (B) Thin-section photomicrograph shows concavo-convex contact between skeletal grains in the (HST 3) at outcrop 16.

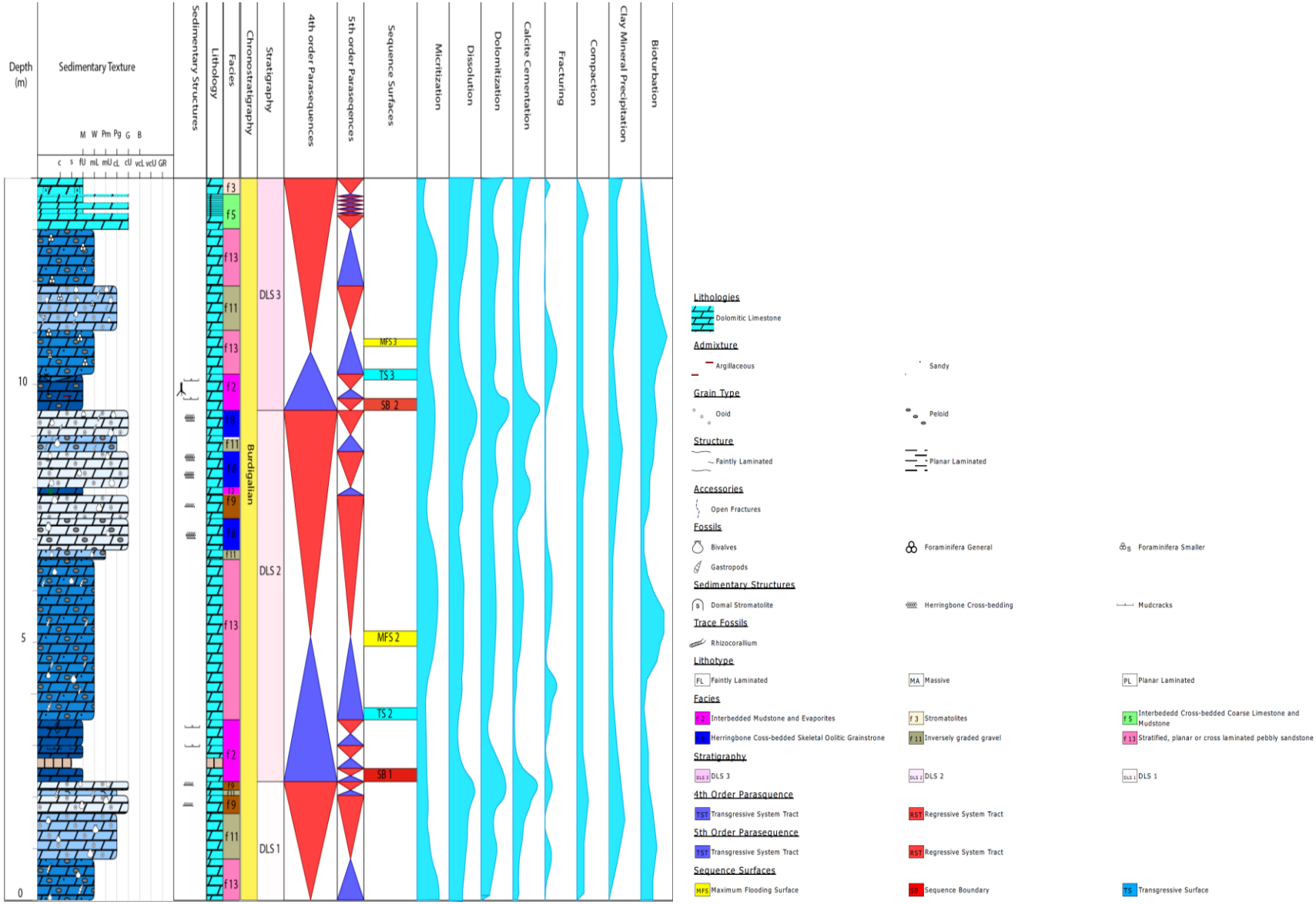

Figure 6.11: Textures, structures, lithology, sequence stratigraphic subdivisions and diagenetic processes of outcrop 2.

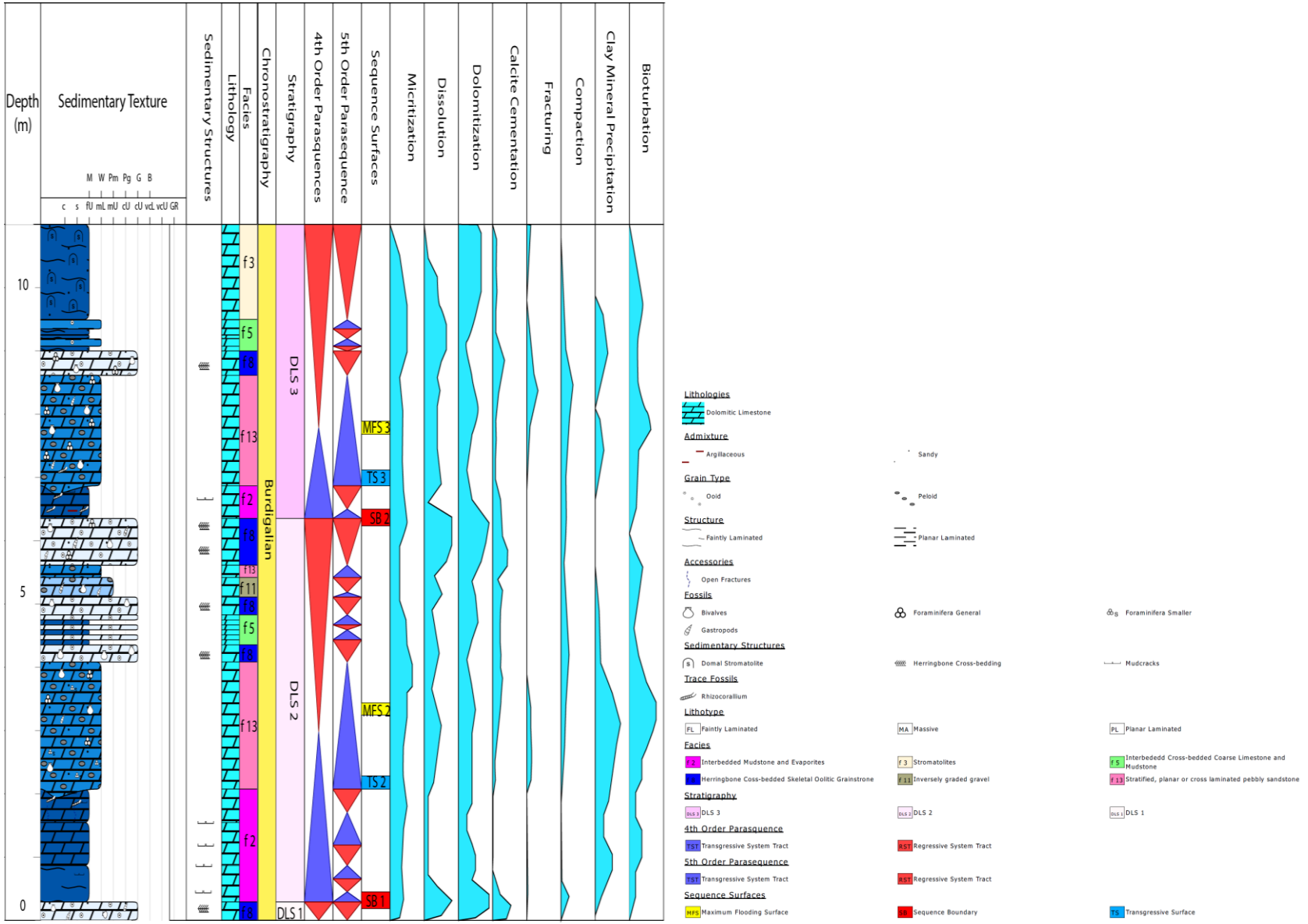

Figure 6.12: Textures, structures, lithology, sequence stratigraphic subdivisions and diagenetic processes of outcrop 1.

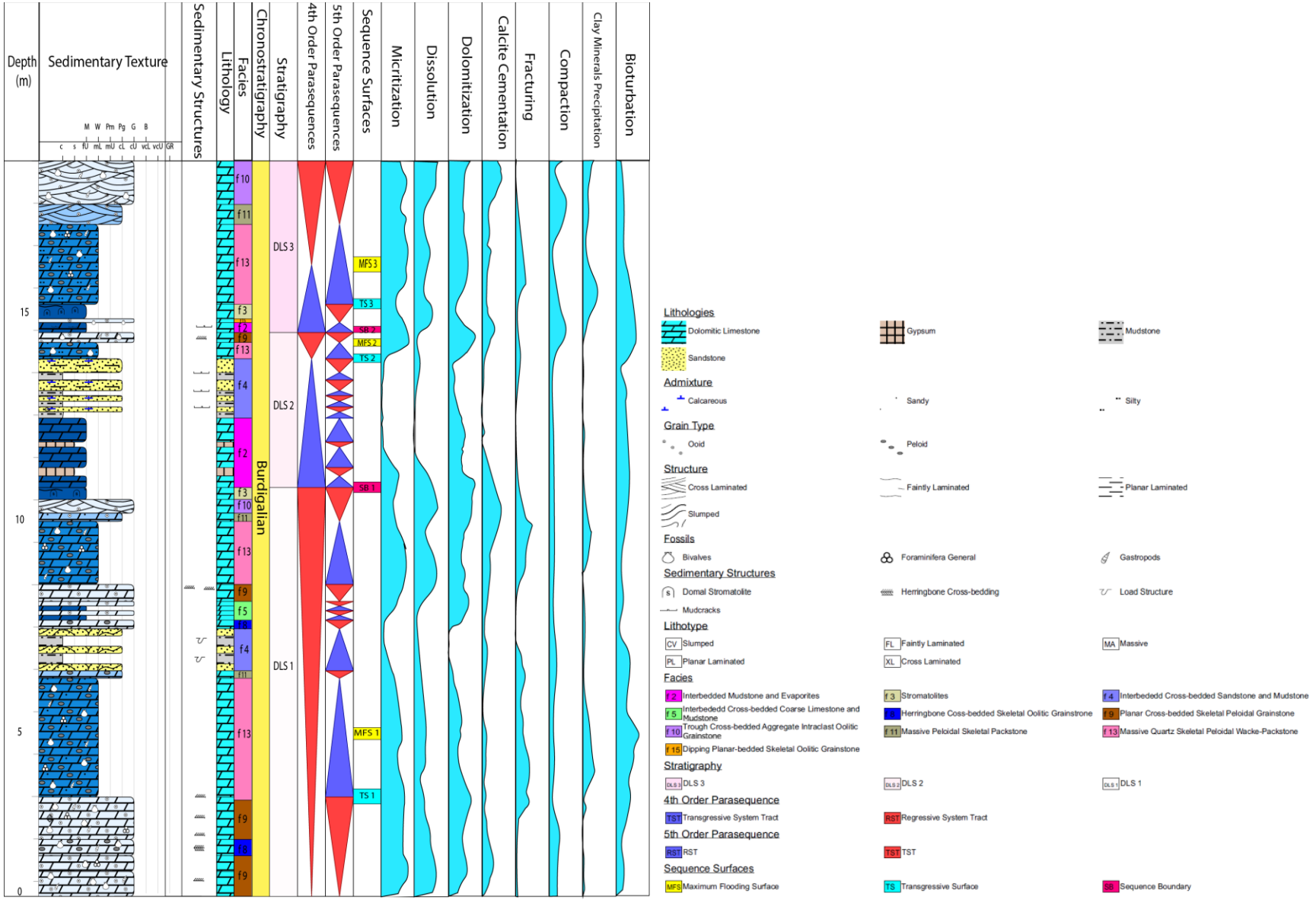

Figure 6.13: Textures, structures, lithology, sequence stratigraphic subdivisions and diagenetic processes of outcrop 23.

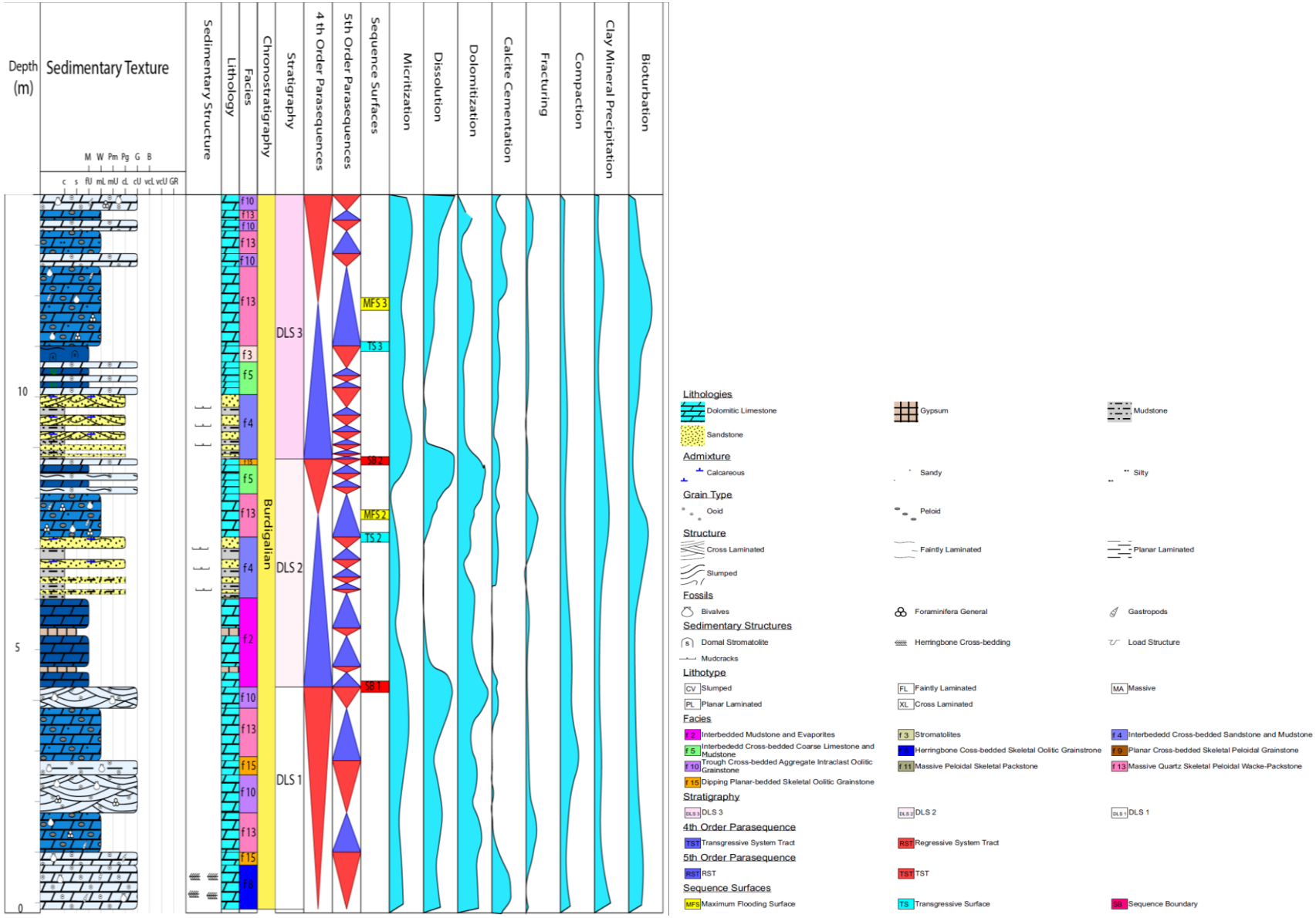

Figure 6.14: Textures, structures, lithology, sequence stratigraphic subdivisions and diagenetic processes of outcrop 8.

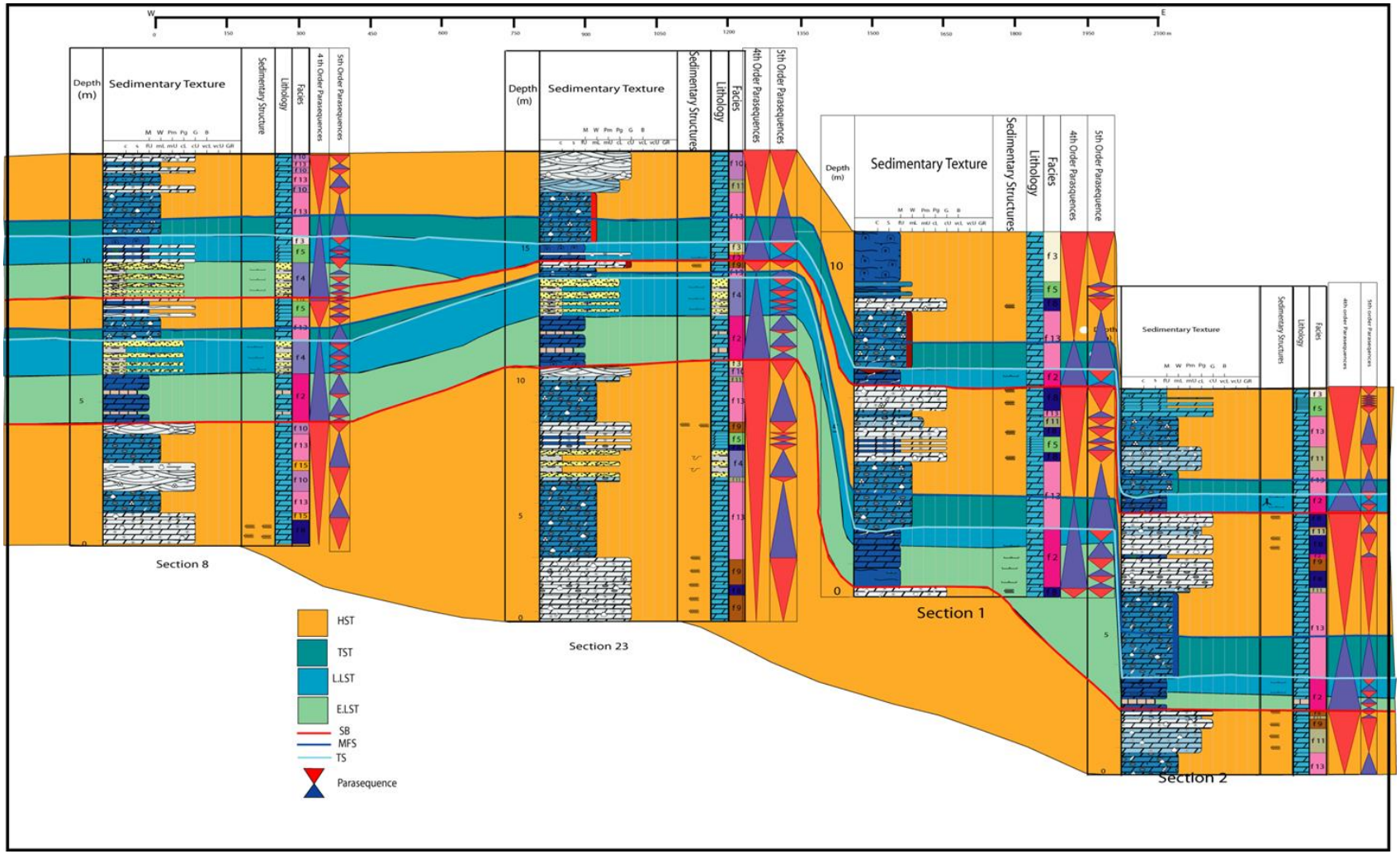

Figure 6.15: Cross section through studied outcrops showing the sequence stratigraphy of the Dam Formation in the study area

CHAPTER 7

DIAGENESIS AND POROSITY EVOLUTION WITHIN A SEQUENCE STRATIGRAPHIC FRAMEWORK

7.1 Introduction

In order to maximize the oil and gas production, understanding porosity types and their distribution is important in reservoir characterization. Focusing on the thin section scale, the characteristics of different porosity types can play a major role in defining reservoir quality. Pore type and size are key parameters that can determine the quality of the porosity and permeability in reservoir intervals. A mixture of the best quality types of the pores within a reservoir unit can produce the optimum reservoir quality. In this study, the pore types were linked with sequence stratigraphy as well as with diagenesis.

When diagenetic porosity and permeability are intimately related to depositional rock properties, reservoir boundaries conform to depositional facies boundaries. If diagenetic changes follow fracture or joint patterns, then determining the size and shape of the reservoir may be a job of interpreting the fracture distribution pattern rather than one of interpreting patterns of diagenesis. In purely diagenetic pore systems that do not conform to fracture or depositional trends, the techniques for analyzing reservoir performance are defined by the type and extent of diagenesis that created the porosity. Reservoir size and shape may depend on the mechanism of diagenesis, the environment of diagenesis, and the size and shape of the zones that were exposed to

diagenesis. In short, diagenetic porosity may or may not correspond to depositional or structural trends (Ahr, 2003).

7.2 Porosity Classification

The size and shape of pores in carbonate sediments are heavily influenced by skeletal material, which can be as varied as the assemblages of organisms that created them.

The Choquette and Pray (1970) porosity classification scheme (Figure 7.1) was used to classify the porosity present in the analyzed samples. On the basis of this classification scheme, more than four hundred thin-section photomicrographs were analyzed. As a result, seven types of porosity were identified from the studied samples. The porosity types include interparticle, intraparticle, moldic, vuggy, intercrystalline, shelter and fracture porosity. The relative abundance of these porosity types are represented in (Figure 7.2).

Using polarized microscope, each one of these porosity types is estimated by point counting method and they can be briefly described as follow;

Interparticle porosity is defined as the pore space between skeletal or non-skeletal grains (Figure 7.3A and 7.3B). In the study area, this type of porosity constitutes the main pore type in oolitic and skeletal grainstones with approximately 36% of the total porosity in the analyzed samples.

Intraparticle porosity is the porosity within individual particle or grain (Figure 7.3C and 7.3D). Much intraparticle porosity in carbonates forms before final deposition of the sedimentary particle or grain (pre-depositional porosity); some forms during or very shortly after final deposition. It occurs in the studied samples as in ooids, forams and skeletal grains and its accounts for approximately 10% of the total porosity in the analyzed samples.

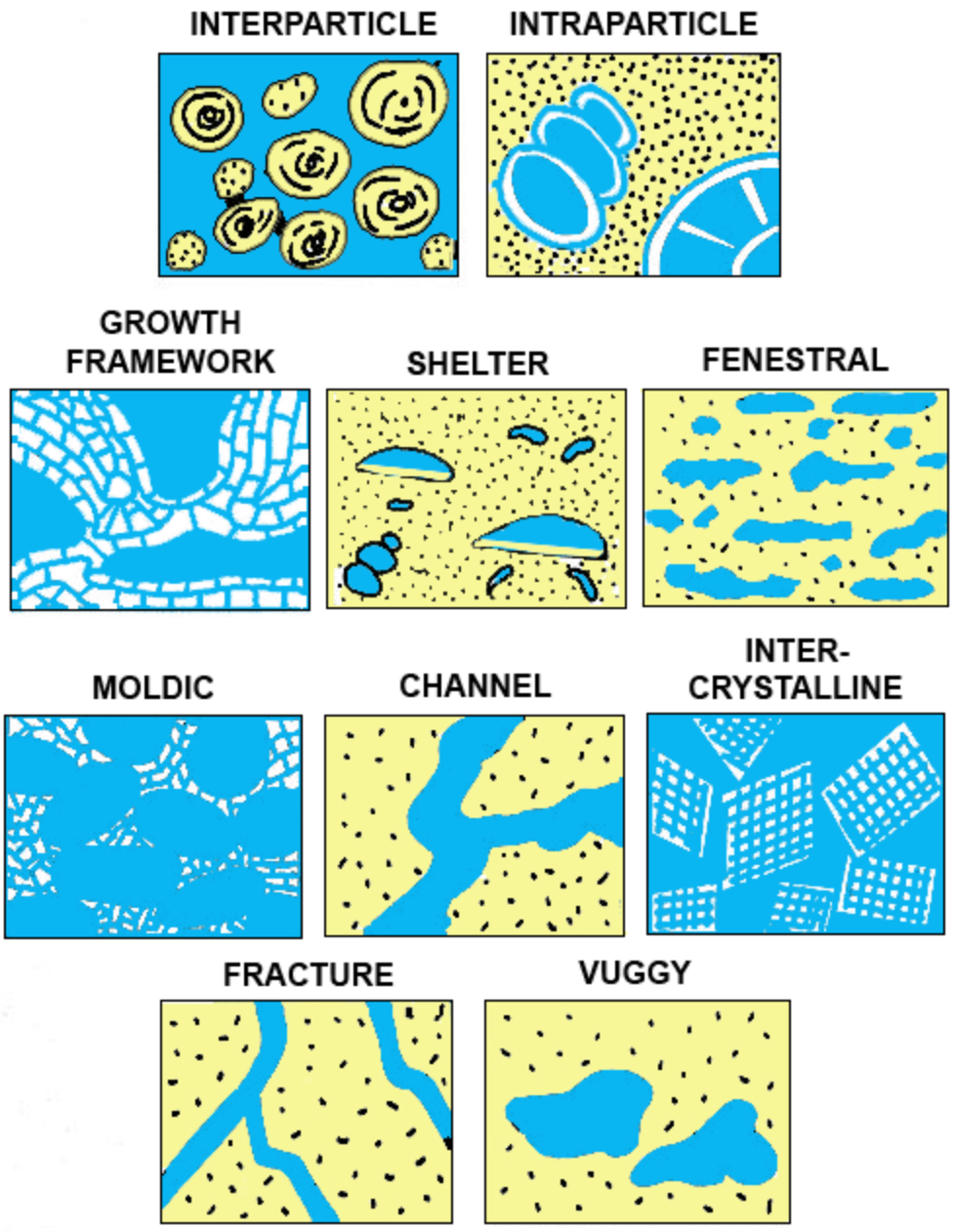

Figure 7.1: Classification of carbonate porosity. After Choquette & Pray 1970.

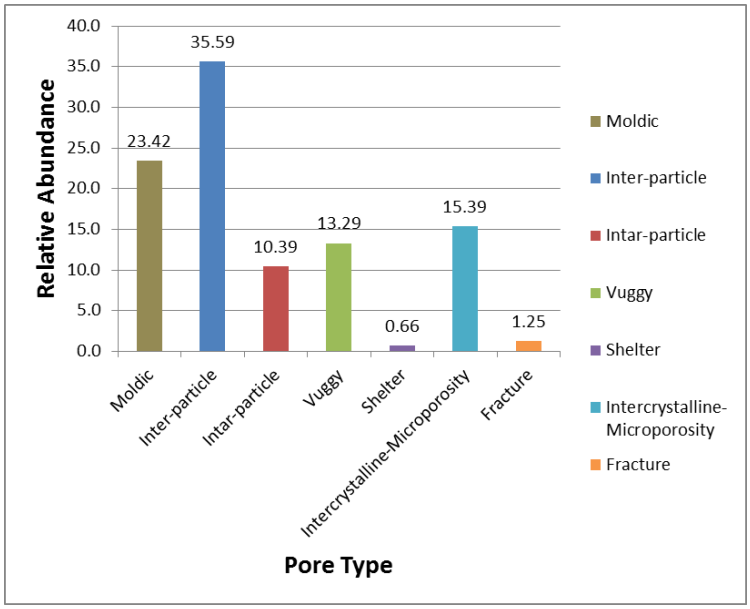

Figure 7.2: Seven basic pore types are distinguished in the analyzed samples of the Dam Formation in Al-Lidam area. Relative proportions (in %) of each pore types are displayed.

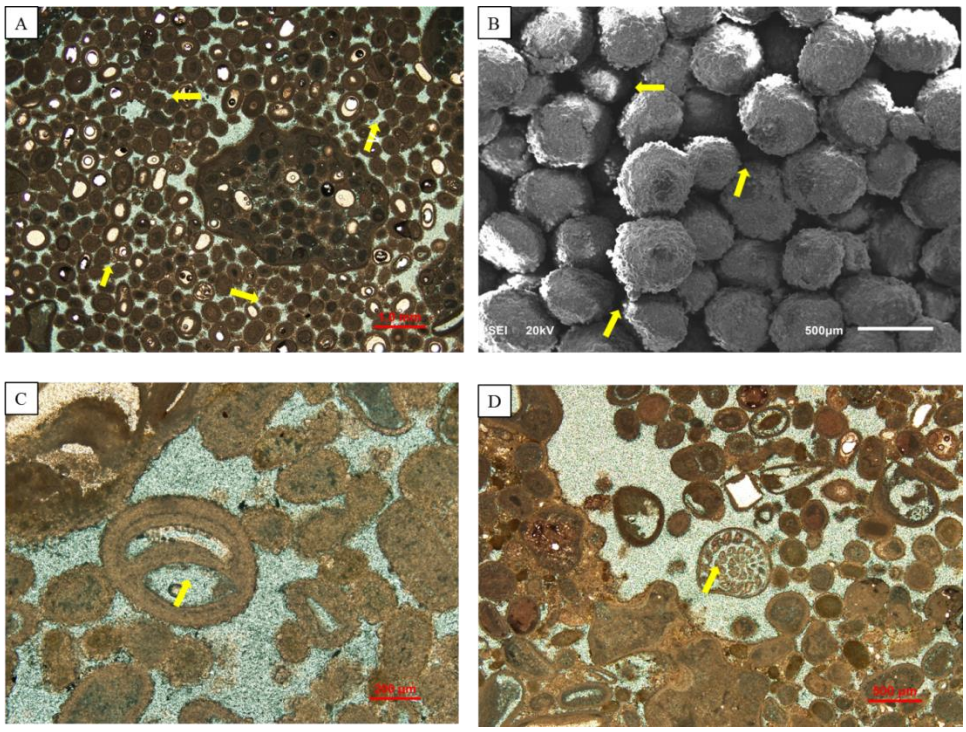

Figure 7.3: Inter-particle porosity between ooids (arrows) as shown under cross polarized microscopy (A), and under SEM (B). Intra-particle porosity under plane polarized microscopy of coated grain (arrow) (C), and within chambers of foraminifera.

Moldic porosity is formed when the metastable grains are dissolved (Figure 7.4A and 7.4B). The moldic pores take the shape, and size of the original grains. Molds are the second dominant pore type, after interparticle porosity, with approximately 23% of the total porosity in the analyzed samples. Some of the molds are complete molds, while other molds are partly or completely filled by calcite cement.

Vuggy porosity typically occurs as large pores and that do not follow any systematic fabric boundaries. This porosity was likely formed as a result of combination of two or more pore types, or by extremely poor mold preservation (Figure 7.4C and 7.4D). Diagenetic dissolution of grains, matrix or cements in the samples might have also allowed the formation of this porosity type. Vugs accounts for about 13% of the total porosity in the analyzed samples.

Intercrystalline porosity is the porosity type that occurs dominantly between dolomite crystals (Figure 7.5A and 7.5B). This porosity type was found in all analyzed samples. It is also associated with micrite cement crystals at micro-scale. Since the crystals are not readily observed using conventional plane-light microscopy, intercrystalline porosity between micrite crystals is considered to be microporosity and quantitatively evaluated by subtracting the visually estimated porosity value from the total plug's porosity in each sample (Cantrell & Hagerty, 1999).This type of porosity increases in the muddy lithofacies and its accounts for approximately 15 % of the total porosity in the analyzed samples.

Shelter porosity is formed when large grains such as bivalve segments act as shelters or “umbrellas” and prevent detrital grains from filling pore space beneath the shelter of the large grain (Figure 7.5C and 7.5D).

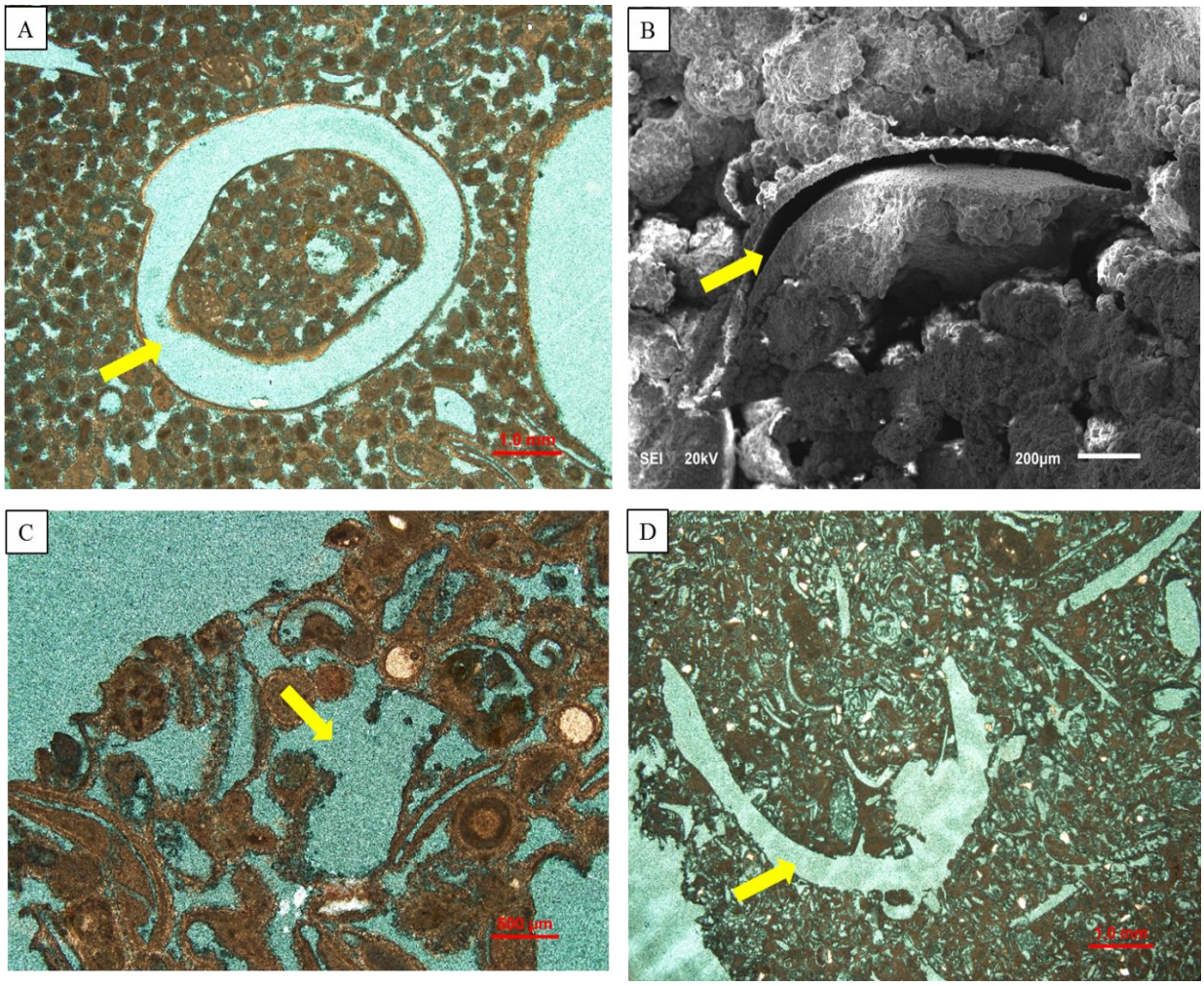

Figure 7.4: Moldic porosity (arrow) formed by complete dissolution of bivalve skeletal grain as shown under polarized microscopy (A), and under SEM (B). Vuggy porosity (arrows) formed by non-selective dissolution of skeletal grains and matrix as shown under polarized microscopy (C) and (D).

This porosity type was found mainly associated with beach grainstone lithofacies, and it accounts for less than 1 % of the total porosity in the analyzed samples.

Fracture porosity is the porosity formed by cracking or fracturing of the matrix and/or the skeletal and non-skeletal grains (Figure 7.6A and 7.6B). These fractures increase the porosity and especially permeability, although it may locally be filled by cement leading to decrease of porosity and permeability. This porosity type was found mainly associated with mud dominated lithofacies, it accounts for about 1 % of the total porosity in the analyzed samples.

7.3 Porosity Distribution

The impact of biological and physical depositional processes in combination with diagenetic overprints can make the distribution of porosity and permeability in carbonates much more heterogeneous than in siliciclastics.

In the studied samples of the Dam Formation in the Al-Lidam area, a plot of porosity Vs permeability shows clear correlation between porosity & permeability values, and the depositional energy of the lithofacies. Generally, the high energy intertidal grain dominated lithofacies have similar porosity values, with higher permeability values than the lower energy subtidal mud dominated lithofacies (Figure 7.7). In terms of lithofacies, the intertidal and beach lithofacies (f 3, f 8, f 9, f 11 and f 15) have the higher permeability values, while the supratidal and subtidal lithofacies (f 2, f 10 and f 13) have lower values (Figure 7.8).

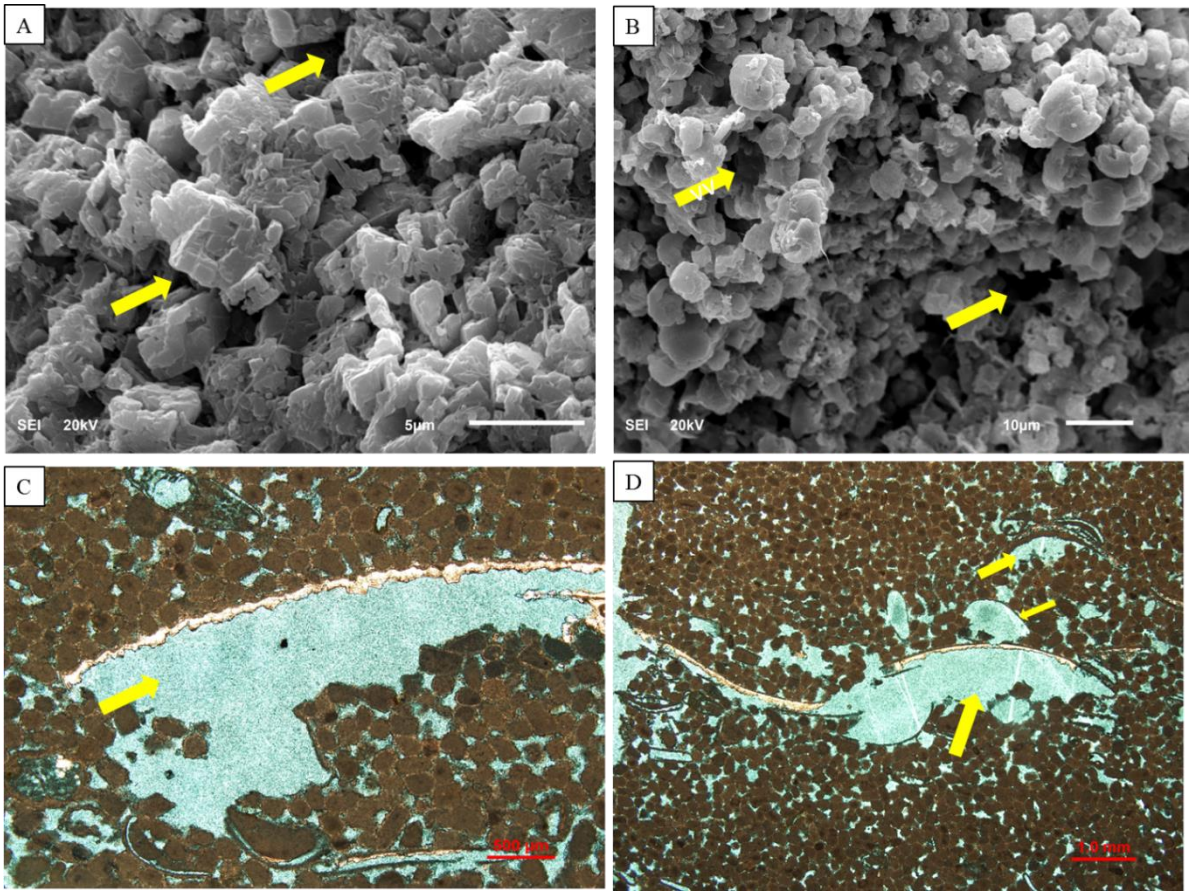

Figure 7.5: Inter-crystalline microporosity between crystals (arrows) as shown under SEM (A) and (B). Shelter porosity (arrows) formed as bivalve grains prevented the pore spaces from being filling by sediments as shown under polarized microscopy (C) and (D).

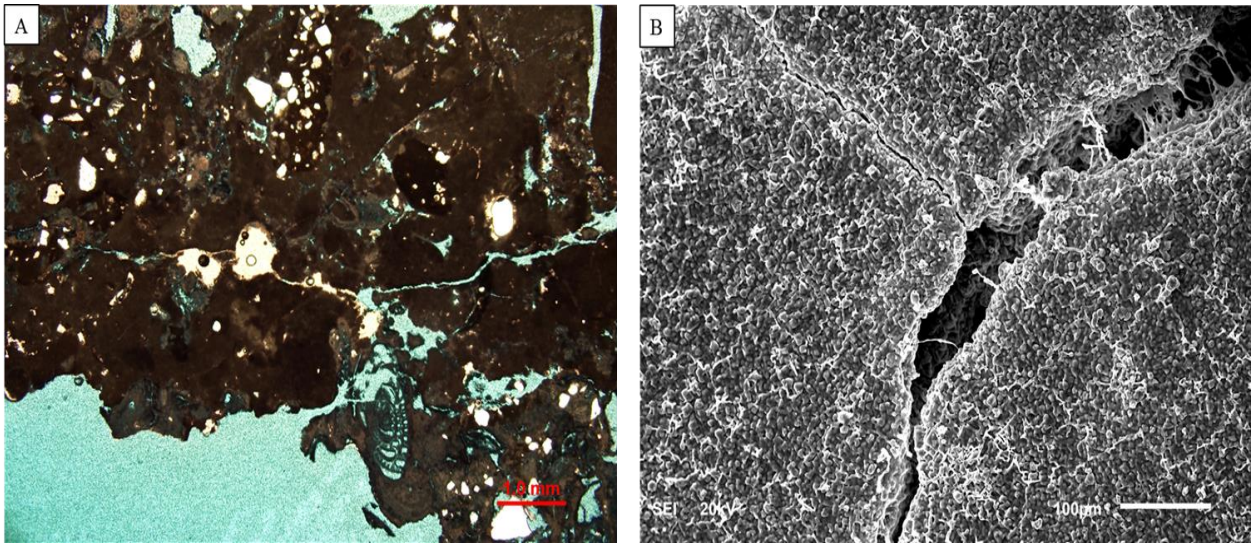

Figure 7.6: Fracture porosity under polarized microscopy (A), and under SEM with some cement filling the fracture (B).

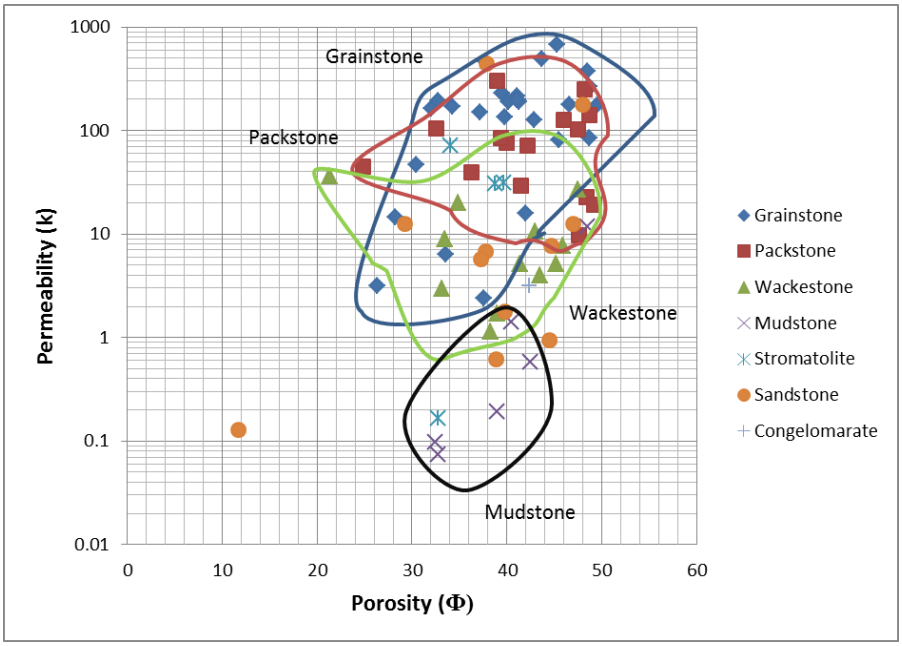

Figure 7.7: Porosity-permeability cross plot based on sedimentary texture, showing that that grain dominated sediments have similar porosity values, with higher permeability values than the mud dominated sediments.

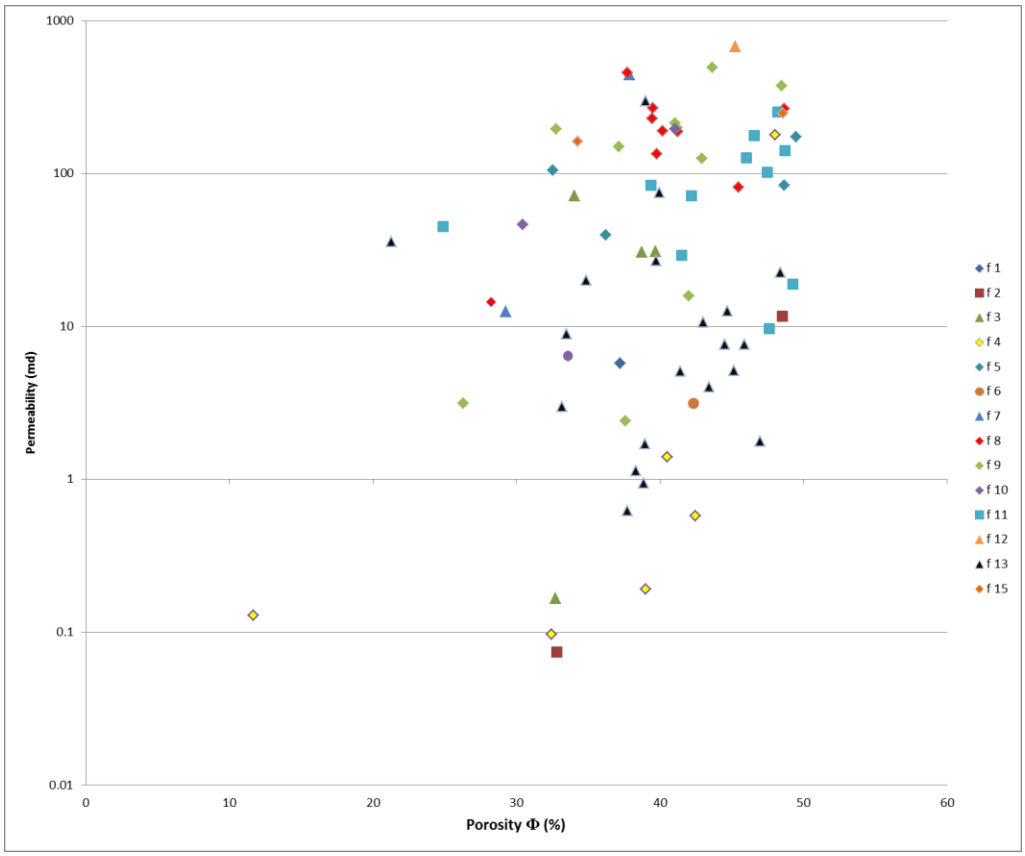

Figure 7.8: Porosity-Permeability cross plot base on identified lithofacies of the Dam Formation in Al-Lidam area, showing that the intertidal lithofacies (f 3, f 5, f 8, f 9 and f 11) have a higher porosity and permeability values than the supratidal and subtidal lithofacies (f 2, f 10 and f 13).

From sequence stratigraphy point of view, the intertidal, grain dominated, high stand system tracts have the higher porosity and permeability values, followed by the subtidal, mud dominated, transgressive system tracts and finally the supratidal, mud dominated, low stand system tracts (Figure 7.9).

The distribution of porosity and permeability within the studied sections indicates primary depositional controls on porosity that have been modified at subsequent stages by diagenesis in response to the fluctuation in the relative sea level.

Porosity type distribution within each lithofacies shows that the interparticle, moldic, vuggy and intraparticle porosity are the dominant porosity types within the intertidal grain dominated lithofacies (f 4, f 5, f 8, f9 and f 11) (Figure 7.10), with lower relative abundance of intercystalline porosity and fracture porosity. The beach grainstone lithofacies (f 15) is dominated by interparticle, moldic, shelter and vuggy porosity with lower relative abundance of intercrystalline, fracture and intraparticle porosity (Figure 7.11). The subtidal mud dominated lithofacies (f 13) are dominated by intercystalline-microporosity with lower relative abundance of moldic and interparticle porosity (Figure 7.12).

In term of sequence stratigraphy, the high stand system tracts are dominated by interparticle, moldic, vuggy and intraparticle porosity, with lower relative abundance of intercrystalline, shelter and fracture porosity (Figure 7.13). The transgressive system tracts are dominated by intercrystalline-microporosity and interparticle porosity with lower relative abundance of moldic, vuggy and intraparticle porosity. It also shows relatively higher abundance of fracture porosity than the high stand system tracts (Figure 7.14). The lowstand system tract is dominated by mudstone facies, which could not be prepared for petrographic analysis.

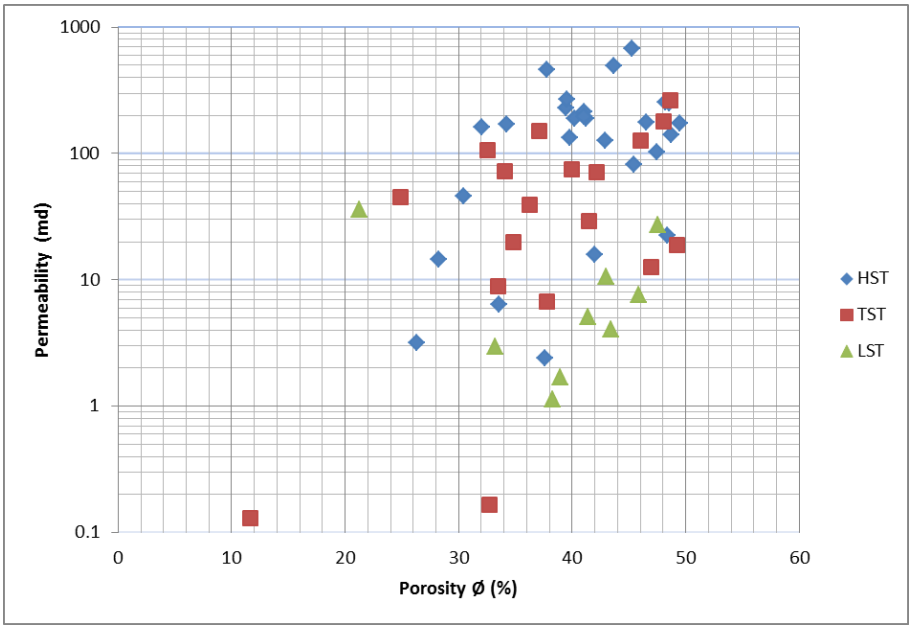

Figure 7.9: Porosity-Permeability cross plot base on interpreted sequence stratigraphic framework of the Miocene Dam Formation in Al-Lidam area, showing that the high stand system tracts (HST) have a similar porosity and higher permeability values than the transgressive and lowstand system tracts (TST and LST).

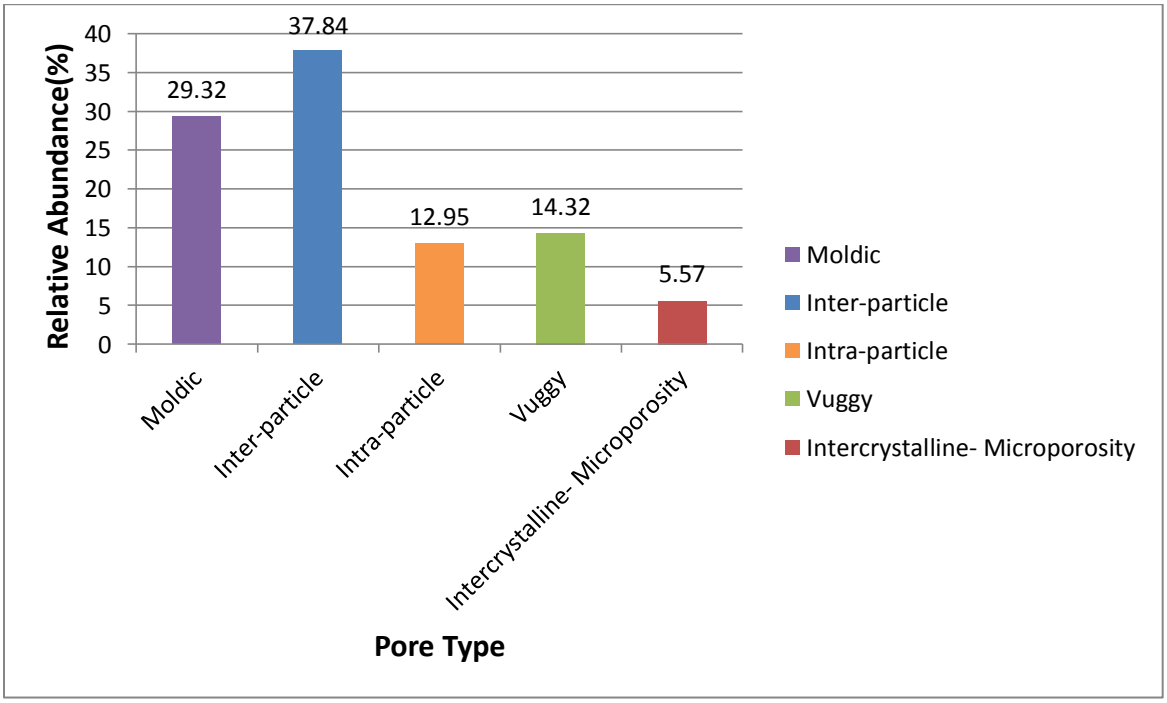

Figure 7.10: Porosity types distribution within the intertidal lithofacies of the Dam formation in Al-Lidam area.

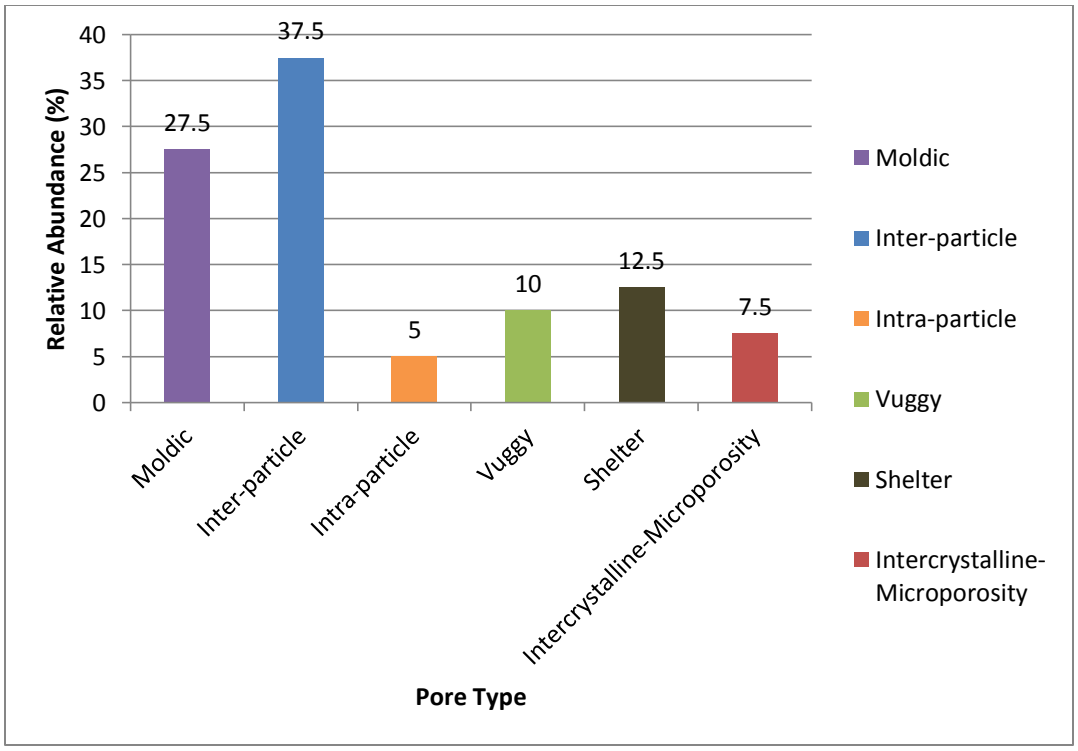

Figure 7.11: Porosity types distribution within the beach lithofacies of the Dam formation in the Al-Lidam area.

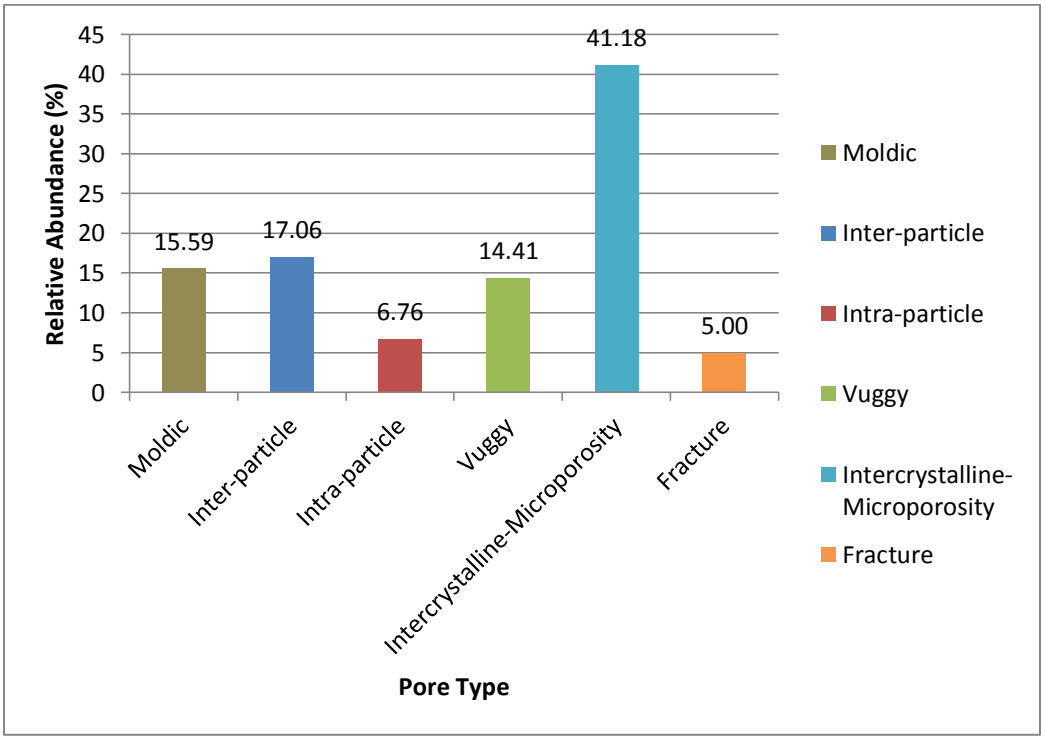

Figure 7.12: Porosity types distribution within the subtidal lithofacies of the Dam formation in the Al-Lidam area.

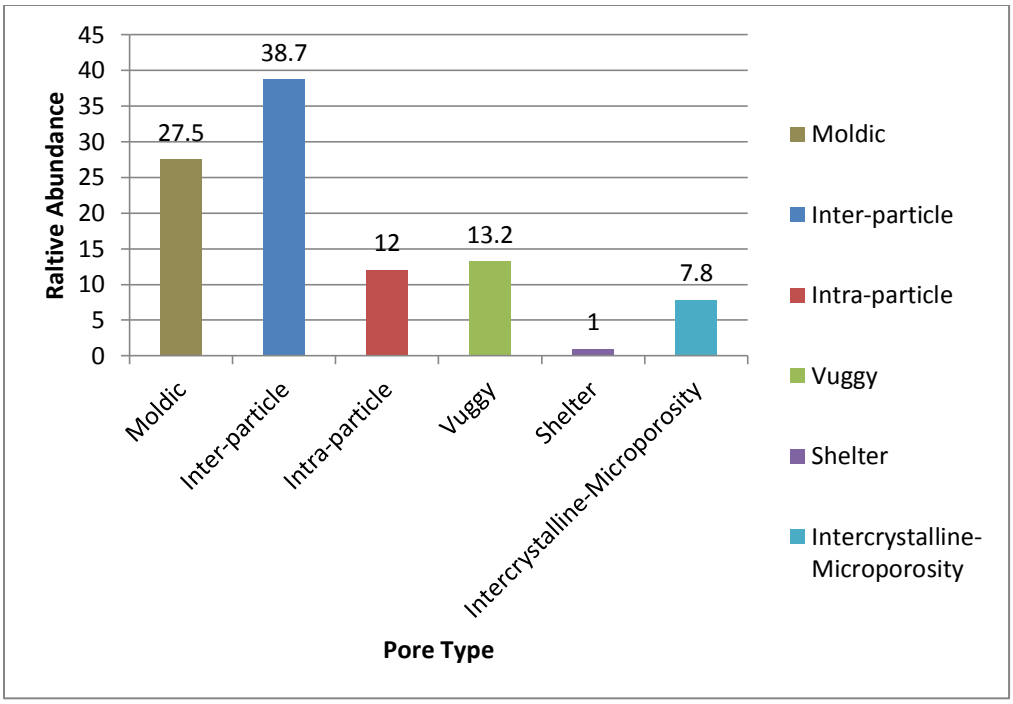

Figure 7.13: Porosity types distribution within the high stand system tracts (HST) of the Dam formation in the Al-Lidam area.

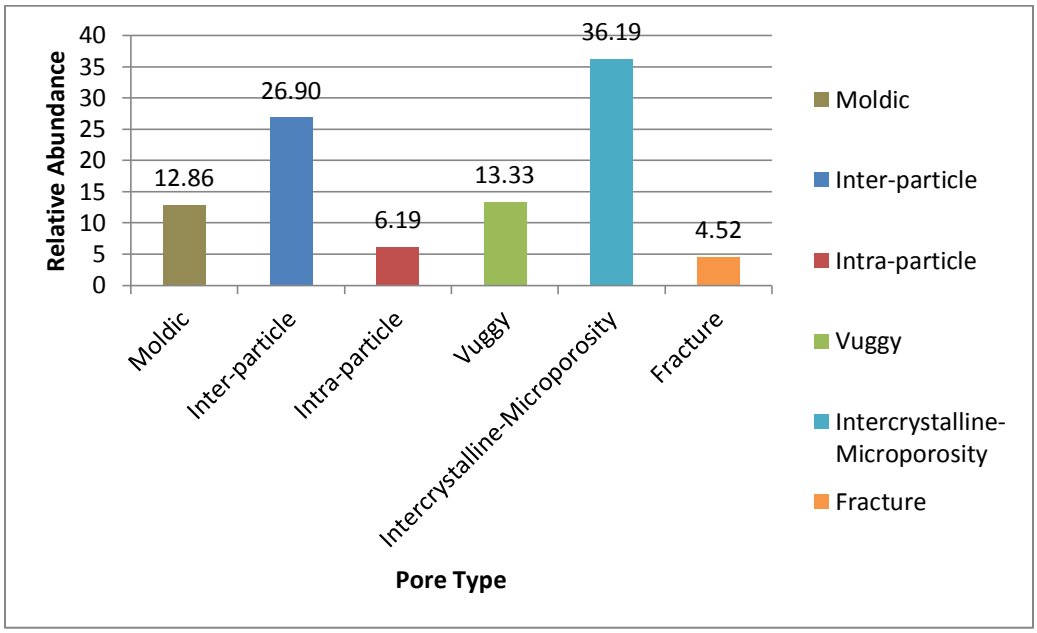

Figure 7.14: Porosity types distribution within the transgressive system tracts (TST) of the Dam formation in the Al-Lidam area.

7.4 Discussion

Most of the intertidal and beach lithofacies are represented by the high stand system tracts, while the subtidal lithofacies are represented by the transgressive system tracts. The supratidal lithofacies are represented by low stand system tracts, but, because they are dominated by mudstone, few plugs were prepared from these lithofacies and all of the thin-sections were not good for analysis.

The higher permeability values within the high stand systems tracts (HST) are attributed to the fact that the high stand systems tracts (HST) were originally grain dominated sediments with higher interparticle porosity, which may have allowed the dissolving meteoric fluids to pass through the sediments forming dissolution-related porosity. Thus, the high stand system tracts (HST) were extensively influenced by meteoric diagenetic processes during periods of subaerial exposure, which occurred as a result of relative sea level fall, and formed the sequence boundary. The most important meteoric diagenetic process that enhanced the porosity is the grain dissolution, forming moldic and vuggy porosity. Other porosity reducing, meteoric diagenetic processes, while less abundant, were also observed within the high stand system tract. These include the meniscus or microstalactitic calcite cement and equant calcite cement.

Another reason that may lead to enhanced porosity of the high stand system tracts (HST) is the increasing impact of dolomitization in the high stand system tract (HST) relative to the transgressive system tract (TST) as shown in (Figure 7.15). The grater abundance of dolomite in (HST) is attributed to the fact that the dolomitizing fluids are sourced from the overlying sequence boundary, which is closer to the HST than the TST sediments.

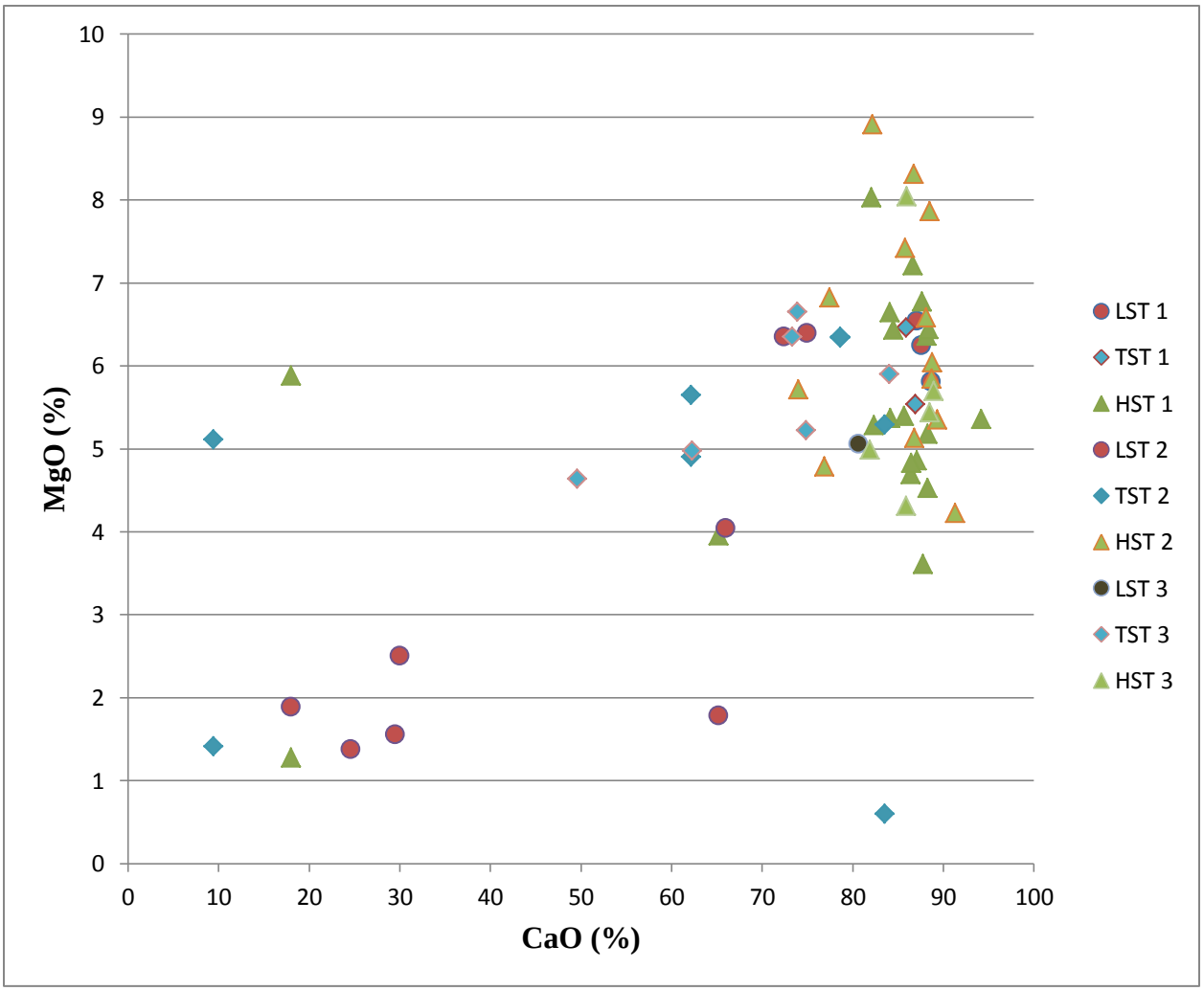

Figure 7.15: Cross plot of magnesium oxide (MgO) vs calcium oxide (CaO) to infer dolomite abundance within a sequence stratigraphic framework. The HST sediments have a higher dolomite content than do the TST sediments.

On the other hand, the lower porosity and permeability values of the transgressive system tracts (TST) are attributed to the fact that they were originally mud dominated sediments with lower interparticle porosity, which may have prevented the dissolving fluids from passing through the sediments to dissolve the metastable grains. Thus, the transgressive system tracts were not extensively influenced by meteoric diagenesis

The presence of meteoric dissolution and equant calcite cementation suggests diagenesis under humid climate. On the other hand, the occurrence of thin evaporites beds and evaporites cementation suggests deposition and diagenesis under arid to semi-arid climate.

The occurrence of both humid and arid climate features indicates that the Miocene time was a period of climatic fluctuation, due to the fluctuation in the greenhouse gases occurrence (mainly CO_2 and water vapor H_2O), where the major change from greenhouse to an icehouse earth occurred (Mutti et al., 2010).

CHAPTER 8

Conclusions and Recommendations

8.1 Conclusions

The conclusion for this study can be summarized as follow;

- The Miocene Dam Formation in Al-Lidam area is composed of a mixed carbonate-siliciclastic succession.
- These successions were deposited on a low angle dipping carbonate ramp under shallow marine conditions that were tidally dominated as well as, to less extent, wave related processes.
- Fifteen lithofacies have been identified based on their lithology, sedimentary structures, fossils content, paleocurrent patterns and morphology.
- The depositional environments show a gradual change from relative deeper conditions in the east toward the shallower water conditions to the west through the studied sections.
- Three 4th order, shallowing upward, sequences have been identified, with two sequence boundaries separating between them.
- Different diagenetic processes were identified from thin-sections, SEM and XRD analysis. This include; micritization, marine cementation, meniscus and microstalictitic calcite cementation, meteoric grain dissolution, meteoric equant calcite cementation, shallow burial compaction, dolomitization and clay minerals precipitation.

- Carbonate diagenesis in the study area is dominated by meteoric dissolution and mimetic replacement dolomitization. However, several marine diagenetic features were observed too.
- A sabkha-evaporative dolomitization model was proposed for the dolomites in the study area.
- Diagenesis follows the sequence stratigraphic pattern related to sea-level fall; that is, dissolution, early cementation, and frequent dolomitization.
- A combination of depositional environment and diagenesis controls reservoir quality.
- Cementation, compaction and clay minerals precipitation reduced porosity, which led to low permeability and poor reservoir quality, while dissolution, dolomitization and fracturing resulted in improved reservoir quality.
- The best reservoir quality occurs in the upper parts of the highstand systems tracts, which contain primary grain supported intervals and/or dissolution porosity.
- This study has revealed that integration of diagenesis and sequence stratigraphy allows a better prediction of the spatial and temporal distribution of diagenetic alteration in carbonate sequences, and outlining of the reservoir quality evolution of carbonate sediments.

8.2 Recommendations

At the end of this study, I recommend looking in some areas where further research may be powerful, these include;

- Application of paleontology and biostratigraphy on the studied sections for better understanding of depositional environments.
- Application of isotope geochemistry (Oxygen, Carbon and Strontium stable isotopes) to delineate the sequences and to define the diagenetic processes and environments more precisely.
- Correlation of the present findings with subsurface data.

References

Ahr, W. M. (2008). GEOLOGY OF CARBONATE The Identification , Description , and Characterization of Hydrocarbon Reservoirs in Carbonate Rocks. Hoboken, New Jersey: Wiley.

Al-husseini, M. I. (2000). Origin of the Arabian Plate Structures : Amar Collision and Najd Rift. GeoArabia, 5(4), 527–542.

Ali, S. A., Clark, W. J., & Dribus, J. R. (2010). Diagenesis and Reservoir Quality. Oilfield Review, 22(2), 14–27.

Al-juboury, A. I., & Mccann, T. (2008). The Middle Miocene Fatha (Lower Fars) Formation , Iraq. GeoArabia, 13(3), 141–174.

Alkhaldi, F. (2009). Controls on Hierarchy of Miocene Buildups within a High Resolution Cycle Stratigraphic Framework of Dam Formation, Lidam Area, Saudi Arabia. M.Sc thesis. King Fahd University of Petroleum & Minerals.

Al-saad, H., & Ibrahim, M. I. (2002). Stratigraphy , micropaleontology , and paleoecology of the Miocene Dam Formation , Qatar. GeoArabia, 7(1), 9–28.

Armstrong, H. A., & Brasier, M. D. (2005). Microfossils (2nd ed.). Malden, MA: Blackwell Publishing.

Beydoun, Z.R., 1993. Evolution of the northeastern Arabian plate margin and shelf: hydrocarbon habitat and conceptual future potential. Revue de l'Institut Francais du Petrole, 48(4): 311–45.

Bjørlykke, K. (1998). Clay Mineral Diagenesis in Sedimentary Basins — A Key to the Prediction of Rock Properties. Examples from the North Sea Basin. Clay Minerals, 33(1), 15–34.

Boggs, S. (2006). Principles of Sedimentology and Stratigraphy (4th ed.). New Jersey: Prentice Hall.

Brown, L. F. Jr., and Fisher, W. L. (1977). Seismic stratigraphic interpretation of depositional systems: examples from Brazilian rift and pull apart basins. In Seismic Stratigraphy–Applications to Hydrocarbon Exploration (C. E. Payton, Ed.), pp. 213–248. American Association of Petroleum Geologists Memoir 26.

Budd, D. A. (1984). Freshwater Diagenesis of Holocene Ooid Sands, Schooner Cays, Bahamas. PhD dissertation. University of Texas at Austin.

Çağatay, M. N. (1990). Palygorskite in the Eocene Rocks of the Dammam Dome, Saudi Arabia. Clays and Clay Minerals, 38(3), 299–307.

Camp, V. E., & Roobol, M. . (1991). Geologic map of the Cenozoic lava field of Harrat Rahat, Kingdom of Saudi Arabia. Saudi Arabian Directorate General of Mineral Resources Geosciences Map GM-123, Scale 1:250,000, with Text 37 P.

Cantrell, D. L., & Hagerty, R. M. (1999). Microporosity in Arab Formation Carbonates , Saudi Arabia. GeoArabia, 4(2), 129–154.

Catuneanu, O., 2006, Principles of Sequence Stratigraphy. Elsevier, Amsterdam, 375 pp.

Catuneanu, O., Galloway, W. E., Kendall, C. G. S. C., Miall, A. D., Posamentier, H. W., Strasser, A., & Tucker, M. E. (2011). Sequence Stratigraphy: Methodology and Nomenclature. Newsletters on Stratigraphy, 44(3), 173–245.

Dill, H. G., Botz, R., Berner, Z., Stüben, D., Nasir, S., & Al-Saad, H. (2005). Sedimentary facies, mineralogy, and geochemistry of the sulphate-bearing Miocene Dam Formation in Qatar. Sedimentary Geology, 174(1-2), 63–96.

Duncan F. Sibley. (1982). The Origin of Common Dolomite Fabrics: Clues from the Pliocene. SEPM Journal of Sedimentary Research, Vol. 52.(4), 967 - 975.

Dunham, R. J. (1962). Classification of carbonate rocks according to depositional texture. In: Ham, W.E. Classification of carbonate rocks. American Association of Petroleum Geologists Memoir. 1. pp. 108–121.

Embry, A. F., & Klovan, J. S. (1971). A Late Devonian reef tract on northeastern Banks Island, N.W.T. Bulletin of Canadian Petroleum Geology, 4, 730–781.

Embry, A.F. 1993. Transgressive-regressive (T-R) sequence analysis of the Jurassic succession of the Sverdrup Basin, Canadian Arctic Archipelago. Canadian Journal of Earth Sciences, 30, 301-320.

Flügel, E. (2010). Diagenesis, Porosity, and Dolomitization. In: Flugel, E., (ed.). Microfacies of Carbonate Rocks (2nd ed., pp. 267–338). Berlin, Heidelberg: Springer Berlin Heidelberg.

Folk, R.L. (1974). The natural history of crystalline calcium carbonate: Effect of magnesium content and salinity. Journal of Sedimentary Petrology, 44, 40–53.

Friedman, G. M. (1993). Carbonate Storm Deposits (Tempestites) of Middle to Upper Cambrian Age in Helan Mountains, Northeast China, Carbonates and Evaporites, 8(2), 181–190.

Gregg, J. M. and, & Sibley, D. F. (1987). Classification of dolomite rock texture. Journal of Sedimentary Research, 57(6), 967 – 975.

Halley, R. B., & Harris, P. M. (1979). Fresh water cementation of a 1,000 yearold oolite. Journal of Sedimentary Petrology, 49, 969–988.

Harrison, R. S. (1975). Porosity in Pleistocene grainstones from Barbados: some preliminary observations. Bulletin of Canadian Petroleum Geology, 23, 383–392.

Helland-Hansen, W. and Gjelberg, J., 1994, Conceptual basis and variability in sequence stratigraphy: a different perspective. Sedimentary Geology, 92, 1-52.

Hsu K.J. (1967). Chemistry of Dolomite Formation. In: Chilingar G.V., Bissell H.J. and Fairbridge R.W., (eds.). Carbonate Rocks – Physical and Chemical Aspects. Developments in Sedimentology, Elsevier, Amsterdam (169–191).

Hunt, D. and Tucker, M. (1992). Stranded parasequences and the forced regressive wedge systems tract:

deposition during base level fall. Sedimentary Geology, 81, 1-9.

Irtem, O. (1986). Miocene Tidal Flats Stomatolites of the Dam Formation, Saudi Arabia. The Arabian Journal for Science and Engineering, 12(2), 145–153.

James, N. ., & Choquette, P. . (1983). Diagenesis 6. Limestones - the sea floor diagenetic environment. Geoscience Canada, 10(4), 162–179.

Kendall, C. G. S. C., & Warren, J. (1987). A review of the origin and setting of tepees and their associated fabrics. Sedimentology, 34(6), 1007–1027.

Konert, G., Afifi, A. M., & Al-hajri, S. 'id. (2001). Paleozoic Stratigraphy and Hydrocarbon Habitat of the Arabian Plate. GeoArabia, 6(3), 407–442.

Koop, W. J., Stoneley, R., Ridd, M. F., Murphy, R. W., Osmaston, M. F., & Kholief, M. M. (1982). Subsidence History of the Middle East Zagros Basin, Permian to Recent. Philosophical Transactions of the Royal Society, 305(1489), 149–168.

Land, L. S., & Epstein, S. (1970). Late Pleistocene Diagenesis and Dolomitization, North Jamaica. Sedimentology, 14(3-4), 187–200.

Land, L. S., & Moore, C. H. (1980). Lithification, micritization and syndepositional Sediment., diagenesis of biolithites on the Jamaican island slope. Journal of Sedimentary Petrology, 50, 357–370.

Longman, M. W. (1980). , Carbonate Diagenetic Textures from Nearsurface Diagenetic Environments., The American Association of Petroleum Geologists Bulletin, 64(4), 461–487.

Lumsden, D. N. & Chimahusky, J. S. (1980). Relationship between dolomite nonstoichiometry and carbonate facies parameters. In SEPM Special Publication 28 (pp. 123 – 137.).

Makhloufi, Y., Collin, P.-Y., Bergerat, F., Casteleyn, L., Claes, S., David, C., … Rigollet, C. (2013). Impact of sedimentology and diagenesis on the petrophysical properties of a tight oolitic carbonate reservoir. The case of the Oolithe Blanche Formation (Bathonian, Paris Basin, France). Marine and Petroleum Geology, 48, 323–340.

Maliński, E., Gasiewicz, A., Witkowski, A., Szafranek, J., Pihlaja, K., Oksman, P., & Wiinamäki, K. (2009). Biomarker features of sabkha-associated microbialites from the Zechstein Platy Dolomite (Upper Permian) of northern Poland. Palaeogeography, Palaeoclimatology, Palaeoecology, 273(1-2), 92–101.

Matthews, R. K. (1974). A process approach to diagenesis of reefs and reefassociated limestones. In: Laporte, L.F. (Ed.), Reefs in Time and Space. SEPM Special Publication 18, pp. 234–256.

Milliman, J. D. (1974). Recent Sedimentary Carbonates . Verlag , Berlin.: Springer.

Mishra, P. K., Kandiri, J. Al, Choudhary, P. K., Hoppe, M., & Meadows, D. (2012). Significance of Palygorskite in the Drilling and Production of Hydrocarbon in the Neogene of North Kuwait. In AAPG International Conference and Exhibition. Singapore.

Mitchum, R. M., Jr., 1977. Seismic stratigraphy and global changes of sea level, part 11: glossary of terms used in seismic stratigraphy. In: Payton, C. E. (ed.), Seismic Stratigraphy – Applications to Hydrocarbon Exploration. American Association of Petroleum Geologists Memoir 26, 205–212.

Moore, C. H. (2013). Carbonate Reservoirs: Porosity Evolution and Diagenesis in a Sequence Stratigraphic Framework . (C. H. Moore & W. J. Wade, Eds.) (2nd ed.). Amsterdam.: Elsevier.

Morad, S., Ketzer, J. M., & De Ros, L. F. (2013). Linking Diagenesis to Sequence Stratigraphy: An Integrated Tool for Understanding and Predicting Reservoir Quality Distribution. In

Morad, S., Ketzer, J. M., & De Ros, L. F.(eds.). Linking Diagenesis to Sequence Stratigraphy (pp. 1–36). West Sussex, UK: John Wiley & Sons, Inc.

Morad, S., Ketzer, J. M., & DeRos, F. (2000). Spatial and temporal distribution of diagenetic alterations in siliciclastic rocks: implication for mass transfer in sedimentary basins. Sedimentology, 47, 95 – 120.

Morse, J. W., & Mackenzie, F. T. (1990). Geochemistry of Sedimentary Carbonates. Amsterdam: Elsevier.

Mutti, M., Piller, W.E., Betzler, C., 2010. Miocene carbonate systems: an introduction. In: Mutti, M., Piller, W.E., Betzler, C. (Eds.), Oligocene – Miocene Carbonate Systems. IAS Spec. Publ., 42, pp. vii – xii.

Muttoni, G., Gaetani, M., Kent, D. V, Sciunnach, D., Berra, F., Garzanti, E., … Zanchi, A. (2009). Opening of the Neo-Tethys Ocean and the Pangea B to Pangea A transformation during the Permian. GeoArabia, 14(4), 17–48.

Palma, R. M., López-Gómez, J., & Piethé, R. D. (2007). Oxfordian ramp system (La Manga Formation) in the Bardas Blancas area (Mendoza Province) Neuquén Basin, Argentina: Facies and depositional sequences. Sedimentary Geology, 195(3-4), 113–134.

Pemberton, S.G., MacEachern, J.A., Dashtgard, S.E., Bann, K.L., Gingras, M.K., and Zonneveld, JP. 2012. Shorefaces, *in* Knaust, D. and Bromley, R. eds., Trace Fossils as Indicators of Sedimentary Environments, Developments in Sedimentology Series 64, 563-606, Elsevier.

Posamentier, H. and Allen, G. 1999, Siliciclastic sequence stratigraphy – concepts and applications. SEPM Concepts in Sedimentology and Paleontology, # 7, 210 pp.

Powers, R., Ramirez, L. F., Redmond, C. D., & Erelbg, JR., E. L. (1966). GEOLOGY OF THE ARABIAN PENINSULA Sedimentary Geology of Saudi Arabia. Washington: U.S. Geological Survey Professional Papaer 560-D.

R. C. Murray. (1960). Origin of Porosity in Carbonate Rocks. Journal of Sedimentary Research, 30(1), 59-84.

Reid, R. P., & Macintyre, I. G. (2000). Microboring Versus Recrystallization: Further Insight into the Micritization Process. Journal of Sedimentary Research, 70(1), 24–28.

Riding, R. (1999). The term stromatolite: towards an essential definition. Lethaia, 32(1), 321–330.

Sawaf, T., Al-saad, D., Gebran, A., Barazangi, M., Best, J. A., & Chaimov, T. A. (1993). Stratigraphy and structure of eastern Syria across the Euphrates depression. Tectonophysics, 220(1-4), 267–281.

Sellwood, B. W., Scott, J., Mikkelsen, P., & Akroyd, P. (1985). Stratigraphy and sedimentology of the Great Oolite Group in the Humbly Grove oilfield, Hampshire, S. England. Marine and Petroleum Geology, 2, 44–55.

Sharland, P.R., R. Archer, D.M. Casey, R.B. Davies, S.H. Hall, A.P. Heward, A.D. Horbury and M.D. Simmons 2001. Arabian Plate Sequence Stratigraphy. GeoArabia Special Publication 2, Gulf PetroLink, Bahrain, 371 p.

Shinn, E. a. (1983). Birdseyes, fenestrae, shrinkage pores, and loferites; a reevaluation. Journal of Sedimentary Research, 53(2), 619–628.

Stampfli, G. M., and Borel, G. D. (2002). A plate tectonic model for the Paleozoic and Mesozoic constrained by dynamic plate boundaries and restored synthetic oceanic isochrons. Earth and Planetary Science Letters, 196(1-2), 17–33.

Steineke, M., Bramkamp, R. A., & Sander, N. J. (1958). Stratigraphic relations of Arabian Jurassic oil in Habitat of oil. American Association of Petroleum Geologists Symposium, Tulsa, 1294–1329.

Stoeser, D. B., & Camp, V. E. (1985). Pan-African microplate accretion of the Arabian Shield. Bulletin of the Geological Society of America, 96, 817–826.

Thralls, H. W., & Hasson, R. C. (1956). Geology and oil resources of eastern Saudi Arabia. Internat. Geol. Cong., 20th, Mexico, Symposium Sobre Yacimentos Do Petroleo Y Gas, 2, 9 - 32.

Thurmond, J. B., Løseth, T. M., Rivenæs, J. C., Martinsen, O. J., & Aiken, C. (2005). Using Outcrop Data in the 21st Century – New methods and applications , with example from the Ainsa Turbidite System . In: Studlick, J, Shew, R., Nilsen, T., and Steffens, G. (eds.) Deep-Water Outcrops of the World Atlas, Tulsa,. American Association of Petroleum Geologists Special Publication.

Tucker, M. E. (1993). Carbonate Diagenesis and Sequence Stratigraphy. In Sedimentology Review 1 (51 – 72).

Tucker, M. E. (2001). Sedimentary Petrology: An Introduction to the Origin of Sedimentary Rocks. Blackwell sciences Ltd.

Tucker, M. E., & Wright, V. P. (1990a). Carbonate sedimentology (1st ed.). Blackwell scientific.

Tucker, M. E., & Wright, P. V. (1990b). Dolomites and dolomitization models. In: Tucker, M. E., & Wright, V. P. Carbonate Sedimentology. Blackwell scientific Ltd.

Van Wagoner, J. C. (1995). Overview of sequence stratigraphy of foreland basin deposits: terminology, summary of papers, and glossary of sequence stratigraphy. In Catuneanu, O., 2006, Principles of Sequence Stratigraphy. Elsevier, Amsterdam, 375 pp.

Van Wagoner, J. C., Mitchum, R. M., Campion, K. M., & Rahmanian, V. D. (1990). Siliciclastic Sequence Stratigraphy in Well Logs, Cores, and Outcrops: Concepts for High-Resolution Correlation of Time and Facies. In: Siliciclastic Sequence Stratigraphy in Well Logs, Cores, and Outcrops: Concepts for High-Resolution Correlation of Time and Facies (pp. 1–55).

Van Wagoner, J. C., Posamentier, H.W., Mitchum, R. M., Vail, P. R., Sarg, J. F., Loutit, T. S., Hardenbol, J., 1988. An overview of sequence stratigraphy and key definitions. In: Wilgus, C. K., Hastings, B. S., Kendall, C. G. St. C., Posamentier, H.W., Ross, C. A., Van Wagoner, J. C. (Eds.), Sea Level Changes – An Integrated Approach. SEPM Special Publication 42, 39 - 45.

Warren, J. (2000). Dolomite: occurrence, evolution and economically important associations. Earth-Science Reviews, 52(1-3), 1–81.

Weijermars, R. (1999). Surface Geology , Lithostratigraphy and Tertiary Growth of the Dammam Dome , Saudi Arabia : A New Field Guide. GeoArabia, 4(2), 199–226.

Wilson, J. L. (1975). Carbonate Facies in Geologic History . Verlag , New York: Springer.

Worden, R., & Morad, S. (2003). Clay minerals in sandstones: controls on formation, distribution and evolution. In: Worden, R., and Morad, S. (eds.). Clay minerals Cement in Sandstones. Int. Assoc. Sedimentol. Spec. Publ. 34, (3 - 41).

Ziegler, M. A. (2001). Late Permian to Holocene Paleofacies Evolution of the Arabian Plate and its Hydrocarbon Occurrences, GeoArabia, 6(3), 445–504.

Vitae

Name :Moaz AbdAltawab Salih

Nationality :Sudanese

Date of Birth :September. 25. 19989

Email :g201205780@kfupm.edu.sa

Address :KFUPM Campus – Dhahran – Saudi Arabia

Academic Background :Geology

Experience

Geologist

at Managem International for Mining Co. Ltd - Sudan

Location: Sudan, Wadi Gabgaba - Abu Hamad

Company Industry: Mining

Job Role: Exploration

March 2012 - December 2012

Responsibilities

- Supervised borehole RC and rotary drilling.
- Lithological description and lithological profile preparation.
- Sample preparation for geochemical analysis.
- Daily report preparation.

- Weekly presentation about the work progress, and supervised a team of seven workers.

Geologist

at Dams Implementation Unit

Location: Sudan, Al shuwak - Gedarif

Company Industry: Construction

Job Role: Exploration

December 2010 - December 2011

Responsibilities

- Supervised borehole drilling.
- Lithological description and lithological profile preparation.
- Daily report writing.
- Handling Geotechnical Investigations & various tests in Station & Tunnel.
- Prepared Geological mapping, Planning, Statigraphy, Geomorphology & Ground water condition.
- Geo-logging of various excavations i.e. shafts & Diaphragm Walls.
- Handling Probing Machine, Dynamic Cone Penetration Test (DCPT).
- Carrying out insitu geotechnical field tests and calculating TCR and RQD of core samples.

Education

Master Degree, Geology

at King Fahd University of Petroleum & Minerals, Saudi Arabia

Completion Date: June 2016

GPA / Percentage: 3.78 out of 4

I got a full scholarship from KFUPM to pursue my master degree in geology. My M.Sc. thesis is about carbonate diagenesis. Three Conference papers were published out of this work. Two journal papers are under preparation

Bachelor Degree, Geology

at University of Khartoum, Sudan

Completion Date: September 2010

GPA / Percentage: 70.7 out of 100

My graduation project was related to seismic interpretation of southwestern Muglad Basin - South Sudan.

Publication

Moaz Salih, Osman Abdulattif, Mazin Bashri (May. 2015), "Carbonate Diagenesis of Miocene Dam Formation. An outcrop approach – al-Lidam area, Eastern Region, Saudi Arabia". 11th International Geological Conference & Exhibition. Riyadh. Saudi Arabia.

Moaz Salih, Osman Abdullatif, Khalid Al-Ramadan, Dave Cantrell, Lamidi Babalola, Mazin Bashri (March 2016), "Impact of Sedimentology and Diagenesis on Petrophysical Properties of Miocene Dam Formation. Outcrop Approach – Al – Lidam Area, Eastern Saudi Arabia". GEO 2016 (12th Middle East Geosciences Conference & Exhibition). Manama. Bahrain.